ISTANBUL TECHNICAL UNIVERSITY ★ GRADUATE SCHOOL OF SCIENCE ENGINEERING AND TECHNOLOGY

ESTIMATIONS OF SEISMIC INPUT ENERGY AND INELASTIC TOP DISPLACEMENT DEMAND IN MOMENT RESISTING FRAME TYPE STRUCTURES

M.Sc. THESIS

Furkan ÇALIM

Department of Civil Engineering

Structural Engineering Programme

JULY 2020

ISTANBUL TECHNICAL UNIVERSITY ★ GRADUATE SCHOOL OF SCIENCE ENGINEERING AND TECHNOLOGY

ESTIMATIONS OF SEISMIC INPUT ENERGY AND INELASTIC TOP DISPLACEMENT DEMAND IN MOMENT RESISTING FRAME TYPE STRUCTURES

M.Sc. THESIS

Furkan ÇALIM
(501181015)

Department of Civil Engineering

Structural Engineering Programme

Thesis Advisor: Prof. Dr. Ercan YÜKSEL

JULY 2020

İSTANBUL TEKNİK ÜNİVERSİTESİ ★ FEN BİLİMLERİ ENSTİTÜSÜ

MOMENT AKTARAN ÇERÇEVE TÜRÜ YAPILARDA SİSMİK GİRİŞ ENERJİSİNİN VE İNELASTİK TEPE YERDEĞİŞTİRMESİ TALEBİNİN TAHMİN EDİLMESİ

YÜKSEK LİSANS TEZİ

Furkan ÇALIM
(501181015)

İnşaat Mühendisliği Anabilim Dalı

Yapı Mühendisliği Programı

Tez Danışmanı: Prof. Dr. Ercan YÜKSEL

TEMMUZ 2020

Furkan Çalım, a M.Sc. student of ITU Graduate School of Science Engineering and Technology student ID 501181015, successfully defended the thesis entitled "ESTIMATIONS OF SEISMIC INPUT ENERGY AND INELASTIC TOP DISPLACEMENT DEMAND IN MOMENT RESISTING FRAME TYPE STRUCTURES", which he prepared after fulfilling the requirements specified in the associated legislations, before the jury whose signatures are below.

Thesis Advisor :	**Prof. Dr. Ercan YÜKSEL** Istanbul Technical University	.....
Jury Members :	**Prof. Dr. Engin ORAKDÖĞEN** Istanbul Technical University	.....
	Asst. Prof. Dr. Melih SÜRMELİ Bursa Technical University	.....

Date of Submission : 15 June 2020
Date of Defense : 14 July 2020

To my family,

FOREWORD

Firstly, I would like to express my sincere thanks to my advisor Prof. Dr. Ercan Yüksel for his endless support, guidance and inspiration. It was an honor for me to work with him and benefit from his valuable knowledge and experience.

I would like to thank Asst. Prof. Dr. Ahmet Güllü as well for his guidance during the thesis.

I also give thanks to The Scientific and Technological Research Council of Turkey (TUBITAK) "2211 – National Graduate Scholarship Programme" for their financial support during my M.Sc. degree education.

July 2020

Furkan ÇALIM
(Civil Engineer)

TABLE OF CONTENTS

Page

ABBREVIATIONS

DBSD	**:** Displacement-Based Seismic Design
EBSD	**:** Energy-Based Seismic Design
EQ	**:** Earthquake
E-SDOF	**:** Equivalent Single Degree of Freedom
FBSD	**:** Force-Based Seismic Design
MDOF	**:** Multi Degree of Freedom
NLTHA	**:** Nonlinear Time History Analysis
PGA	**:** Peak Ground Acceleration
PGV	**:** Peak Ground Velocity
RC	**:** Reinforced Concrete
SAC	**:** A Partnership of the Structural Engineers Association of California, the Applied Technology Council, and the California Universities for Research in Earthquake Engineering
SD	**:** Spectral Displacement
SDOF	**:** Single Degree of Freedom
SRSS	**:** Square-Root of Sum of Squares
SV	**:** Spectral Velocity

SYMBOLS

E_d	: Damping Energy
E_H	: Dissipated Hysteretic Energy
E_H/m	: Mass-Normalized Dissipated Hysteretic Energy
E_I	: Input Energy
E_I/m	: Mass-Normalized Input Energy
E_k	: Kinetic Energy
E_s	: Strain Energy
R	: Reduction Factor
T	: Vibrational Period
T_{ref}	: Reference Period
V_{s30}	: Average Shear-Wave Velocity in the top 30 m of the Soil
Γ	: Modal Participation Factor
δ_{top}	: Top Displacement
ϕ	: Mode Shape
ω	: Angular Frequency
ε	: Relative Percentage Difference

LIST OF TABLES

Page

LIST OF FIGURES

Page

ESTIMATIONS OF SEISMIC INPUT ENERGY AND INELASTIC TOP DISPLACEMENT DEMAND IN MOMENT RESISTING FRAME TYPE STRUCTURES

SUMMARY

Energy-based seismic design (*EBSD*) methodology has an edge over force-based seismic design (*FBSD*) and displacement-based seismic design (*DBSD*) methodologies in many ways. Unlike *FBSD* and *DBSD* used in the current seismic design codes, it accounts for the type (near-fault, far-fault, etc.), frequency content, and total duration of the *EQ* record. Also, it takes the cumulative damage potential of an earthquake excitation into account.

A basis for the *EBSD* was created in the content of this thesis study by proposing a methodology to calculate the seismic demands of a moment resisting frame fast and with an acceptable level of accuracy. Firstly, mass-normalized input energy response spectrum is calculated for *SDOF* systems using the ground acceleration and velocity response of the structure. Input energies (E_I) imparted into each story of a *MDOF* system are estimated using the suggested formula which uses mode shapes, modal participation factors, and E_I/m spectra constructed for *SDOF* systems. After total E_I per unit mass is estimated, maximum inelastic top displacement (δ_{top}) of a *MDOF* system during a seismic excitation is predicted using the proposed relation between E_I/m and δ_{top}.

Model frames and *EQ* records to be used in the application and verification of the methodology were selected and nonlinear time history analyses (*NLTHA*) were performed on the model frames using Perform 3D software. In order to make sure that the methodology can be applied on moment resisting frames using different materials and with different number of stories, three-story reinforced concrete *Manoukas* frame, three- and six-story steel *Akbas* frames, nine- and twenty-story steel *SAC-LA* frames were selected. For the selection of *EQ* records, energy-displacement capacity curves were calculated for the model frames using the force-displacement capacity curves that were obtained after running static push-over analyses. 92 *EQ* records causing a higher energy input to the frames than the yield energy were selected.

After seismic demands (input energy demands on story level and inelastic top displacement demand) of the set of 92 *EQ* records were estimated by the proposed methodology, they were compared with the results of the *NLTHA*. Relative percentage differences between the predicted and true values were computed.

Using all 92 *EQ* records, arithmetic means of the relative percentage differences in the prediction of total E_I/m, story E_I, and δ_{top} were computed as 12.6%, 19.5%, 19.6%, respectively for the steel frames and 38.6%, 37.0%, 53.1%, respectively for the *RC* frame.

Using the 35 *EQ* records with a *PGV* less than 50 m/s (ordinary non-pulse-like motion), arithmetic means of the relative percentage differences in the prediction of total E_I/m, story E_I, and δ_{top} were computed as 7.3%, 13.6%, 17.3%, respectively for the steel frames and 17.1%, 18.7%, 20.9%, respectively for the *RC* frame.

It was observed that the methodology yields better results for ordinary type *EQ* records ($PGV \leq 50$ m/s) compared to pulse-like type *EQ* records. For steel frames, it predicts the seismic demands with a very strong correlation. For *RC* frame, it predicts the seismic demands with a moderate correlation in the case of pulse-like records, and with a very strong correlation in the case of ordinary non-pulse-like records.

MOMENT AKTARAN ÇERÇEVE TÜRÜ YAPILARDA SİSMİK GİRİŞ ENERJİSİNİN VE İNELASTİK TEPE YERDEĞİŞTİRMESİ TALEBİNİN TAHMİN EDİLMESİ

ÖZET

Mevcut deprem yönetmeliklerinde (ASCE/SEI 7, FEMA 356, Eurocode 8, TBDY 2018 gibi) kuvvet esaslı ve yerdeğiştirme esaslı sismik tasarım yöntemleri kullanılmaktadır. Kuvvet esaslı tasarım yönteminde, daha önceden belirlenmiş bina performans hedefi için sistem sünekliği ve malzeme dayanım fazlalığı katsayısına karşı gelen azaltma katsayısı "*R*" belirlenir. Elastik ivme spektrumu kullanılarak elde edilen elastik deprem kuvvetleri *R* katsayısı ile küçültülerek tasarım deprem kuvvetleri hesaplanır. Bu azaltma, yapının tasarım deprem kuvvetleri altında doğrusal olmayan davranış göstereceği varsayılarak yapılır. Yapısal elemanların tasarım deprem kuvvetlerini güvenle taşıdığı durumda yeterli sismik tasarım elde edilmiş olur. Yerdeğiştirme esaslı tasarım yönteminde ise, öncelikle yapının kuvvet-yerdeğiştirme ilişkisi hesaplanır. Elde edilen kapasite eğrisi kullanılarak yapının yerdeğiştirme talepleri belirlenir. Yerdeğiştirme taleplerinin yönetmeliklerde verilen limitlerden daha az olduğu durumda yeterli sismik tasarım elde edilmiş olur.

Geleneksel sismik tasarım yöntemleri (kuvvet esaslı ve yerdeğiştirme esaslı) depreme ait bazı önemli özellikleri hesaba katmadıkları için güvenilir bir sismik tasarım ortaya koyma konusunda büyük bir eksikliğe sahiplerdir. Özellikle Türkiye gibi depreme sıklıkla maruz kalan ülkelerin yönetmeliklerinde bahsi geçen yöntemlerin kullanılması yerine, bu eksiklikleri bünyesinde barındırmayan yeni bir sismik tasarım yöntemi geliştirilmelidir.

Henüz mevcut yönetmeliklerde yer almayan enerji esaslı tasarım yöntemi ise bu yöntemlerin olumlu özelliklerini barındırmasına ek olarak; depremin türü, süresi ve frekans içeriği gibi kuvvet ve yerdeğiştirme esaslı yöntemlerce göz ardı edilen önemli özellikleri de dikkate almaktadır. Böylece enerji esaslı tasarım yöntemi, deprem süresine bağlı kümülatif hasar durumunu da göz ardı etmemesiyle, kuvvet ve yerdeğiştirme esaslı yöntemlere kıyasla daha güvenilir hale gelmektedir. Enerji esaslı sismik tasarım yönteminde, deprem hareketinden kaynaklanan enerji taleplerinin yapısal eleman enerji kapasitelerinden daha az olduğu durumda yeterli sismik tasarım elde edilmiş olur.

Tezin birinci bölümünde tezin amacından, literatürde konu ile ilgili daha önce yapılmış çalışmalardan ve tez ile birlikte sunulan hipotezden bahsedilmiştir.

Bu yüksek lisans tez çalışması ile; enerji esaslı sismik tasarım yöntemi geliştirilmesi kapsamında kullanılmak üzere, yapıların maruz kaldığı deprem hareketleri altında yapısal elemanlarda oluşacak inelastik tepe yerdeğiştirmesi taleplerinin ve sismik giriş enerjisinin katlar arasında dağıtılmasıyla enerji taleplerinin belirlenmesi için -doğrusal olmayan zaman tanım alanında analiz uygulayarak doğrulaması yapılmış- bir metodoloji geliştirilmesi hedeflenmektedir. Tez kapsamında geliştirilen metodoloji ile yapının sismik enerji ve yerdeğiştirme taleplerinin sadece deprem kaydı ve yapının

modal özellikleri kullanılarak hızlı ve doğru değerlere olabildiğince yakın bir şekilde tahmin edilmesi amaçlanmaktadır.

Tezin ikinci bölümünde Perform 3D yazılımında oluşturulan sayısal modellerden ve doğrusal olmayan zaman tanım alanında analizlerde kullanılan deprem kayıtlarından bahsedilmiştir. Tezde önerilen metodolojinin kontrolü ve doğrulamasını yapmak amacıyla farklı kat sayılarına sahip moment aktaran iki boyutlu çerçeve sistemler seçilmiştir. Tez içerisinde *Manoukas* 3-St, *Akbas* 3-St, *Akbas* 6-St, *SAC-LA* 9-St ve *SAC-LA* 20-St olarak adlandırılan, daha önce literatürdeki bazı çalışmalarda da kullanılmış olan üç katlı bir adet betonarme ve üç, altı, dokuz, yirmi katlı dört adet çelik olmak üzere toplam beş adet moment aktaran çerçeve sistem seçilmiştir. Yapısal elemanların doğrusal olmayan davranışını hesaba katmak için plastik mafsal teorisi kullanılmış ve elemanların her iki ucuna plastik mafsallar tanımlanırken orta kısımları ise elastik tanımlanmıştır. Plastik mafsal uzunlukları, her bir kesit yüksekliğinin yarısı olarak alınmıştır.

Deprem kayıtlarının seçimi için öncelikle model çerçevelere statik itme analizi yapılarak kuvvet-yerdeğiştirme kapasite eğrisi elde edilmiştir. Sonrasında ise enerji-yerdeğiştirme kapasite eğrisi hesaplanmış ve her bir model yapıya ait akma enerjisi değerleri elde edilmiştir. *Akbas* 3-St, *Akbas* 6-St, *SAC-LA* 9-St, *SAC-LA* 20-St çelik çerçeveleri için akma enerjileri sırasıyla 0.156 m^2/s^2, 0.208 m^2/s^2, 0.402 m^2/s^2 ve 0.307 m^2/s^2 olarak hesaplanmıştır. Akma enerjisinden daha yüksek bir enerji girişine sebep olacak 92 adet deprem kaydı, toplam 1094 deprem kaydı arasından seçilmiştir. Analizler sırasında %5 sönüm oranı kullanılmıştır. Ayrıca kayıtlarda herhangi bir ölçeklendirme yapılmamış, dolayısıyla seçilen deprem kayıtlarının içeriği bozulmamıştır.

Seçilen 92 deprem kaydından 32 tanesi uzak deprem karakteristiklerini içerisinde barındıran "ordinary non-pulse-like", 60 tanesi ise yakın fay depremi karakteristiklerini içerisinde barındıran "pulse-like" kayıtlardır. Yakın fay depremleri genellikle yapılarda daha yüksek sismik taleplerin (taban kesme kuvveti, kat yerdeğiştirmeleri, sismik giriş enerjisi, v.s.) oluşmasına sebep olurlar ve genellikle yüksek *PGV* (en büyük yer hızı) değerine sahiplerdir. Tez kapsamında önerilen metodolojinin uzak deprem kayıtları için, veya başka bir deyişle *PGV* değeri daha az olan deprem kayıtları için ($PGV \leq 50$ cm/s) çok daha iyi sonuç verdiği görülmüştür.

Tezin üçüncü bölümünde bir deprem hareketi sırasında çok serbestlik dereceli sistemlere (*ÇSDS*) etkiyen maksimum giriş enerjisinin tahmini için önerilen yöntemden bahsedilmiştir. Önerilen yöntemde, kümülatif olarak bina toplam kütlesinin %95'inden daha fazla modal etkin kütleyi sağlayacak sayıda mod kullanılmıştır. Bu bağlamda Manoukas 3-St ve *Akbas* 3-St çerçeveleri için ikişer mod (sırasıyla %96.58 ve %97.01 kümülatif modal etkin kütle), *Akbas* 6-St, *SAC-LA* 9-St, *SAC-LA* 20-St çerçeveleri için ise üçer mod (sırasıyla %97.10, %97.70 ve %95.16 kümülatif modal etkin kütle) kullanılmıştır.

Öncelikle her bir deprem kaydı kullanılarak tek serbestlik dereceli sistemlere (*TSDS*) ait giriş enerjisi spekturumu oluşturulmuştur. Yapıya ait mod şekli, modal katkı çarpanı ve *TSDS* için oluşturulmuş giriş enerjisi spekturumu kullanılarak bir formülasyon önerilmiş ve *ÇŞDS* için maksimum giriş enerjisi tahmin edilmeye çalışılmıştır. Tahmin edilen giriş enerjisi değerleri sonraki bölümlerde önce inelastik tepe yerdeğiştirmesi, sonrasında ise kat yerdeğiştirmelerinin tahmininde kullanılacağı için yapılan tahminlerin gerçek değerlere oldukça yakın olması gerekmektedir.

Giriş enerjisi tahmini için 92 adet deprem kaydı kullanılarak elde edilen sonuçlar, doğrusal olmayan zaman tanım alanında analiz sonuçları ile karşılaştırılmış ve *Manoukas* 3-St, *Akbas* 3-St, *Akbas* 6-St, *SAC-LA* 9-St, *SAC-LA* 20-St çerçeveleri için rölatif yüzde farklarının aritmetik ortalamaları sırasıyla %38.6, %11.3, %13.6, %11.7 ve %13.9 olarak hesaplanmıştır. Korelasyon katsayıları ise sırasıyla 0.739, 0.974, 0.932, 0.959 ve 0.914 olarak hesaplanmıştır. Bu sonuçlar, çelik çerçeveler için tahminlerin çok yüksek korelasyon derecesi ile, betonarme çerçeve için ise tahminlerin yüksek korelasyon derecesi ile yapıldığını göstermektedir.

Giriş enerjisi tahmini için 50 cm/s daha düşük bir *PGV* değerine sahip 35 adet deprem kaydı kullanıldığında *Manoukas* 3-St, *Akbas* 3-St, *Akbas* 6-St, *SAC-LA* 9-St, *SAC-LA* 20-St çerçeveleri için rölatif yüzde farklarının aritmetik ortalamaları sırasıyla %17.1, %5.8, %7.7, %6.0 ve %9.3 olarak hesaplanmıştır.

Tezin dördüncü bölümünde moment aktaran çerçeveye etkiyen toplam giriş enerjisinin yapının katları arasında dağıtılmasından bahsedilmiştir. Literatürde giriş enerjisinin katlar arasında dağılımının tahminine yönelik bir çalışma olmazken, histeretik enerjinin dağılımına yoğunlaşılmıştır. Literatürdeki bir çok çalışmada deprem karakteristiklerinden bağımsız olarak yapının sadece modal özellikleri kullanılarak histeretik enerji dağılımının tahmin edilmesine çalışılmış, dolayısıyla her yapı için tek bir enerji dağılım düzeni önerilmiştir. Ancak bu tezde elde edilen doğrusal olmayan zaman tanım alanında analiz sonuçları da göstermiştir ki, enerji dağılımını deprem kaydından bağımsız olarak temsil etmek mümkün değildir. Bu yüzden, bir önceki bölümde önerilen ve her bir deprem kaydına özgü giriş enerjisi spektrumunun kullanıldığı yöntem ile giriş enerjisinin katlar arasında dağılımı düşük rölatif yüzde farkları ile tahmin edilebilmektedir.

Giriş enerjisinin yapıların katları arasında dağıtılmasının tahmini için 92 adet deprem kaydı kullanılarak elde edilen sonuçlar, doğrusal olmayan zaman tanım alanında analiz sonuçları ile karşılaştırılmış ve *Manoukas* 3-St, *Akbas* 3-St, *Akbas* 6-St, *SAC-LA* 9-St, *SAC-LA* 20-St çerçeveleri için rölatif yüzde farklarının aritmetik ortalamaları sırasıyla %37.0, %15.4, %16.9, %16.5 ve %29.4 olarak hesaplanmıştır.

Giriş enerjisi yapıların katları arasında dağıtılmasının tahmini için 50 cm/s daha düşük bir *PGV* değerine sahip 35 adet deprem kaydı kullanıldığında *Manoukas* 3-St, *Akbas* 3-St, *Akbas* 6-St, *SAC-LA* 9-St, *SAC-LA* 20-St çerçeveleri için rölatif yüzde farklarının aritmetik ortalamaları sırasıyla %18.7, %13.1, %12.3, %10.1 ve %19.3 olarak hesaplanmıştır.

Tezin beşinci bölümünde ise yapının inelastik tepe yerdeğiştirmesi talebinin tahmini için önerilen yöntemden bahsedilmiştir. Literatürde bulunan ve giriş enerjisi ile tepe yerdeğiştirme arasındaki ilişkiyi gösteren formülasyon, yapının diğer modlarının katkısını da göz önünde bulundurmak için tanımlanan "referans periyot, T_{ref}" kullanılarak güncellenmiş ve tezin üçüncü bölümünde tahmin edilen giriş enerjisi kullanılarak yapının maksimum tepe yerdeğiştirmesi tahmin edilmiştir. Bu yönteme göre, giriş enerjisi ile maksimum tepe deplasmanı arasında ikinci dereceden parabolik bir ilişki elde edilmiştir.

Yapının bir deprem hareketi sırasında meydana gelen maksimum tepe yerdeğiştirmesi değeri genel doğrusal olmayan statik prosedürler için bir giriş bilgisi olarak kullanıldığından, bu değerin olabilidiğince az bir rölatif hata ile tahmin edilebilmesi önem arz etmektedir.

Tepe yerdeğiştirmesi tahmini için 92 adet deprem kaydı kullanılarak elde edilen sonuçlar, doğrusal olmayan zaman tanım alanında analiz sonuçları ile karşılaştırılmış ve *Manoukas* 3-St, *Akbas* 3-St, *Akbas* 6-St, *SAC-LA* 9-St, *SAC-LA* 20-St çerçeveleri için rölatif yüzde farklarının aritmetik ortalamaları sırasıyla %53.1, %18.3, %20.6, %18.8 ve %20.9 olarak hesaplanmıştır. Korelasyon katsayıları ise sırasıyla 0.546, 0.857, 0.849, 0.878 ve 0.883 olarak hesaplanmıştır. Bu sonuçlar, çelik çerçeveler için tahminlerin çok yüksek korelasyon derecesi ile, betonarme çerçeve için ise tahminlerin orta korelasyon derecesi ile yapıldığını göstermektedir.

Tepe yerdeğiştirmesi tahmini için 50 cm/s'den daha düşük bir *PGV* değerine sahip 35 adet deprem kaydı kullanıldığında *Manoukas* 3-St, *Akbas* 3-St, *Akbas* 6-St, *SAC-LA* 9-St, *SAC-LA* 20-St çerçeveleri için rölatif yüzde farklarının aritmetik ortalamaları sırasıyla %20.9, %15.8, %14.8, %19.8 ve %18.8 olarak hesaplanmıştır.

Tez kapsamında önerilen metodoloji ile, sismik giriş enerjisi ve inelastik tepe yerdeğiştirmesi tahminlerini çelik çerçeveler için çok yüksek korelasyon derecesi ile yapmak mümkünken, betonarme çerçeve için tahminler sadece uzak deprem ($PGV \leq$ 50 cm/s) durumunda çok yüksek korelasyon derecesi ile yapılabilmektedir.

1. INTRODUCTION

In the current seismic design codes (such as ASCE/SEI 7, FEMA 356, Eurocode 8, and TBEC 2018: Turkish Building Earthquake Code-2018), two design philosophies are used, namely force-based seismic design (*FBSD*) and displacement-based seismic design (*DBSD*). In *FBSD*, a reduction factor "*R*" corresponding to the ductility of the structure is determined for predefined target performance level. Elastic forces obtained using the elastic acceleration spectrum are reduced by the factor *R* to calculate the design seismic forces. This reduction is implemented by assuming the structure will show inelastic nonlinear behavior under the design seismic forces. The satisfactory design is obtained when the structural members can safely carry the design seismic forces. In *DBSD*, force-displacement relation of the structure is obtained with the nonlinear modelling strategy. Displacement demand of the structure is then calculated using the structural capacity curve. The satisfactory design is obtained when the displacement demand is less than or equal to the limits given in the design codes corresponding to the prevenient performance level.

However, these approaches disregard some important earthquake-dependent parameters such as the frequency content and duration of the excitation. They only consider the peak responses in the assessment of demands of the structures. Because of the deficiencies in *FBSD* and *DBSD*, a more extensive design philosophy was needed. Thus, "Energy Based Seismic Design" (*EBSD*) is firstly introduced by Housner in 1956 and studied by many researchers since. *EBSD* can be considered as a more reliable design procedure as it also accounts for the cumulative damage potential of the earthquake record alongside comprising the positive sides of the current design methodologies.

Two unscaled earthquake records with similar *PGA* values but different total durations (Chile Llolleo, 1985 and San Salvador, 1986) were selected in order to demonstrate the deficiencies in the current seismic design methodologies, Figure 1.1. They result in almost the same acceleration spectra (Figure 1.2) but quite different input energy spectra (Figure 1.3) for 5% damping ratio. Since some parameters like earthquake

duration are not considered in the traditional design methods, similar seismic demands are obtained using the acceleration spectra. Yet, more realistic seismic demands are obtained using the input energy spectra in *EBSD*.

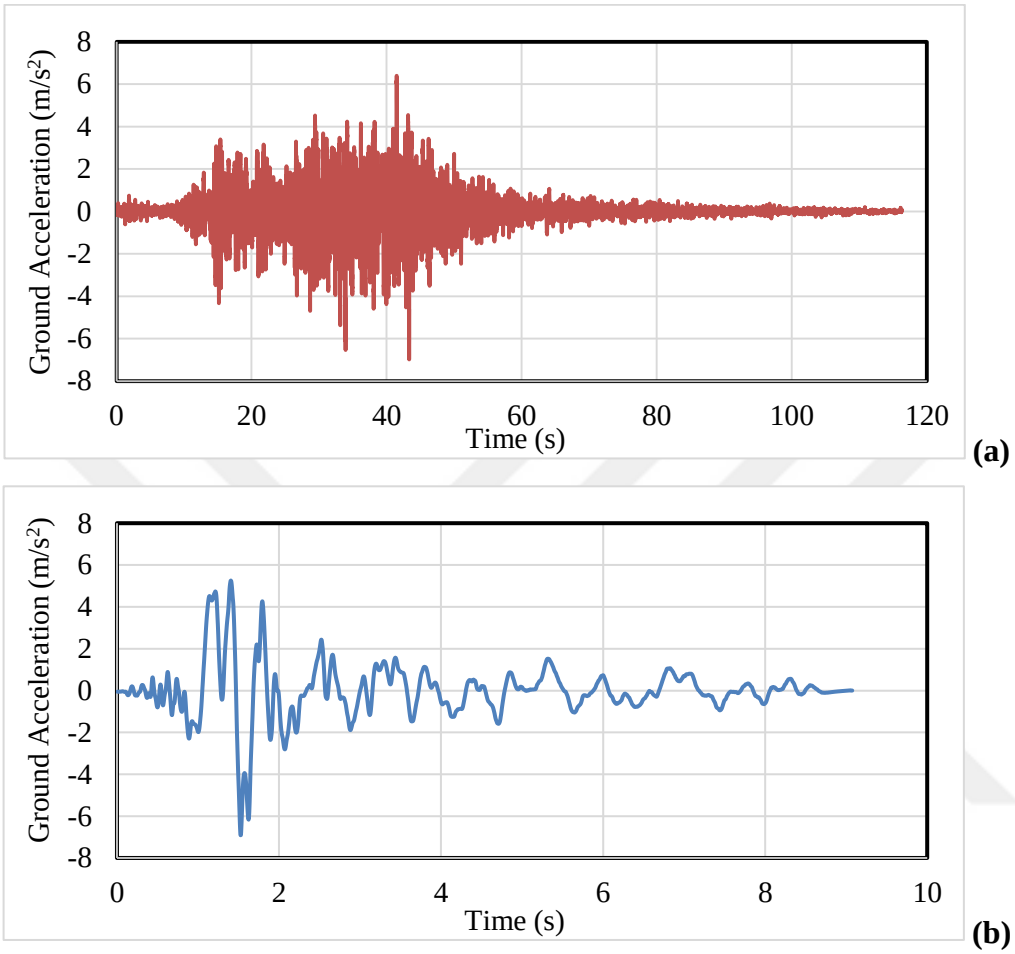

Figure 1.1 : Ground accelerations: (a) Chile Llolleo. (b) San Salvador.

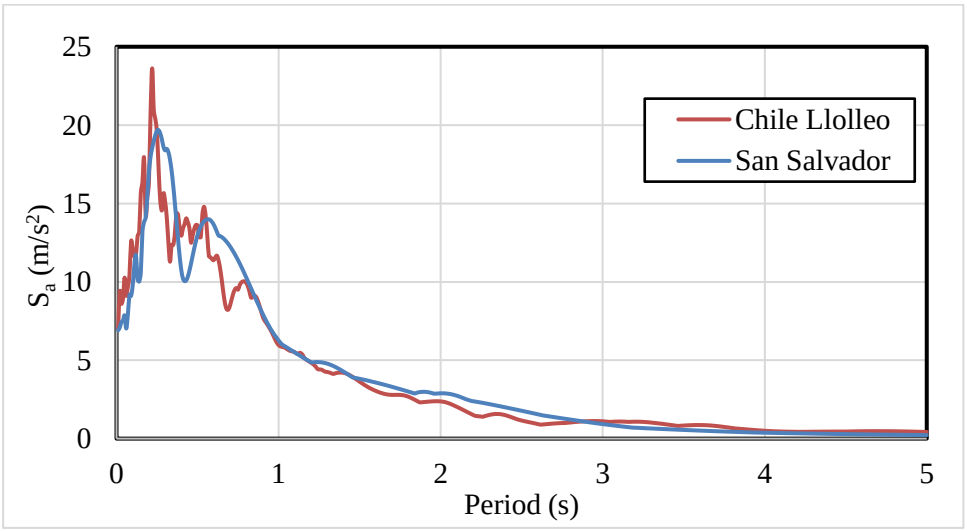

Figure 1.2 : Acceleration spectra for the sample *EQ* records.

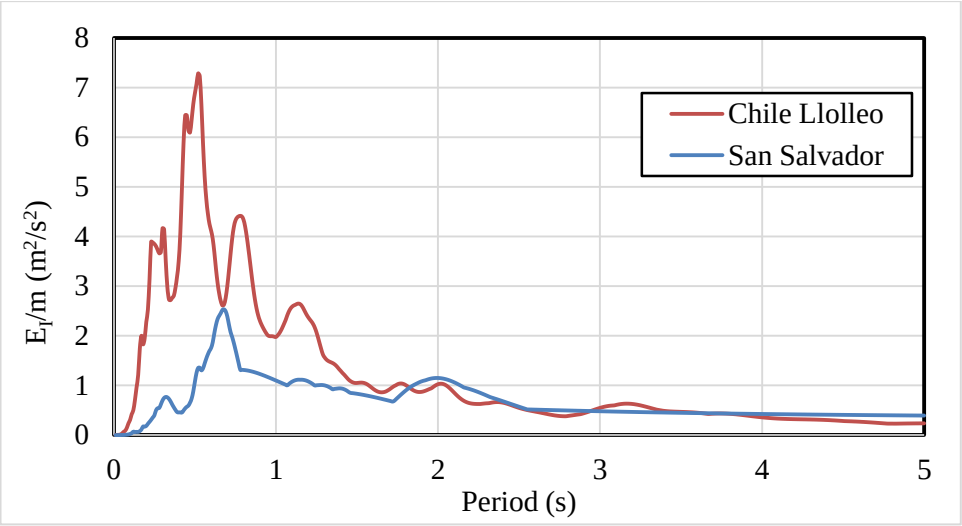

Figure 1.3 : Input energy spectra for the sample *EQ* records.

1.1 Purpose of Thesis

With this M.Sc. thesis, it is aimed to propose a methodology in order to determine the earthquake demands of moment resisting frame type structures using energy-based approach. Using the proposed methodology; the seismic input energy imparted into a structure during an earthquake, its distribution among the stories, and inelastic top displacement demand are expected to be estimated with a high precision only using the modal properties of the structure and the input energy spectrum of the earthquake record.

1.2 Literature Review

External and internal energy terms can be obtained using the dynamic equation of motion of a *SDOF* system under a seismic excitation, equation (1.1) where "*m*" is mass, "*c*" is damping, "*k*" is stiffness, "*u*" is displacement response, "$\dot{u}$" is velocity response, "$\ddot{u}$" is acceleration response of the system, and "$\ddot{u}_g$" is ground acceleration.

$$m\cdot\ddot{u}(t)+c\cdot\dot{u}(t)+k\cdot u(t)=-m\cdot\ddot{u}_g(t) \tag{1.1}$$

Multiplying both sides of the equation (1.1) by "$\dot{u}dt$" term and integrating it over the total earthquake duration yields equation (1.2). Left-hand side of the equation represents the energy components of the structure, namely kinetic energy (E_k), damping energy (E_d) which is the amount of dissipated energy due to damping, and

strain energy (E_s) which is composed of recoverable elastic and irrecoverable inelastic energies. Right-hand side of the equation represents the input energy (E_I), equation (1.3) (Akiyama, 1985).

$$m\int_0^t \ddot{u}(t)\cdot\dot{u}(t)dt + c\int_0^t \dot{u}(t)\cdot\dot{u}(t)dt + k\int_0^t u(t)\cdot\dot{u}(t)dt = -m\int_0^t \ddot{u}_g(t)\cdot\dot{u}(t)dt \tag{1.2}$$

$$E_k + E_d + E_s = E_I \tag{1.3}$$

In order to calculate the mass-normalized input energy for a *SDOF* system, Akiyama (1985) proposed empirical relation, equation (1.4). The equivalent velocity (V_E) used in the estimation of the input energy per unit mass is calculated using the predominant period of the ground motion (T_c), equation (1.5).

$$E_I / m = \frac{V_E^2}{2} \tag{1.4}$$

$$V_E = \begin{cases} 2.5T & T \le T_c \\ 2.5T_c & T > T_c \end{cases} \tag{1.5}$$

Kuwamura and Galambos (1989) used the same equation with Akiyama but recommended equation (1.6) in the calculation of V_E. "I_e" term is calculated using equation (1.7).

$$V_E = \begin{cases} \dfrac{\sqrt{T_c I_e}}{2}\dfrac{1.2T}{T_c} & T \le T_c \\ \dfrac{\sqrt{T_c I_e}}{2} & T > T_c \end{cases} \tag{1.6}$$

$$I_e = \int_0^t \ddot{u}_g^2(t)dt \tag{1.7}$$

Two methods are suggested by Uang and Bertero (1990) to calculate mass-normalized input energy. In the first method, it was calculated by derivation of the absolute equation of motion, equation (1.8) whereas in the second method, it was calculated by derivation of the relative equation of motion, equation (1.9). Idea of calculating the

input energy in terms of the relative equation of motion as in equation (1.9) is considered to be more reasonable in the literature.

$$E_I / m = \int_0^t \dot{u}_g(t) \cdot \ddot{u}(t) dt \tag{1.8}$$

$$E_I / m = -\int_0^t \ddot{u}_g(t) \cdot \dot{u}(t) dt \tag{1.9}$$

In order to obtain a reliable relationship between the energy and displacement demands, Fajfar (1992) and Fajfar and Vidic (1994) proposed a non-dimensional parameter (γ) for *SDOF* systems, equation (1.10). With this expression, mass normalized dissipated hysteretic energy (E_H) and the maximum displacement of a *SDOF* system (δ) are correlated.

$$\gamma = \frac{\sqrt{E_H / m}}{\omega \times \delta} \tag{1.10}$$

Teran-Gilmore (1996) suggested a more stable parameter (ζ) to indicate the relation between energy and displacement demand of *SDOF* systems where input energy (E_I) is used instead of dissipated hysteretic energy (E_H), equation (1.11).

$$\zeta = \frac{\sqrt{E_I / m}}{\omega \times \delta} \tag{1.11}$$

For the application of these expressions on *MDOF* systems, Mollaioli et al. (2011) studied the correlation between top displacement demand of a *MDOF* system and energy demand in terms of both E_H and E_I. In this study, equations (1.10) and (1.11) were modified using the angular frequency corresponding to the first mode (ω_1) and top displacement of the structure (δ_{top}) and two new parameters (γ' and ζ') were introduced, equations (1.12) and (1.13).

$$\gamma' = \frac{\sqrt{E_H / m}}{\omega_1 \times \delta_{top}} \tag{1.12}$$

$$\zeta' = \frac{\sqrt{E_I / m}}{\omega_1 \times \delta_{top}} \tag{1.13}$$

By the suggestion of two new parameters, it is now possible to determine the maximum displacement of *SDOF* systems and the maximum top displacement of *MDOF* systems using both input energy and hysteretic energy approaches (Mollaioli et al, 2011). In this study, calculating the seismic demands of *MDOF* systems using the input energy will be the focus of interest, Figure 1.4.

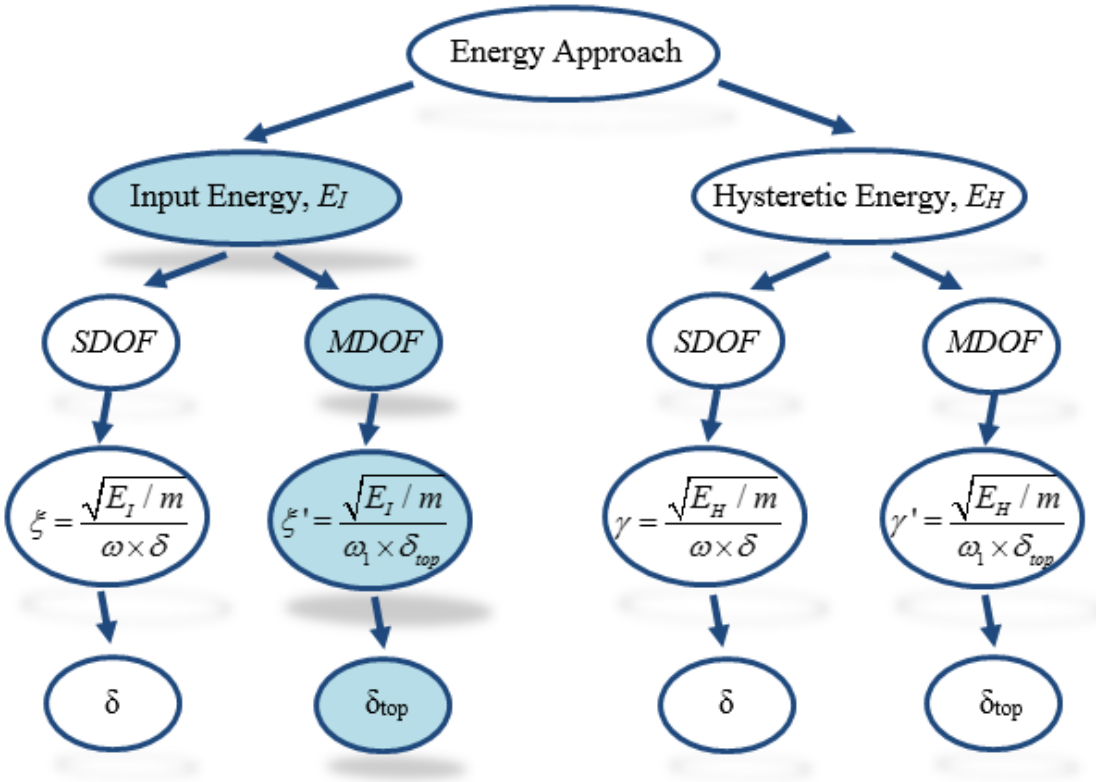

Figure 1.4 : Energy approaches for the determination of δ_{top}.

The change in the parameter ζ′, which was defined in order to associate the energy with the top displacement demand in *MDOF* systems using input energy approach, with respect to period for different types of stiffness patterns is shown in Figure 1.5. Here, the stiffness pattern A represents parabolic stiffness distribution along the height of a stiff foundation structure, the stiffness pattern B represents parabolic stiffness distribution along the height of a flexible foundation structure, and the stiffness pattern U represents uniform stiffness distribution along the height of a stiff foundation structure (Mollaioli et al, 2011). It can be observed that the parameter ζ′ is almost pegged on the value of 0.80 after T = 0.75 s for all three stiffness patterns.

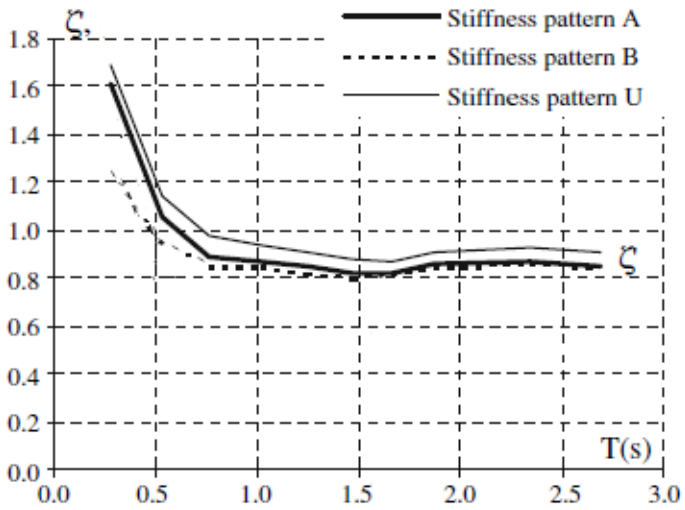

Figure 1.5 : ζ' spectra (Mollaioli et al, 2011).

1.3 Hypothesis

Seismic input energy of a *MDOF* system can be estimated on story levels by means of its modal properties and the energy spectrum obtained for a *SDOF* system. Using the predicted input energy, inelastic top displacement demand of a frame type system can be calculated. Thus, a basis for the energy-based seismic design (*EBSD*) is created with this M.Sc. thesis by proposing a methodology to determine the seismic demands (input energy and inelastic displacement) of moment resisting frame type structures.

2. NUMERICAL MODELS

In order to compute the seismic input energy for each *MDOF* model frame under the effect of different seismic excitations, Perform 3D software was used in the modelling of the frames and performing the nonlinear time history analysis. The program computes input energy with an acceptable numerical accuracy as it provides an energy balance between internal (strain, kinetic, inelastic, and damping) energies and external (input) energy.

2.1 Selected Model Frames

In this study, seismic input energy and inelastic displacement demand estimations were carried out for a set of five model frames which are three-story reinforced concrete frame and three-, six-, nine-, and twenty-story steel frames. The model frames to be used in the application and verification of the methodology have been studied on in the literature before.

2.1.1 Three-story reinforced concrete frame

The three-story and one-bay frame used by Manoukas et al. (2011) was selected as the only *RC* frame to be used in this study, Figure 2.1. The frame has a bay width of 4.0 m and a story height of 4.0 m. The columns are fixed at the base. The columns have a rectangular cross-section of 40×40 with 8Φ16 longitudinal reinforcement. The beams have a rectangular cross-section of 25×40 with 4Φ12 longitudinal reinforcement. Concrete quality of C16/20 is used whereas the reinforcing bars are S400. Seismic mass of the structure is 30 tons in total (each story is 10 tons).

Natural periods, effective masses, and modal participation factors of the three-story *RC* frame (*Manoukas* 3-St) are listed in Table 2.1. Normalized mode shapes to be used in the following chapters are shown in Table 2.2 for the first three modes.

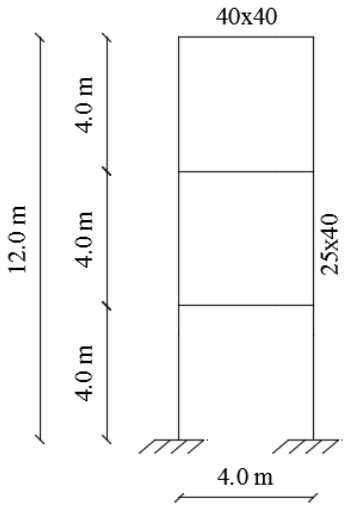

Figure 2.1 : *Manoukas* 3-St frame.

Table 2.1 : The dynamic properties of *Manoukas* 3-St frame.

Mode	Period (s)	Effective Mass (%)	Participation Factor (Γ)
1	0.51	84.20	5.07
2	0.15	12.38	-1.94
3	0.08	3.42	1.02

Table 2.2 : Mode shapes for *Manoukas* 3-St frame.

Story #	1st mode	2nd mode	3rd mode
1	0.073	-0.205	0.226
2	0.177	-0.161	-0.203
3	0.249	0.175	0.078

2.1.2 Three-story steel frame

The three-story and four-bay frame used by Akbas et al. (2001) was selected as the low-rise steel frame to be used in this study, Figure 2.2. The frame has a bay width of 9.15 m and a story height of 4.27 m for the first story and 3.51 m for the rest. The columns are fixed at the base. W360×122 and W360×262 sections are used as column elements whereas W460×52 and W610×101 sections are used as beam elements. A36 steel is used in both columns and beams. Seismic mass of the structure is 515 kNs^2/m in total.

Natural periods, effective masses, and modal participation factors of the three-story steel frame (*Akbas* 3-St) are listed in Table 2.3. Normalized mode shapes to be used in the following chapters are shown in Table 2.4 for the first three modes.

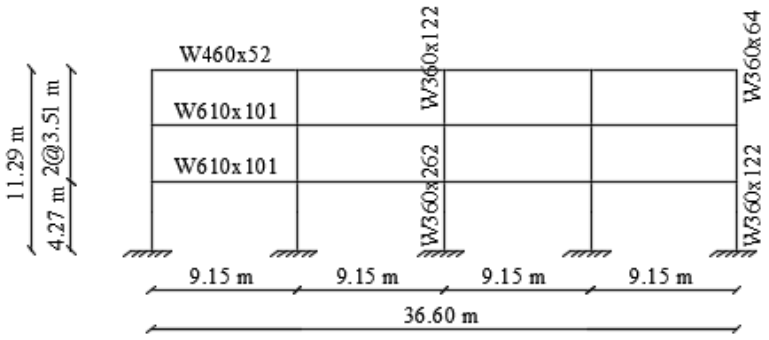

Figure 2.2 : *Akbas* 3-St frame.

Table 2.3 : The dynamic properties of *Akbas* 3-St frame.

Mode	Period (s)	Effective Mass (%)	Participation Factor (Γ)
1	0.80	86.23	21.07
2	0.30	10.78	7.45
3	0.14	2.99	3.92

Table 2.4 : Mode shapes for *Akbas* 3-St frame.

Story #	1st mode	2nd mode	3rd mode
1	0.022	0.042	0.056
2	0.043	0.038	-0.046
3	0.064	-0.053	0.015

2.1.3 Six-story steel frame

The six-story and four-bay frame used by Akbas et al. (2001) was selected as one of the mid-rise steel frames to be used in this study, Figure 2.3. The frame has a bay width of 9.15 m and a story height of 4.27 m for the first story and 3.51 m for the rest. The columns are fixed at the base. W360×147, W360×179, and W360×314 sections are used as column elements whereas W610×82 and W610×101 sections are used as beam elements. A36 steel is used in both columns and beams. Seismic mass of the structure is 1076 kNs^2/m in total.

Natural periods, effective masses, and modal participation factors of the six-story steel frame (*Akbas* 6-St) are listed in Table 2.5. Normalized mode shapes to be used in the following chapters are shown in Table 2.6 for the first three modes.

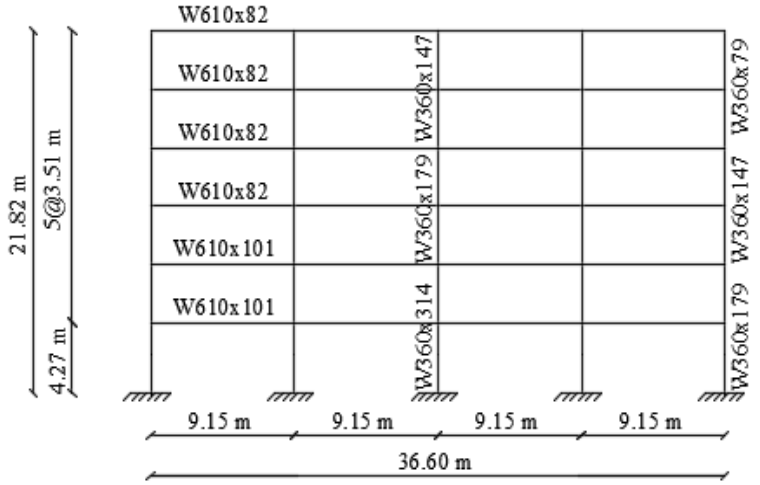

Figure 2.3 : *Akbas* 6-St frame.

Table 2.5 : The dynamic properties of *Akbas* 6-St frame.

Mode	Period (s)	Effective Mass (%)	Participation Factor (Γ)
1	1.58	81.00	29.53
2	0.53	12.07	-11.40
3	0.30	4.03	-6.59

Table 2.6 : Mode shapes for *Akbas* 6-St frame.

Story #	1st mode	2nd mode	3rd mode
1	0.007	-0.021	-0.031
2	0.016	-0.038	-0.034
3	0.025	-0.037	0.006
4	0.034	-0.016	0.041
5	0.041	0.019	0.014
6	0.045	0.044	-0.041

2.1.4 Nine-story steel frame

The nine-story and five-bay frame used by Gupta and Krawinkler (1999) was selected as one of the mid-rise steel frames to be used in this study, Figure 2.4. The frame has a bay width of 9.15 m and a story height of 5.49 m for the first story and 3.96 m for the rest. It also has a basement story with a height of 3.65 m. The columns are pinned at the base. A36 steel is used in beams and A572 Gr. 50 steel is used in columns. Seismic mass of the structure is 4500 kNs^2/m in total.

Natural periods, effective masses, and modal participation factors of the nine-story steel frame (*SAC-LA* 9-St) are listed in Table 2.7. Normalized mode shapes to be used in the following chapters are shown in Table 2.8 for the first three modes.

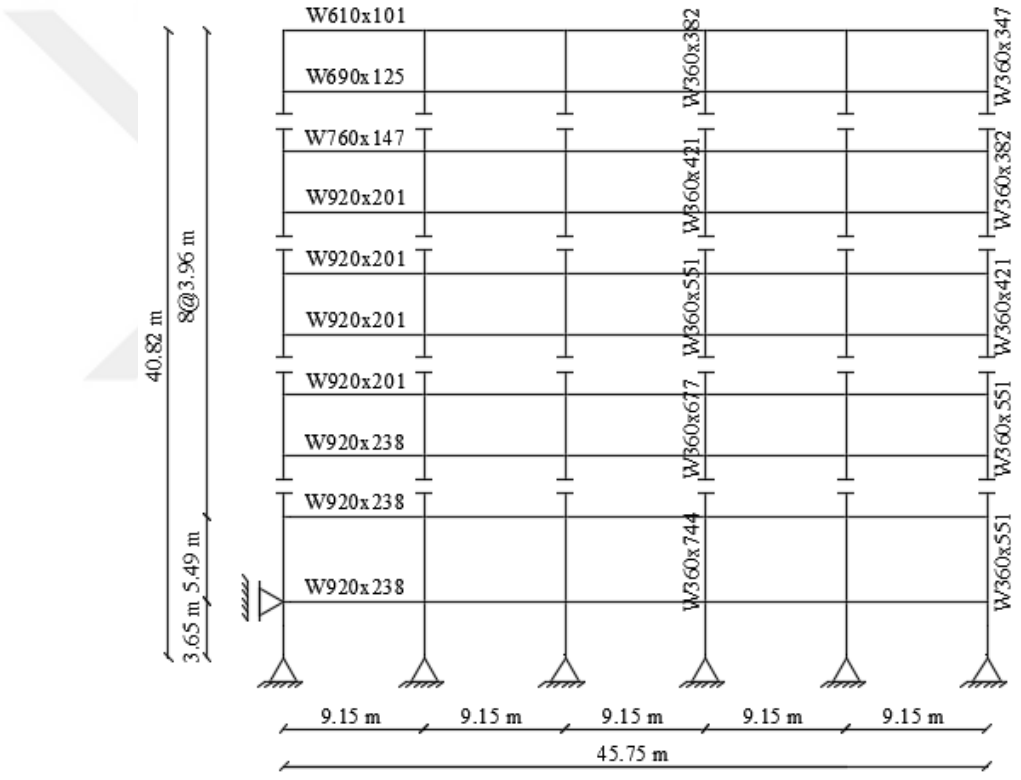

Figure 2.4 : *SAC-LA* 9-St frame.

Table 2.7 : The dynamic properties of *SAC-LA* 9-St frame.

Mode	Period (s)	Effective Mass (%)	Participation Factor (Γ)
1	2.27	83.10	61.24
2	0.85	10.90	22.14
3	0.49	3.70	12.95

Table 2.8 : Mode shapes for *SAC-LA* 9-St frame.

Story #	1st mode	2nd mode	3rd mode
1	0.004	0.009	0.015
2	0.006	0.014	0.019
3	0.009	0.017	0.016
4	0.011	0.018	0.005
5	0.014	0.015	-0.009
6	0.016	0.010	-0.019
7	0.018	0.000	-0.018
8	0.021	-0.013	-0.003
9	0.022	-0.024	0.019

2.1.5 Twenty-story steel frame

The twenty-story and five-bay frame used by Gupta and Krawinkler (1999) was selected as the high-rise steel frame to be used in this study, Figure 2.5. The frame has a bay width of 6.10 m and a story height of 5.49 m for the first story and 3.96 m for the rest. It also has two basement stories with a height of 3.65 m. The columns are pinned at the base. A36 steel is used in beams and A572 Gr. 50 steel is used in columns. Seismic mass of the structure is 5526 kNs^2/m in total.

Natural periods, effective masses, and modal participation factors of the twenty-story steel frame (*SAC-LA* 20-St) are listed in Table 2.9. Normalized mode shapes to be used in the following chapters are shown in Table 2.10 for the first three modes.

Table 2.9 : The dynamic properties of *SAC-LA* 20-St frame.

Mode	Period (s)	Effective Mass (%)	Participation Factor (Γ)
1	3.82	80.00	66.53
2	1.32	11.80	25.50
3	0.77	3.50	13.89
4	0.54	1.80	9.86
5	0.41	1.00	-7.38

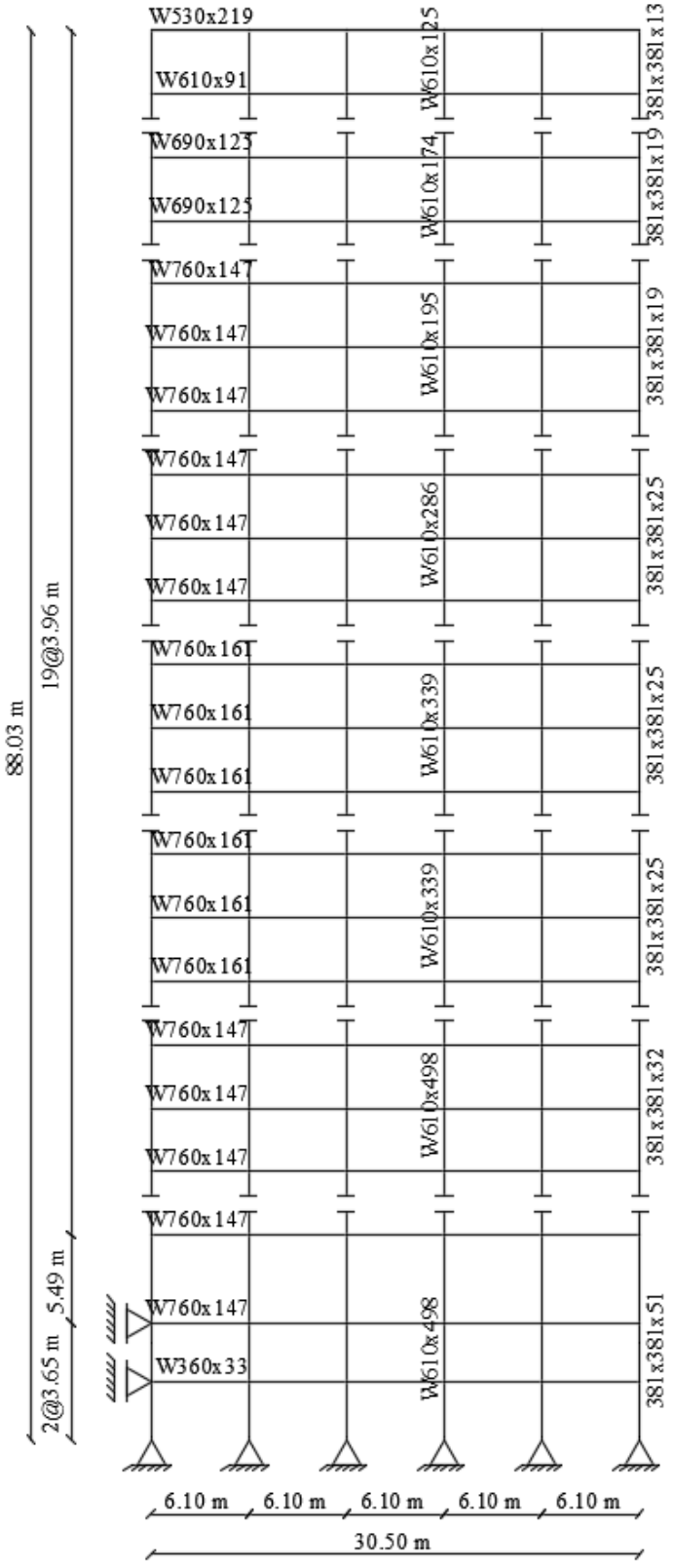

Figure 2.5 : *SAC-LA* 20-St frame.

Table 2.10 : Mode shapes for *SAC-LA* 20-St frame.

Story #	1st mode	2nd mode	3rd mode
1	0.001	0.004	0.007
2	0.003	0.008	0.012
3	0.004	0.011	0.015
4	0.005	0.013	0.017
5	0.006	0.015	0.017
6	0.007	0.017	0.015
7	0.009	0.018	0.011
8	0.010	0.017	0.006
9	0.011	0.017	0.001
10	0.012	0.015	-0.005
11	0.013	0.013	-0.011
12	0.014	0.010	-0.015
13	0.015	0.007	-0.018
14	0.016	0.003	-0.018
15	0.017	-0.002	-0.016
16	0.018	-0.006	-0.011
17	0.019	-0.010	-0.004
18	0.019	-0.015	0.005
19	0.020	-0.019	0.015
20	0.021	-0.023	0.024

2.2 Modelling Strategy

After the set of five model frames were drawn in Perform 3D software, movement of the frame was restricted in H2 direction by assigning supports at every joint in order to perform the analysis in plane frame. Self and additional masses were concentrated on the joints, Figure 2.6.

For all the systems, a damping ratio of 5% was considered in the analyses.

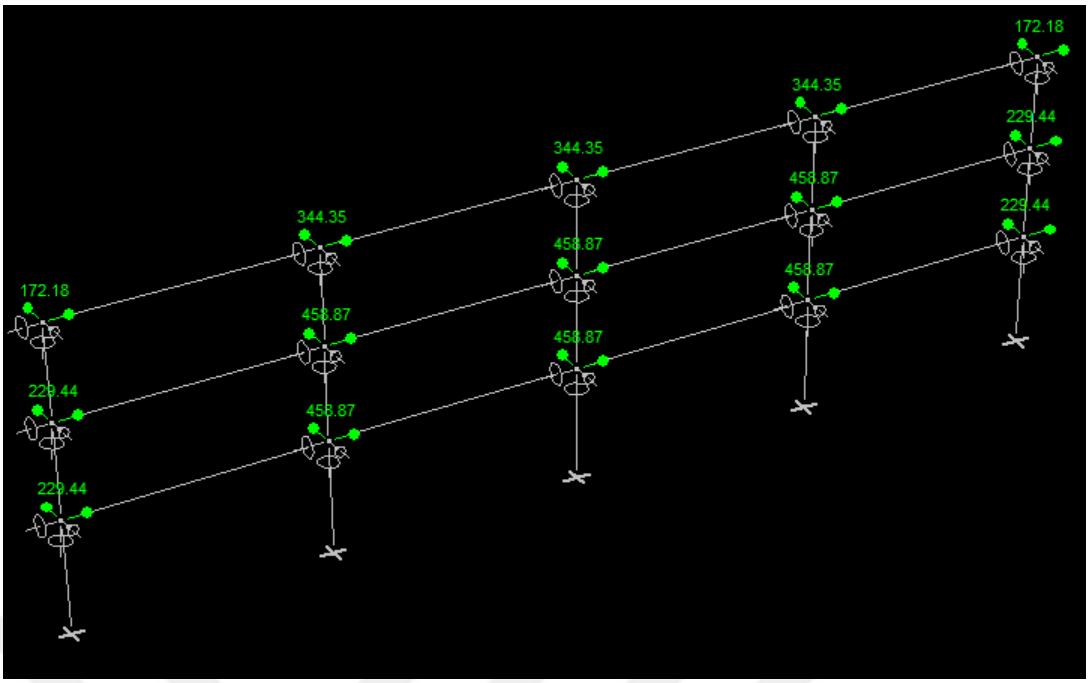

Figure 2.6 : Perform 3D model for *Akbas* 3-St frame.

Using the plastic hinge theory, nonlinear behavior of the frame elements was taken into account. While middle section of the members was considered to behave elastic under the excitation, the curvature type plastic hinges were assigned at the end sections. For the beam type frame elements, curvature type moment hinges were defined whereas for the column type frame elements, curvature type P-M2-M3 hinges were defined at the end zones of the frame elements. Material models of the middle section were represented by linear force-displacement relation, Figure 2.7 (a). Material models of the end sections were represented by elastic-perfectly plastic (e-p-p) force-displacement relation with no cyclic degradation, Figure 2.7 (b).

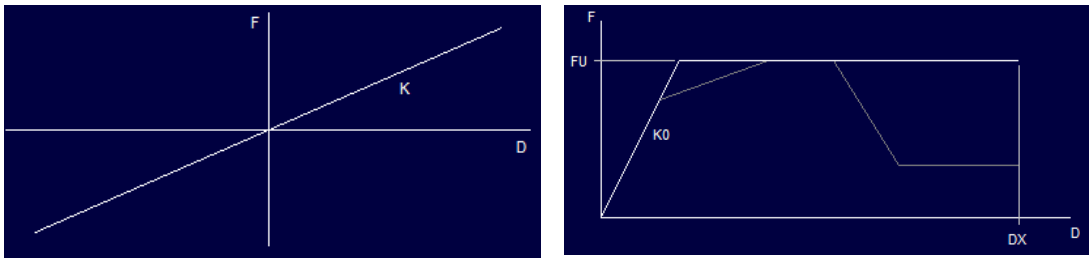

(a) **(b)**

Figure 2.7 : Basic F-D relationship: (a) Middle section. (b) End sections.

For P-M2-M3 type plastic hinges assigned to the column elements, yield surface parameters were defined. P exponent (alpha) was taken as 2.0 for P-M2 and P-M3 interactions in both compression and tension regions. M exponent (beta) was taken as

1.1 for P-M interaction. M exponent (gamma) was taken as 1.4 for M-M interaction, Figure 2.8.

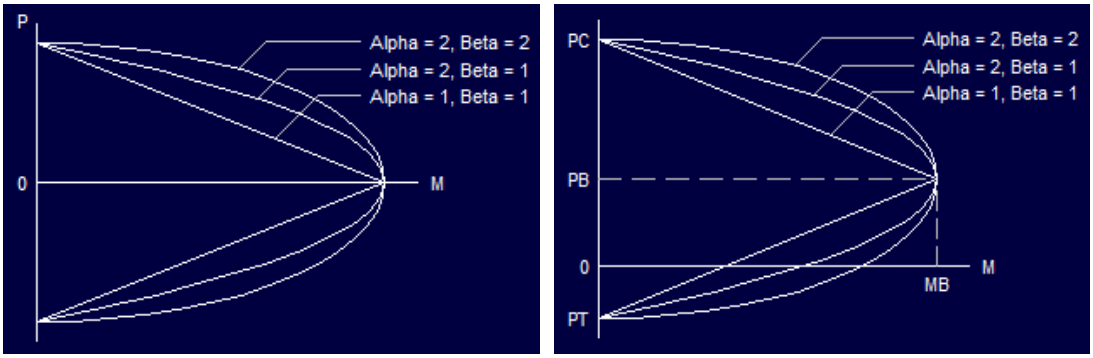

(a) **(b)**

Figure 2.8 : P-M interaction yield surface parameters: (a) Steel sections. (b) *RC* sections.

In order to define the inelastic section properties of the plastic hinges, Xtrack software was used. First, bilinear material properties were defined. For the beam sections, moment-curvature relationship about x-axis was obtained and maximum moment value was defined as "axis 3 bending" in Perform 3D, Figure 2.9. For the column sections, P-M interaction diagram and moment-curvature relationship about both x- and y-axis were obtained. Axial force values for pure tension and pure compression cases were defined as "tension" and "compression", maximum moment value about x-axis was defined as "axis 3 bending" , and maximum moment value about y-axis was defined as "axis 2 bending" in Perform 3D, Figure 2.10.

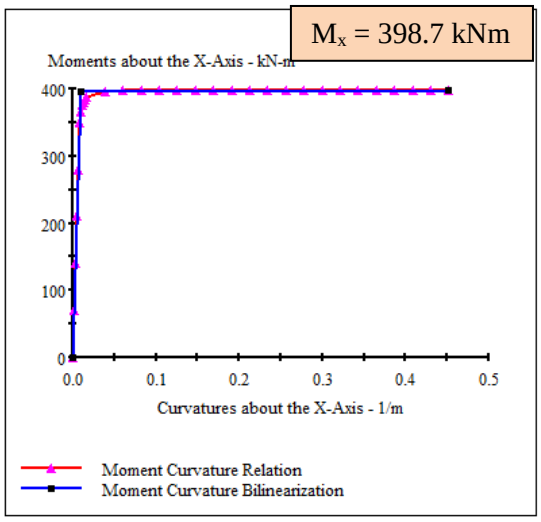

Figure 2.9 : Section properties for a sample beam section (W460×52).

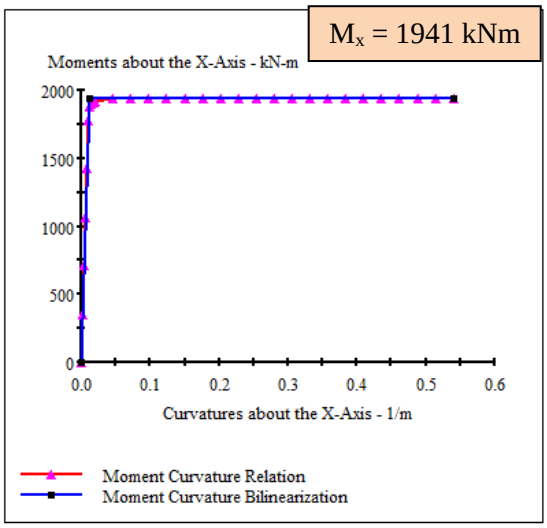

(a) Moment-curvature relationship about x-axis (“axis 3 bending”)

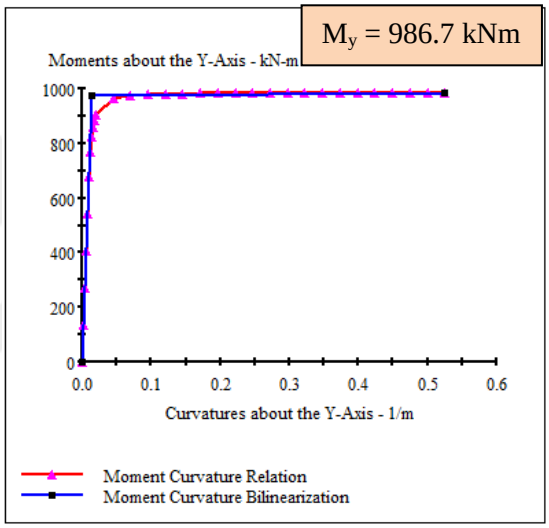

(b) Moment-curvature relationship about y-axis (“axis 2 bending”)

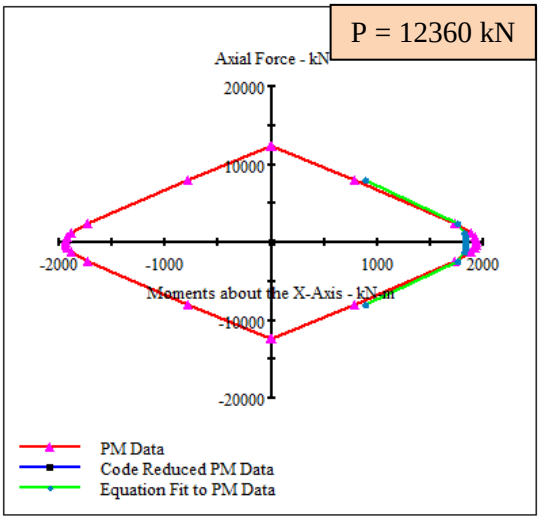

(c) P-M interaction diagram (“tension” and “compression”)

Figure 2.10 : Section properties for a sample column section (W360×262).

After elastic region and plastic hinges were defined for all the structural members, compounds were generated. The length of the plastic hinges was taken as half of the section height, Figure 2.11 (a). For the column sections, P-M2-M3 hinges were defined at both ends, Figure 2.11 (b). For the beam sections, moment hinges were defined at both ends, Figure 2.11 (c).

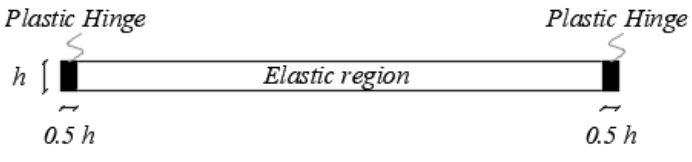

(a)

No.	Component Type	Component Name	Length	Propn
1	P-M2-M3 Hinge, Steel Curvature Type	W360x262	(0.1935	0
2	Column, Steel Type, Nonstandard Section	XecColS-w360x262		1
3	P-M2-M3 Hinge, Steel Curvature Type	W360x262	(0.1935	0

(b)

No.	Component Type	Component Name	Length	Propn
1	Moment Hinge, Curvature Type	W460x52	(0.225)	0
2	Beam, Steel Type, Nonstandard Section	XecBmS-w460x52		1
3	Moment Hinge, Curvature Type	W460x52	(0.225)	0

(c)

Figure 2.11 : Sectional properties used in Perform 3D: (a) Assigning plastic hinges. (b) Example for forming a column section. (c) Example for forming a beam section.

2.3 Selection of the Earthquake Records

In order to determine the yield energy values for the set of four model frames, push-over analyses were performed using the first mode load patterns. After force-displacement capacity curves were obtained, energy-displacement capacity curve for each model frame was calculated and yield energies were obtained (Figure 2.12) where the force-displacement capacity curve is shown with orange and the energy-displacement capacity curve is shown with blue.

Using *PEER NGA* database, a total of 1094 earthquake records were downloaded. Among those, 92 earthquake records which cause a seismic input energy larger than the yield energy were selected. Earthquake records to be used in the nonlinear time history analysis are listed in Table A.1.

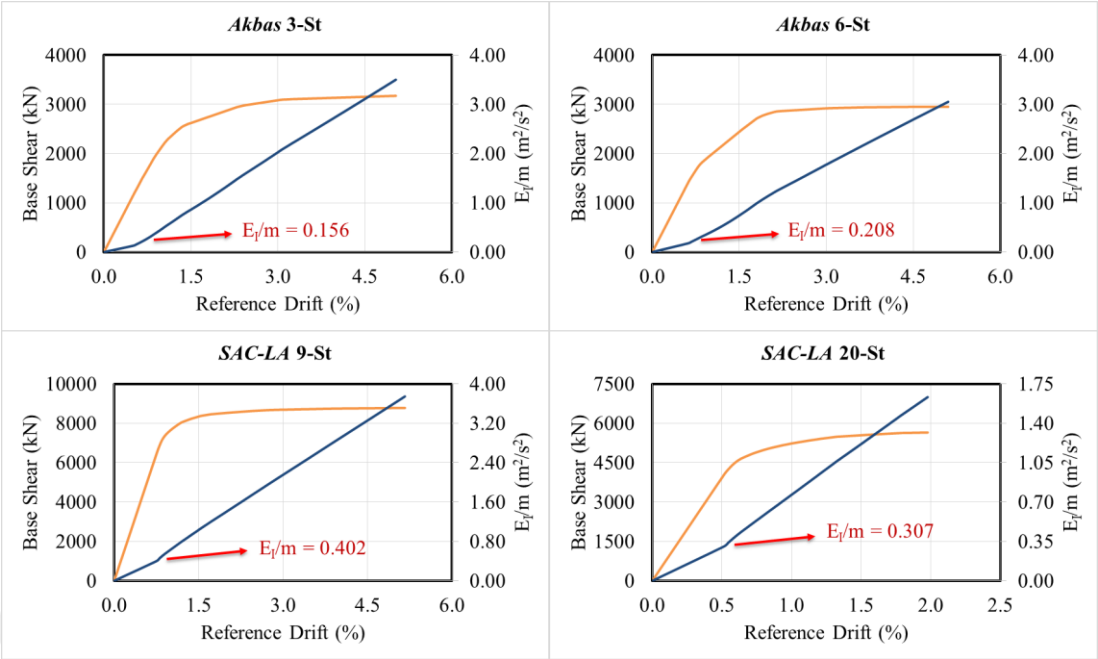

Figure 2.12 : Energy-displacement capacity curves and calculated yield energy values.

Both ordinary type and pulse-like type records were selected and split into groups in terms of V_{s30}, the average shear-wave velocity in the top 30 m of the soil, as shown in Table 2.11. In total, 32 ordinary type and 60 pulse-like type *EQ* records were used in the analyses and no scaling was made.

The pulse-like *EQ* ground motions generally have the characteristics of low frequency and cause higher seismic responses (base shear, story displacements, input energy, etc.) compared to the ordinary non-pulse-like *EQ* ground motions. Near-fault ground motions can often be classified as pulse-like type records whereas far-fault ground motions can often be classified as ordinary type records. Peak ground velocity (*PGV*) can be used as an indicator of the *EQ* type (pulse-like / ordinary non-pulse-like). *PGV* values for the set of 92 *EQ* records are listed in Table 2.12. Here, it can be seen that the ordinary non-pulse-like records (the ones shown with red color) generally have lower *PGV* values compared to the pulse-like records.

Table 2.11 : Classification of the chosen earthquake records.

Group #	Description	EQ #
G1	Ordinary Records with $V_{s30} < 180$	1, 2, 3, 4, 5, 6, 7, 8, 9, 10, 11, 12, 13
G2	Pulse-Like Records with $V_{s30} < 180$	14, 15, 16, 17, 18, 19, 20, 21, 22
G3	Ordinary Records with $180 \leq V_{s30} < 360$	23, 24, 25, 26, 27, 28, 29, 30, 31, 32, 33, 34, 35, 36, 37
G4	Pulse-Like Records with $180 \leq V_{s30} < 360$	38, 39, 40, 41, 42, 43, 44, 45, 46, 47, 48, 49, 50, 51, 52, 53, 54, 55, 56, 57
G5	Pulse-Like Records with $360 \leq V_{s30} < 760$	58, 59, 60, 61, 62, 63, 64, 65, 66, 67, 68, 69, 70, 71, 72, 73, 74, 75, 76, 77
G6	Ordinary Records with $760 \leq V_{s30} < 1500$	78, 79
G7	Pulse-Like Records with $760 \leq V_{s30} < 1500$	80, 81, 82, 83, 84, 85, 86
G8	Ordinary Records with $1500 \leq V_{s30}$	87, 88
G9	Pulse-Like Records with $1500 \leq V_{s30}$	89, 90, 91, 92

Table 2.12 : *PGV* values for the chosen earthquake records.

EQ #	PGV (cm/s)	EQ #	PGV (cm/s)	EQ #	PGV (cm/s)
1	36.21	32	36.07	63	130.38
2	46.31	33	31.03	64	111.48
3	31.67	34	36.03	65	77.78
4	35.10	35	29.16	66	76.16
5	16.03	36	29.95	67	91.72
6	33.21	37	52.09	68	67.40
7	18.60	38	113.15	69	264.11
8	31.95	39	97.45	70	120.97
9	12.88	40	67.02	71	60.43
10	29.33	41	68.54	72	74.85
11	36.53	42	96.92	73	43.98
12	18.27	43	59.20	74	88.98
13	17.77	44	108.81	75	71.96
14	86.57	45	41.75	76	89.15
15	62.18	46	65.01	77	76.49
16	48.26	47	76.14	78	55.54
17	81.40	48	86.34	79	30.41
18	47.98	49	72.96	80	123.59
19	63.97	50	54.05	81	99.05
20	54.24	51	69.86	82	95.86
21	63.81	52	62.72	83	85.84
22	26.63	53	52.06	84	133.61
23	33.02	54	75.82	85	38.28
24	46.76	55	81.31	86	28.25
25	44.95	56	76.09	87	19.13
26	67.69	57	65.94	88	10.43
27	26.33	58	151.21	89	114.50
28	31.36	59	249.60	90	103.60
29	66.31	60	66.43	91	57.43
30	54.50	61	172.34	92	54.81
31	42.81	62	97.36		

3. SEISMIC INPUT ENERGY ESTIMATION

Seismic input energy should first be accurately calculated in order to make an estimation about the inelastic top displacement demand of a structure. After seismic input energy spectrum for a *SDOF* system is obtained, total input energy amount that a *MDOF* system is subjected to during a seismic excitation can be estimated with the suggested method.

3.1 Seismic Input Energy Spectrum

A MATLAB based code was generated in order to obtain seismic input energy spectrum for *SDOF* systems. As the first step, earthquake responses (u, $\dot{u}$, and $\ddot{u}$) were calculated as a function of time using the "Piecewise Exact Method" for a series of oscillators constructed with the same mass but different rigidities, thus different natural vibration periods (Figure 3.1). Then, calculated velocity response ($\dot{u}$) was multiplied with the ground acceleration and integrated over the total duration of the excitation, equation (1.9). Finally, seismic input energy spectrum for a *SDOF* system was constructed plotting absolute maximum values of the time series for each oscillator with respect to natural vibration periods (Figure 3.2). The mass-normalized input energy spectra for all 92 *EQ* records are shown in Figure A.1.

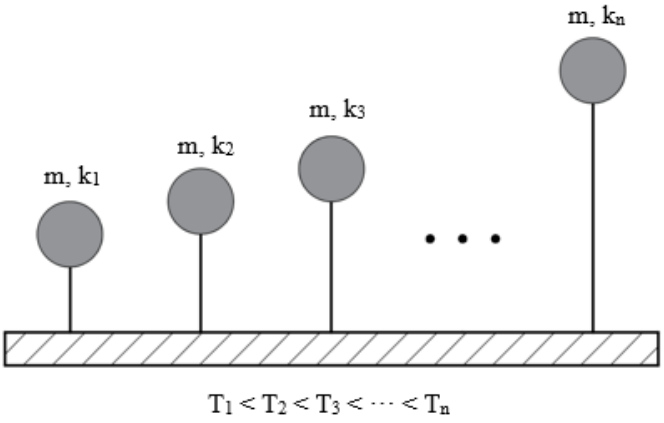

Figure 3.1 : Oscillators with different natural vibration periods.

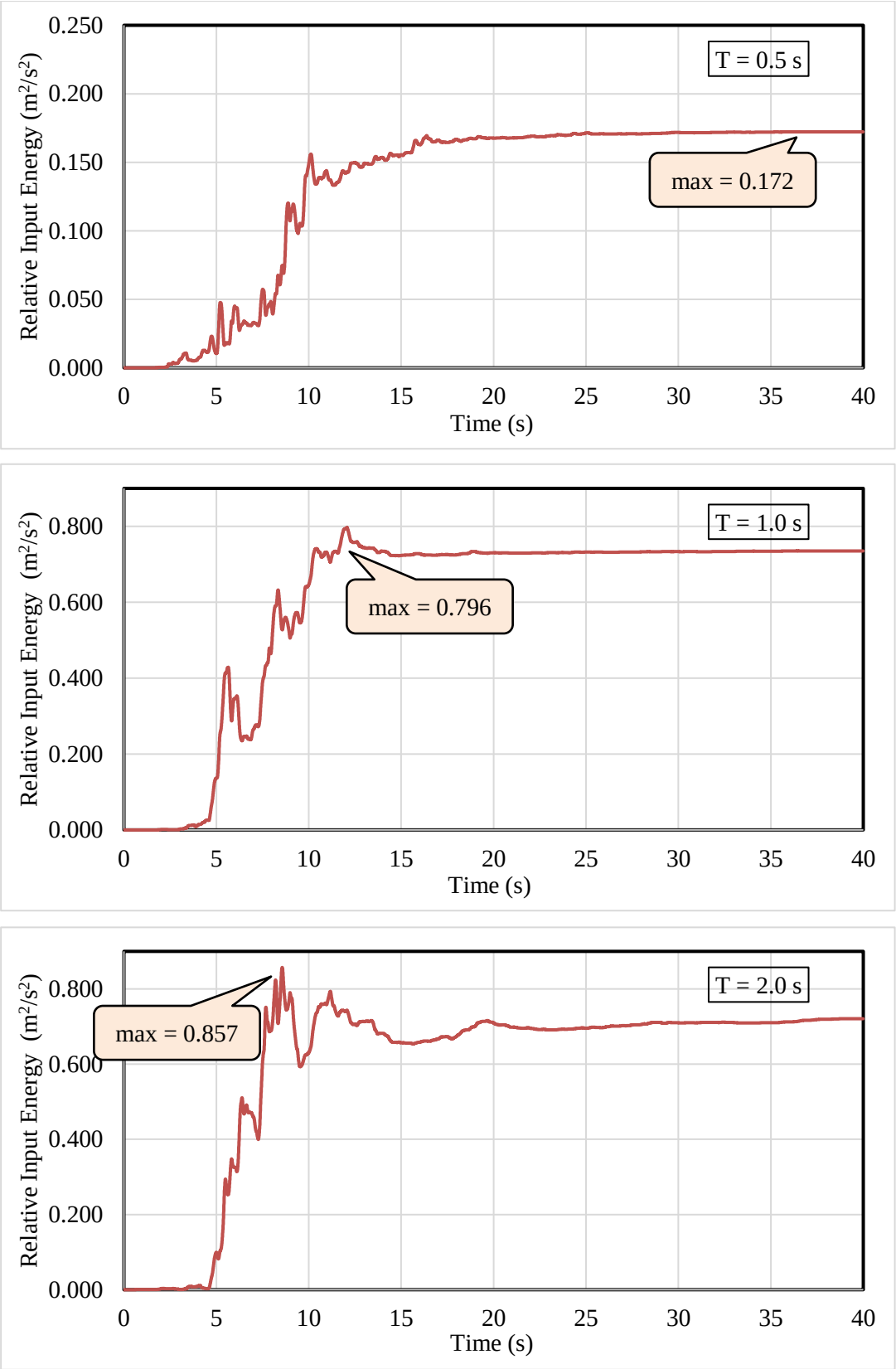

Figure 3.2 : Obtaining input energy spectrum for a sample *EQ* record.

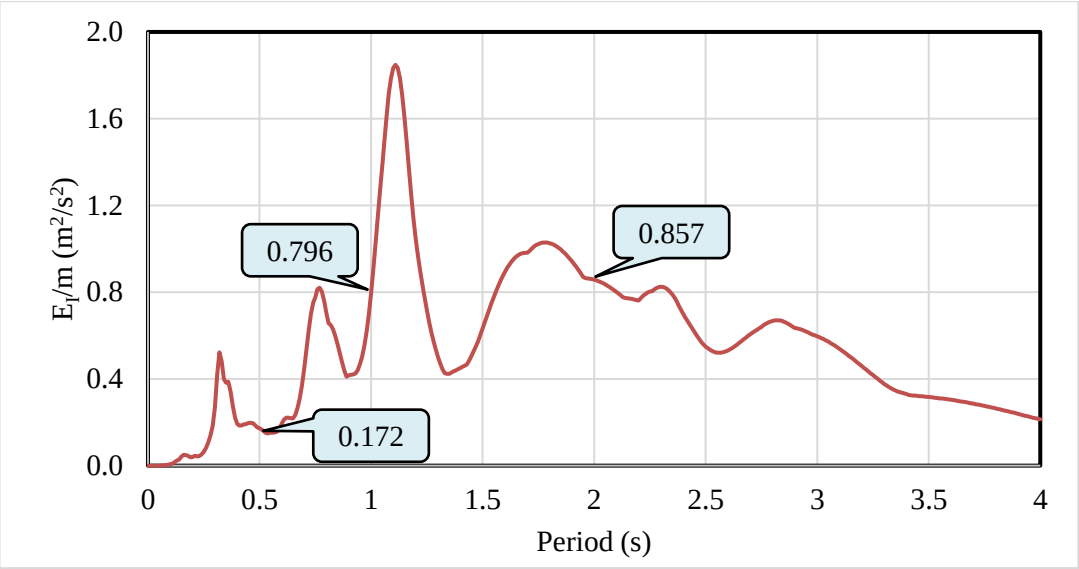

Figure 3.2 (continued) : Obtaining input energy spectrum for a sample *EQ* record.

3.2 Suggested Method to Estimate the Seismic Input Energy for *MDOF* Systems

The method requires the usage of dynamic properties of the structures, as shown in Table 2.1 and 2.2 for the selected set of model frames. The number of modes to be used in the analysis is taken as the mode number making the cumulative summation of the effective masses greater than 95% of the total mass. For three-story *Manoukas* frame and three-story *Akbas* frame, two modes with a cumulative summation of the effective masses of 96.58% and 97.01%, respectively were used in the analysis. For six-story *Akbas* frame, nine- and twenty-story *SAC-LA* frames, three modes with a cumulative summation of the effective masses of 97.10%, 97.70%, and 95.16%, respectively were considered in the application of the methodology.

Using the proposed method, seismic input energy per unit mass for a *MDOF* system can be estimated by equation (3.1), where N is the number of modes used in the analysis, n is the number of degrees of freedom, Φ_{ij} is the i^{th} story mode shape for the j^{th} mode, Γ_j is the modal participation factor, and $(E_I/m)_j$ is the mass-normalized input energies corresponding to each period in the input energy spectrum, Figure 3.3.

$$(E_I/m) = \frac{\sum_{j=1}^{N}\sum_{i=1}^{n}\phi_{ij}\cdot(E_I/m)_j\cdot\Gamma_j}{\sum_{j=1}^{N}\sum_{i=1}^{n}\phi_{ij}\cdot\Gamma_j} \qquad (3.1)$$

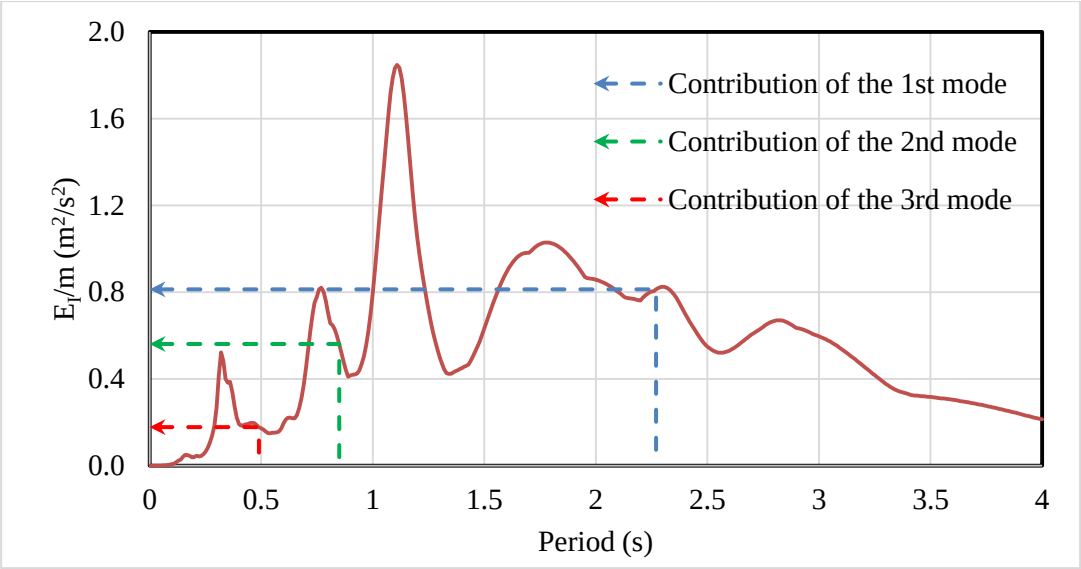

Figure 3.3 : Mass-normalized input energies corresponding to each mode.

Mass-normalized input energy predictions ($(E_I / m)_{pre}$) were made using the suggested method in this study, equation (3.1). After that, they were compared with the numerical results obtained after running nonlinear time history analysis for a total of 92 earthquake records in five model structures in Perform 3D software ($(E_I / m)_{num}$). The relative percentage differences between the predictions and numerical results (ε_{EI}) were calculated using equation (3.2).

$$\varepsilon_{EI} = \frac{\left|(E_I / m)_{pre} - (E_I / m)_{num}\right|}{\left[(E_I / m)_{pre} + (E_I / m)_{num}\right] / 2} \qquad (3.2)$$

3.3 Discussion on the Results

Numerical and predicted E_I/m and the relative percentage differences between them (ε) are listed in Tables B.1 and B.2 and also visualized in Figures B.1, B.2, B.3, B.4 and B.5 for the set of five model frames. In order to comment on the results, arithmetic means of ε were calculated. Arithmetic mean was calculated by summing up ε values and dividing by n, where n is the number of ε values used.

It can be observed from these results that the methodology proposed in this study gives better output for ordinary type (with far-fault characteristics and lower *PGV*) earthquake records in terms of predicting the input energy for *MDOF* systems.

Using the suggested method in this study, for the set of 92 earthquake records on *Manoukas* 3-St *RC* frame, arithmetic mean of ε_{EI} was calculated as 38.6%. The correlation coefficient was calculated as 0.739, indicating a strong correlation, Figure 3.4.

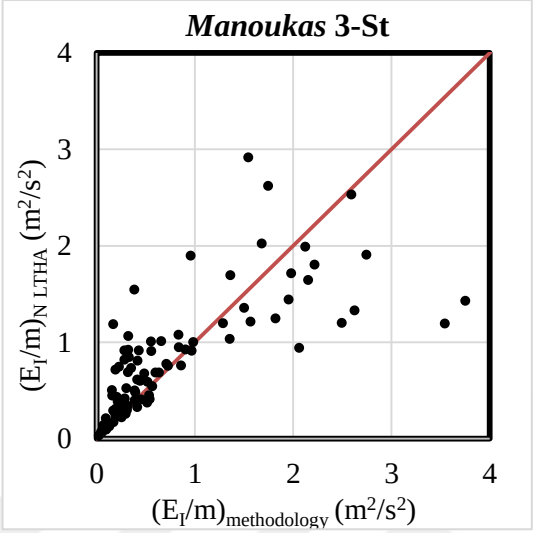

Figure 3.4 : Correlation between the estimated and numerical E_I/m for the set of 92 *EQ* records on *RC* frame.

For 35 *EQ* records with a $PGV \leq 50$ cm/s on *Manoukas* 3-St, arithmetic mean of ε_{EI} was calculated as 18.7%. The correlation coefficient was calculated as 0.961, indicating a very strong correlation, Figure 3.5.

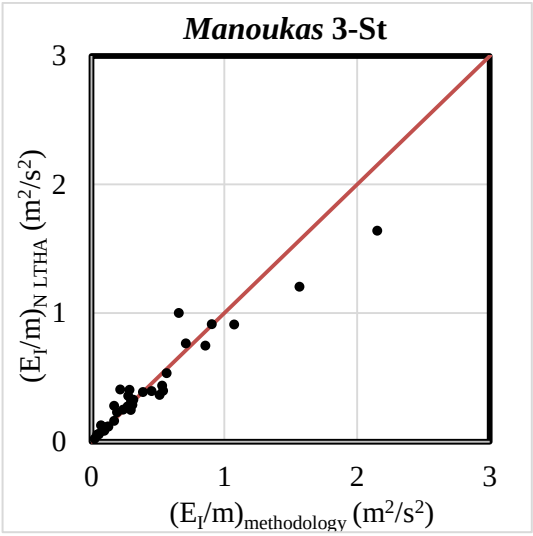

Figure 3.5 : Correlation between the estimated and numerical E_I/m for the *EQ* records with a $PGV \leq 50$ cm/s on *RC* frame.

Using the suggested method in this study, for the set of 92 earthquake records on *Akbas* 3-St, *Akbas* 6-St, *SAC-LA* 9-St, and *SAC-LA* 20-St steel frames, arithmetic means of ε_{EI} were calculated as 11.3%, 13.6%, 11.7%, and 13.9%, respectively.

The correlation coefficients for the steel frames examined in this study were calculated as 0.974, 0.932, 0.959, and 0.914, respectively. These results represent that there is a very strong correlation between the estimated and numerical input energies, Figure 3.6.

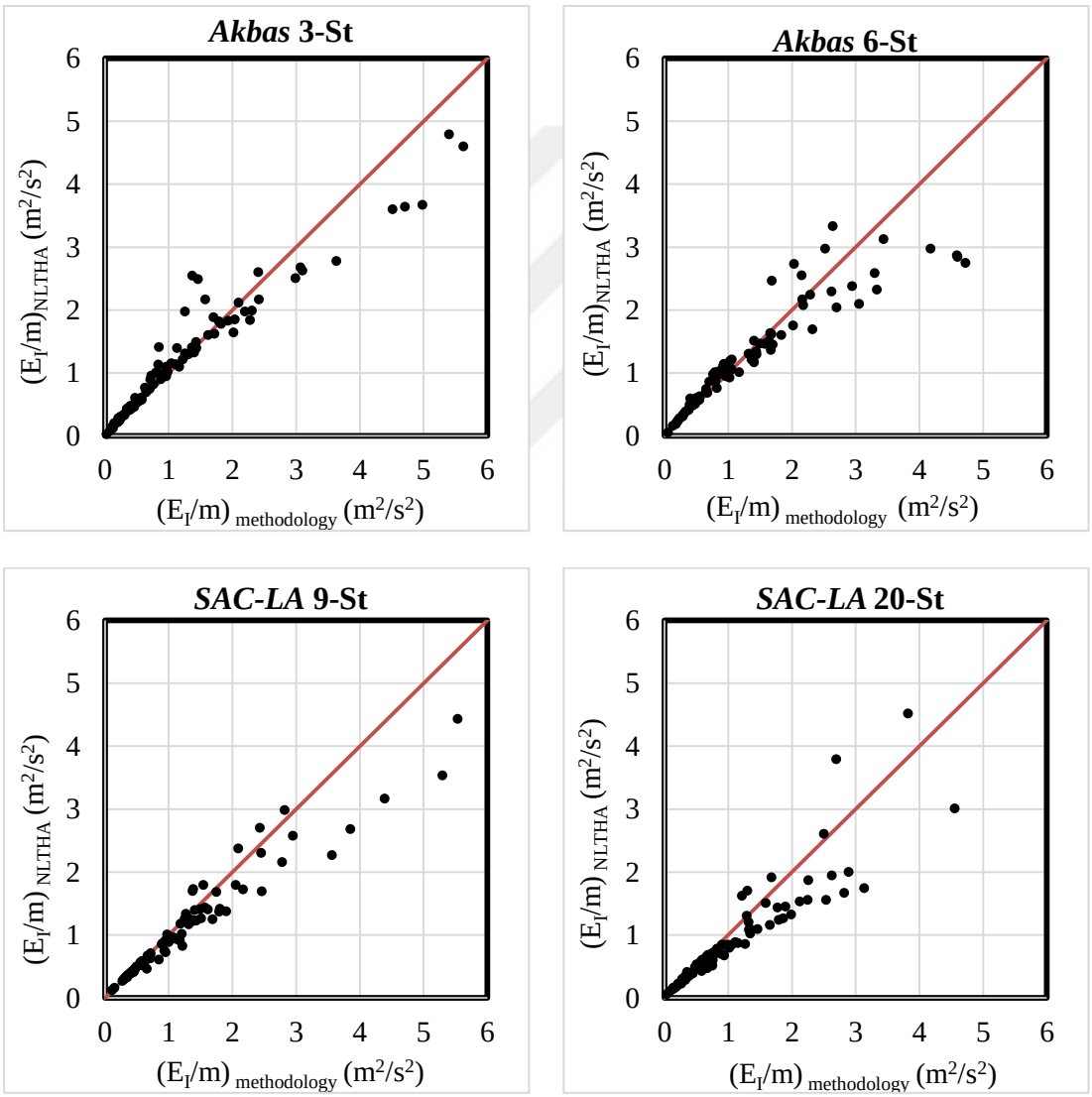

Figure 3.6 : Correlation between the estimated and numerical E_I/m for the set of 92 *EQ* records on steel frames.

Using the suggested method in this study, for 35 *EQ* records with a $PGV \leq 50$ cm/s on *Akbas* 3-St, *Akbas* 6-St, *SAC-LA* 9-St, and *SAC-LA* 20-St steel frames, arithmetic means of ε_{EI} were calculated as 5.8%, 7.7%, 6.0%, and 9.3%, respectively.

The correlation coefficients for the steel frames examined in this study were calculated as 0.994, 0.986, 0.990, and 0.948, respectively. These results represent that there is a very strong correlation between the estimated and numerical input energies, Figure 3.7.

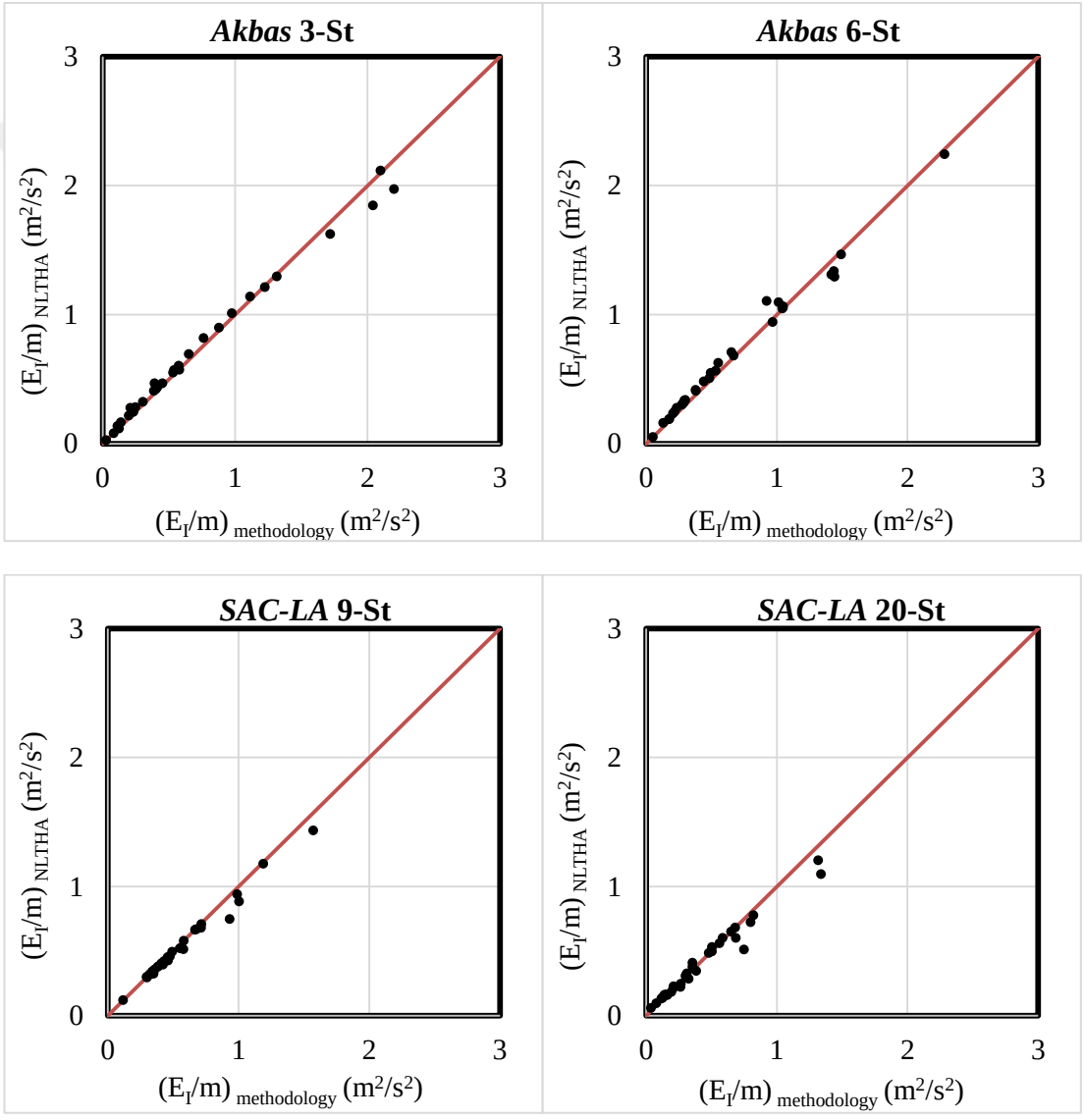

Figure 3.7 : Correlation between the estimated and numerical E_I/m for the *EQ* records with a $PGV \leq 50$ cm/s on steel frames.

Distribution of the relative percentage differences between mass-normalized input energies calculated with the suggested method and "true" mass-normalized input energies obtained using Perform 3D with respect to 35 *EQ* records with a $PGV \leq 50$ cm/s are shown in Figure 3.8.

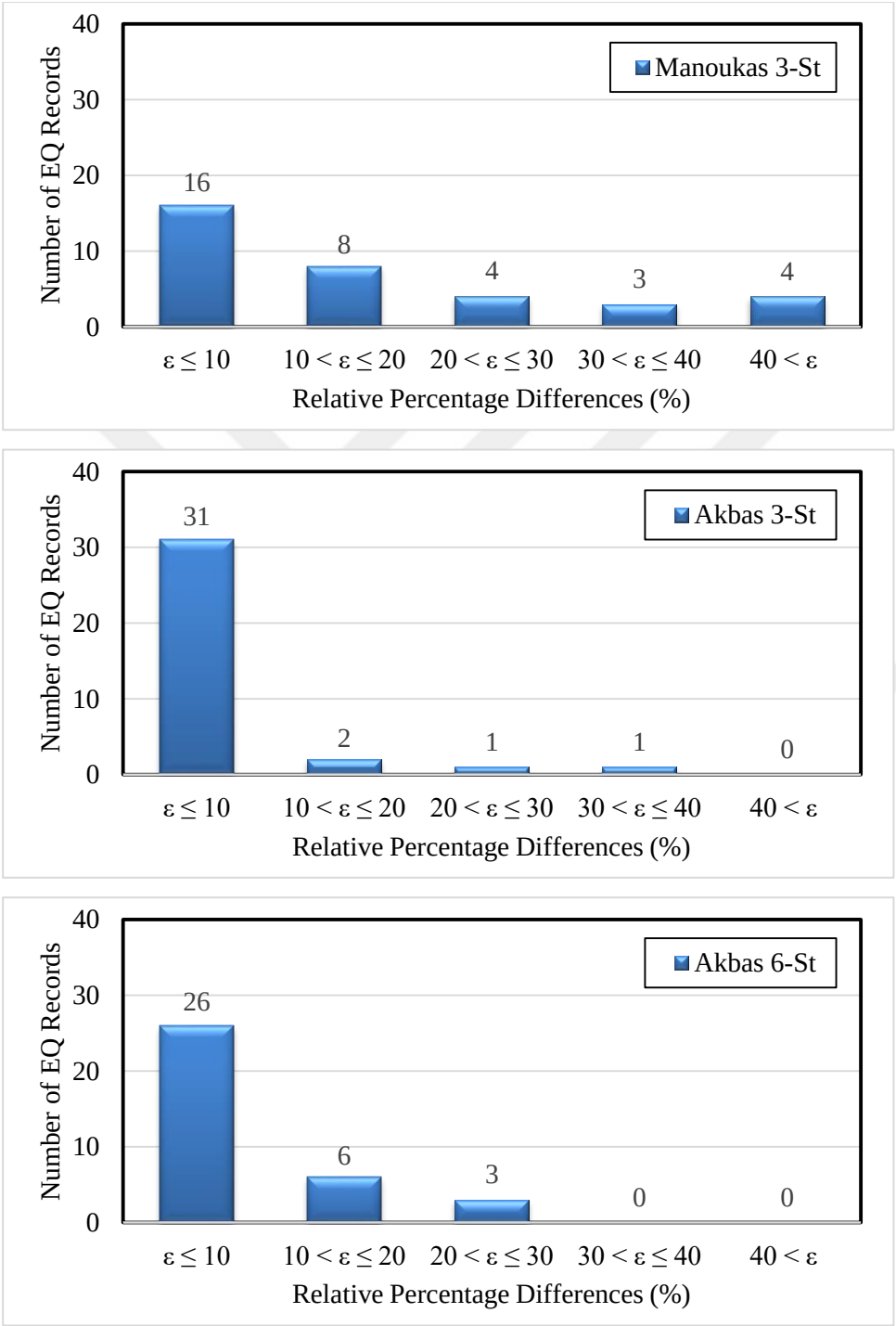

Figure 3.8 : Relative percentage difference distribution for E_I/m estimation.

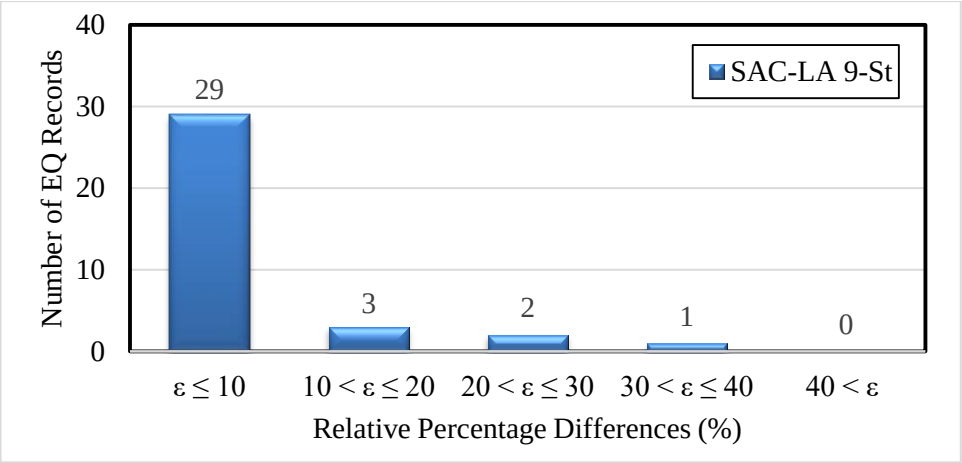

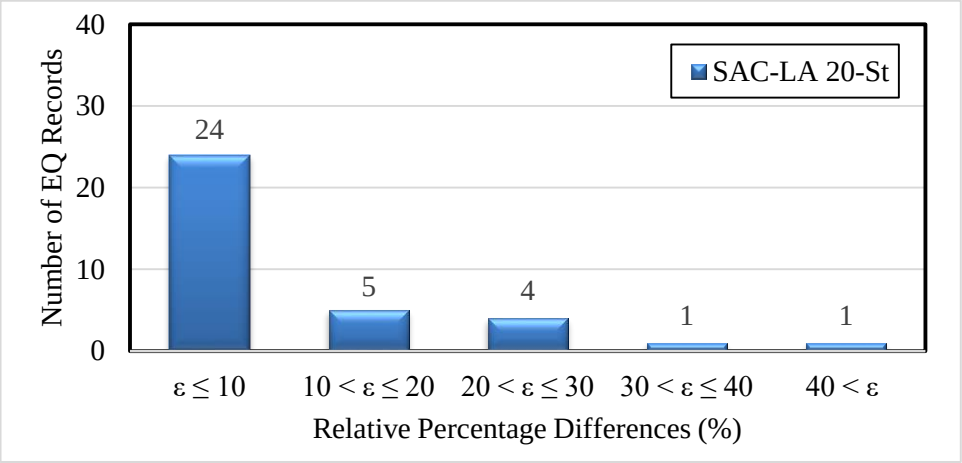

Figure 3.8 (continued) : Relative percentage difference distribution for E_I/m estimation.

3.4 Comparison with Other Methods in the Literature

3.4.1 Method proposed by Kalkan and Kunnath (2007)

For the estimation of the input energy for *MDOF* systems, Kalkan and Kunnath (2007) suggested a formula where input energies calculated for *E-SDOF* systems (Figure 3.9) are combined using the modal participation factor (Γ). In general, it can be estimated using up to the first three modes, equation (3.3).

In case the mode vectors are not normalized ($M_i^* \neq 1$), equation (3.3) becomes identical with equation (3.4) (Ucar, 2020).

$$E_{I(MDOF)} = \sum_{i=1}^{n} E_{I(E-SDOF)_i} \cdot \Gamma_i^2 \tag{3.3}$$

$$E_{I(MDOF)} = \sum_{i=1}^{n} E_{I(E-SDOF)_i} \cdot M_i^* \tag{3.4}$$

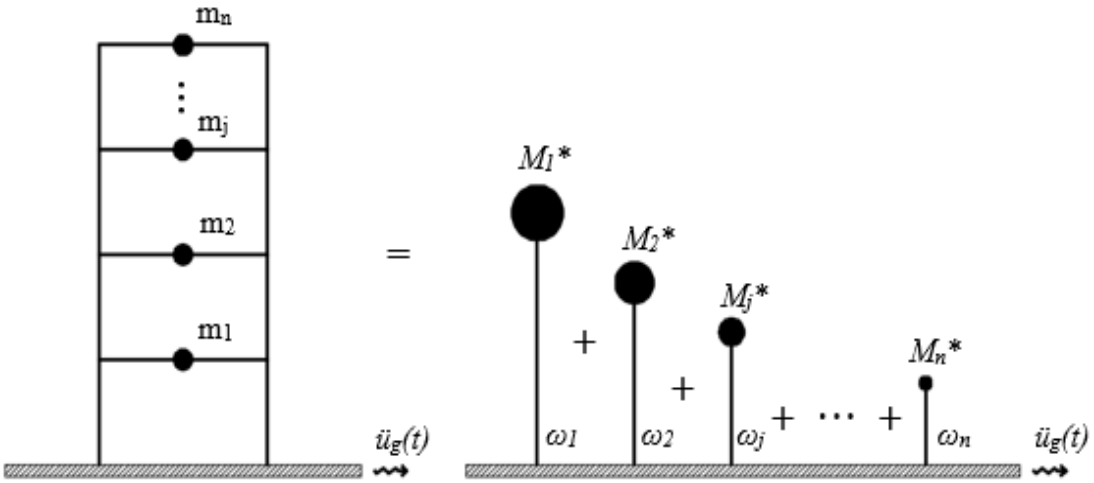

Figure 3.9 : "*n*" number of *E-SDOF* systems of a *MDOF* system.

Here, the time histories of input energy for *E-SDOF* systems are calculated using equation (1.9).

Using the method proposed by Kalkan and Kunnath (2007), for the set of 92 earthquake records on *Manoukas* 3-St, *Akbas* 3-St, *Akbas* 6-St, *SAC-LA* 9-St, and *SAC-LA* 20-St frames, arithmetic means of ε_{EI} were calculated as 39.2%, 11.7%, 12.8%, 13.2%, and 21.1%, respectively.

3.4.2 Method proposed by Güllü (2018)

Instead of using *E-SDOF* systems, Güllü (2018) proposed a method to estimate the seismic input energy for a *MDOF* system using the spectrum constructed for a *SDOF* system by equation (1.9). In this method, mass-normalized input energies (E_I / m) corresponding to an adequate number of vibrational modes of the structure are multiplied with the modal participation factors (Γ_j), equation (3.5).

$$(E_I / m)_{MDOF} = \frac{\sum_{j=1}^{N} (E_I / m)_j \cdot \Gamma_j}{\sum_{j=1}^{N} \Gamma_j} \tag{3.5}$$

Using the method proposed by Güllü (2018), for the set of 92 earthquake records on *Manoukas* 3-St, *Akbas* 3-St, *Akbas* 6-St, *SAC-LA* 9-St, and *SAC-LA* 20-St frames,

arithmetic means of ε_{EI} were calculated as 55.1%, 19.7%, 20.1%, 20.8%, and 32.7%, respectively.

It shows that the proposed method in this study gives better results than the ones Kalkan and Kunnath (2007) and Güllü (2018) suggested in terms of making a prediction about the total input energy in *MDOF* systems, especially for the frames with high number of stories, Table 3.1.

Table 3.1 : Comparison for arithmetic means of ε_{EI} (%).

Methodology	*Manoukas* 3-St	*Akbas* 3-St	*Akbas* 6-St	*SAC-LA* 9-St	*SAC-LA* 20-St
Kalkan and Kunnath (2007)	39.2	11.7	**12.8**	13.2	21.1
Güllü (2018)	55.1	19.7	20.1	20.8	32.7
This study	**38.6**	**11.3**	13.6	**11.7**	**13.9**

4. SEISMIC INPUT ENERGY DISTRIBUTION AMONG STORIES

Since the damage potential of an earthquake is directly dependent on the maximum dissipated hysteretic energy demand, estimation of it for a *MDOF* system is a crucial work for *EBSD*. In the literature, calculation of the dissipated hysteretic energy (E_H) and the distribution of it among stories have been the main focus of interest (Decanini et al. 2001, Chou and Uang 2003, Wang and Yi 2012, Mezgebo and Lui 2017, etc.). Structural properties (mass, modal shape, etc.) were generally used in order to distribute E_H among stories. Thus, a single E_H distribution pattern for each *MDOF* system (independent of the earthquake records) was obtained using these proposed methods.

4.1 Suggested Method to Estimate the Input Energy Distribution Pattern

This study follows a different approach and focuses on the prediction of E_I distribution pattern unlike the current methodologies in the literature focusing on the prediction of E_H distribution pattern. The formulation suggested in the previous chapter to predict the total input energy demand for a *MDOF* system (equation (3.1)) is modified here in order to predict the input energy demand in each story level, equation (4.1). Since there exists an earthquake-dependent term of $(E_I/m)_j$ in this equation (mass-normalized input energy values corresponding to each mode on the input energy spectra), it results in an E_I distribution pattern specific to each earthquake record. When E_H / E_I ratio is known, E_H distribution pattern can also be predicted with a high accuracy in the further studies.

$$(E_I)_i = \frac{\sum_{j=1}^{N} \phi_{ij} \cdot (E_I/m)_j \cdot \Gamma_j}{\sum_{j=1}^{N} \sum_{i=1}^{n} \phi_{ij} \cdot \Gamma_j} \cdot m_{total} \tag{4.1}$$

4.2 Numerical Calculation of the Seismic Input Energy Distribution

Since the distribution of the seismic input energy among the stories cannot be taken from Perform 3D software directly, it was calculated via a MATLAB-based code.

First, the time series of velocity responses ($\dot{u}$) at each story level with respect to the reference point (ground level) were taken from Perform 3D after nonlinear time history analyses were performed for each earthquake record in five model frames, Figure 4.1.

After velocity responses are calculated at each story level, input energy distribution among stories can be calculated using either equation (4.2) or equation (4.3). Since the mass matrix (*[M]*) of the frame type structures with lateral degrees of freedom only is a diagonal matrix, they both give the same result.

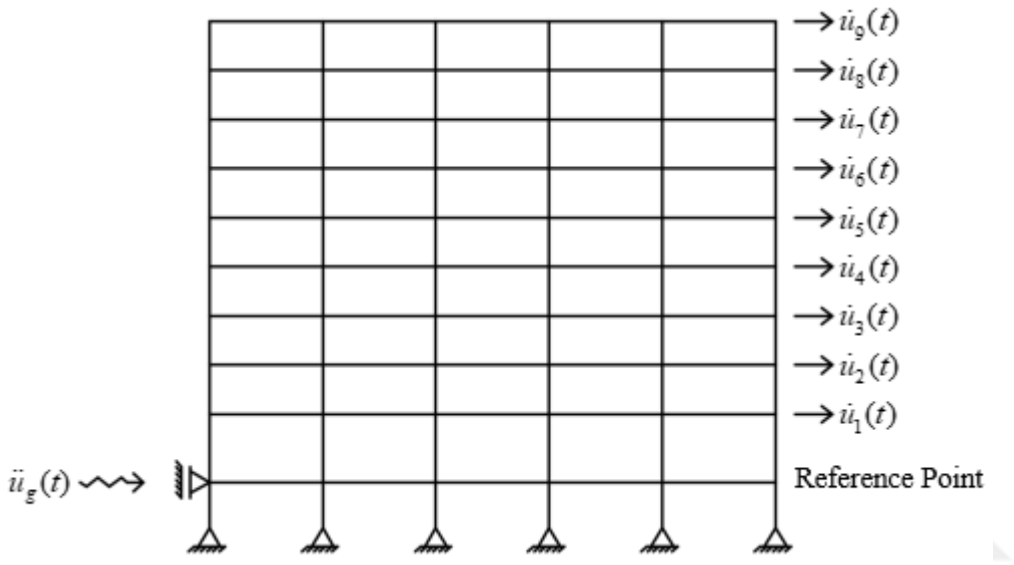

Figure 4.1 : An example for obtaining velocity responses at each story level.

$$\{E_I\} = -[M]\int_0^t \ddot{u}_g \{\dot{u}\} dt \tag{4.2}$$

$$E_{I,i} = -m_i \int_0^t \ddot{u}_g \dot{u}_i dt \tag{4.3}$$

It was observed that as the story level increases, input energy per unit mass imparted into the story tends to increase due to higher velocity responses. When the input energy time series for all stories numerically calculated using the MATLAB-based code were summed up, a value almost equal to the total E_I value read from Perform 3D was obtained, Figure 4.2.

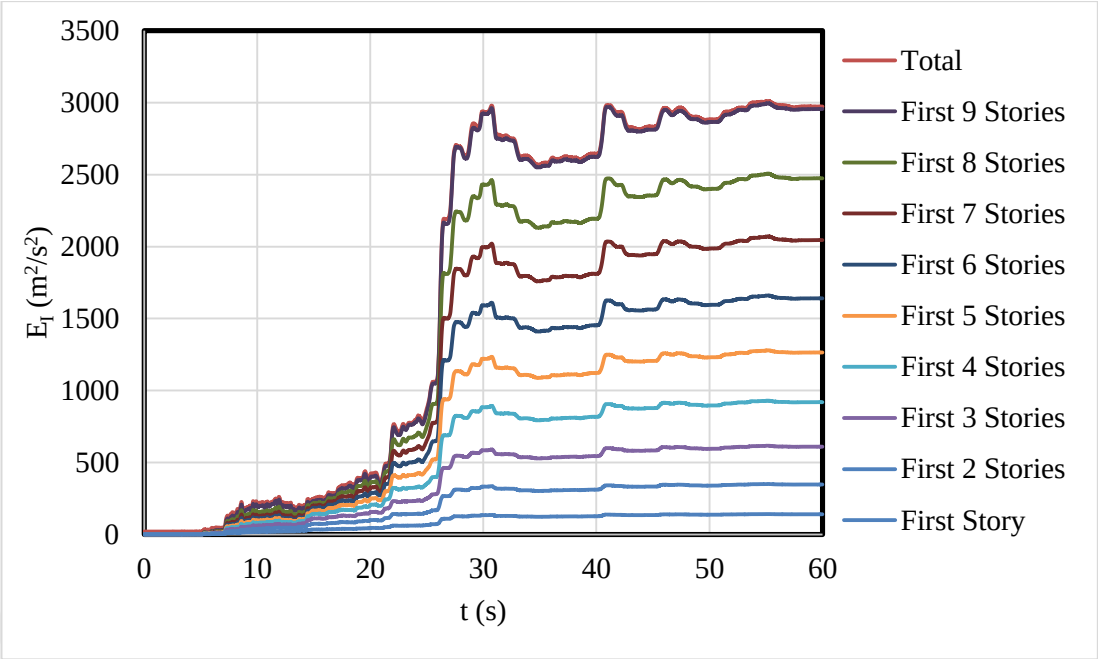

Figure 4.2 : An example for input energy time history at story levels.

Peak values of the input energy time series were calculated for all 92 earthquake records in each story level of five model frames. Their distribution is shown in Figures 4.3, 4.4, 4.5, 4.6 and 4.7. Figures prove that it is not possible to represent the input energy distribution among stories with a single pattern regardless of the earthquake characteristics.

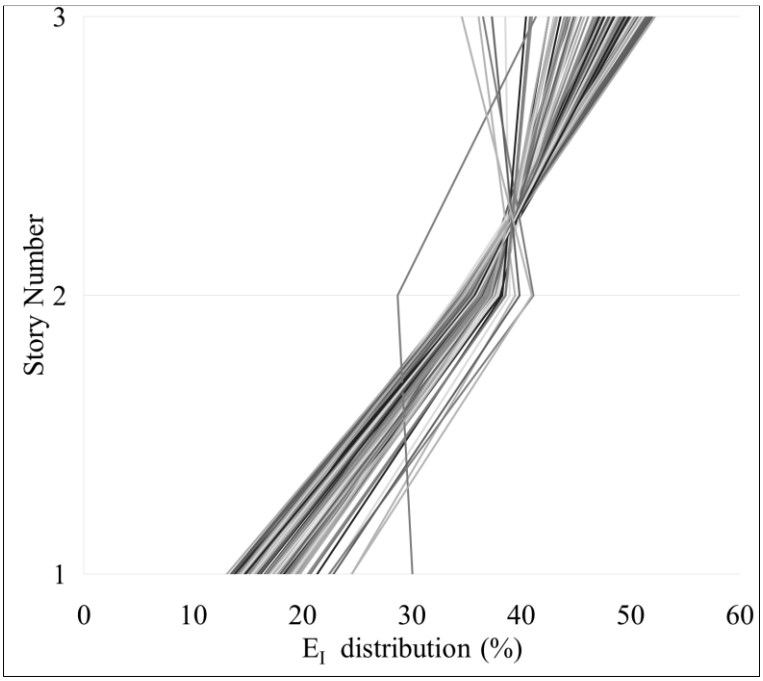

Figure 4.3 : E_I distribution of *Manoukas* 3-St for 92 *EQ* records.

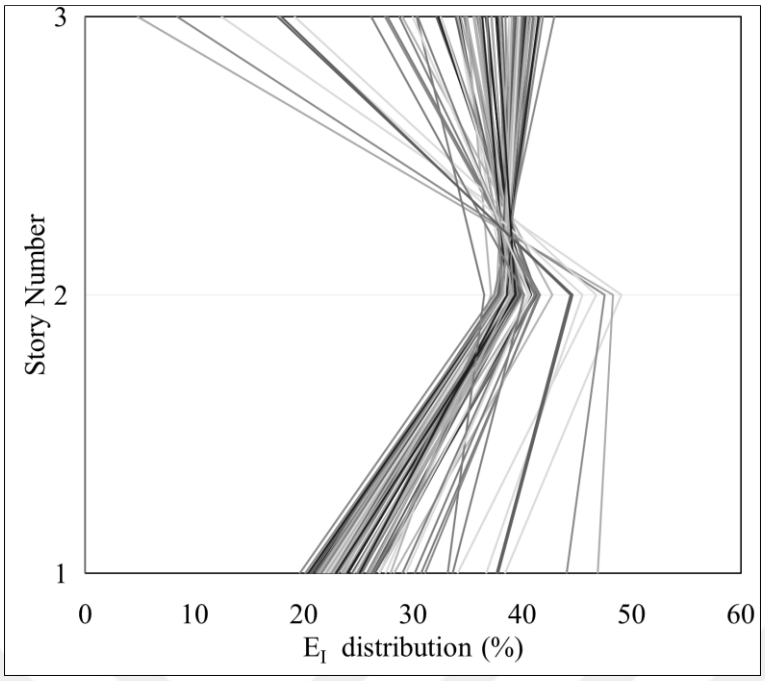

Figure 4.4 : E_I distribution of *Akbas* 3-St for 92 *EQ* records.

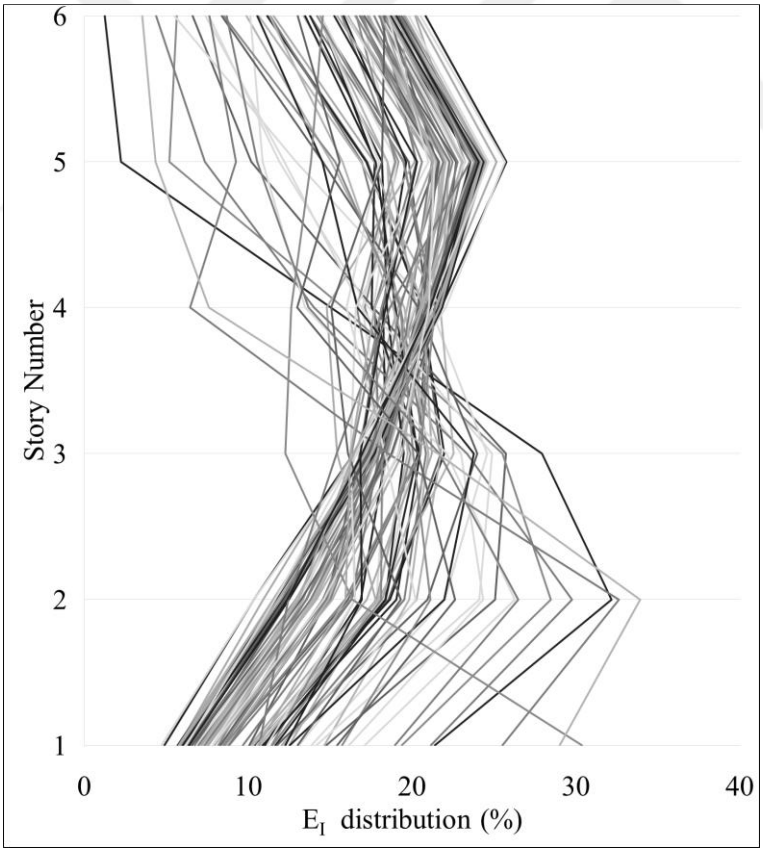

Figure 4.5 : E_I distribution of *Akbas* 6-St for 92 *EQ* records.

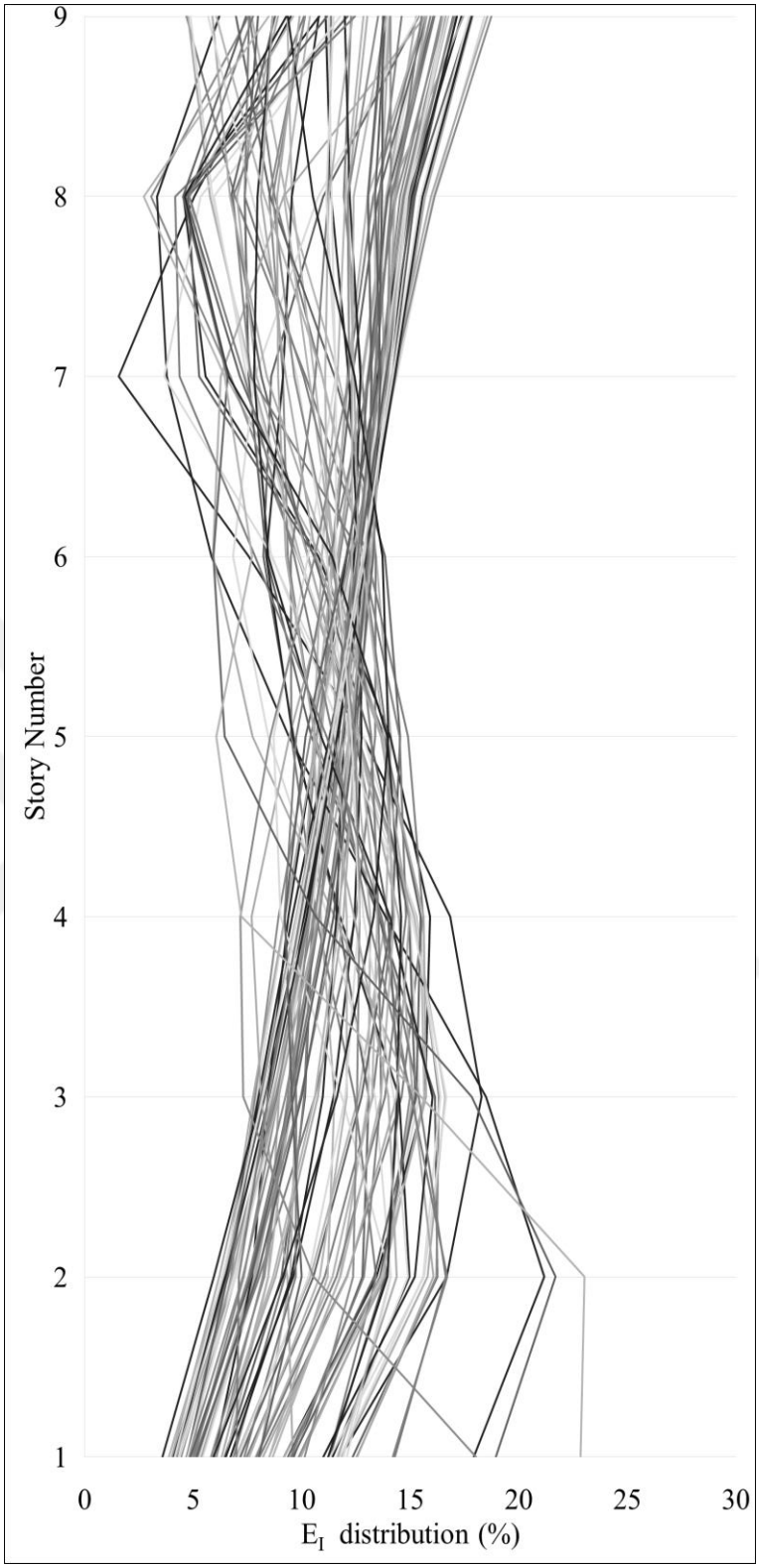

Figure 4.6 : E_I distribution of *SAC-LA* 9-St for 92 *EQ* records.

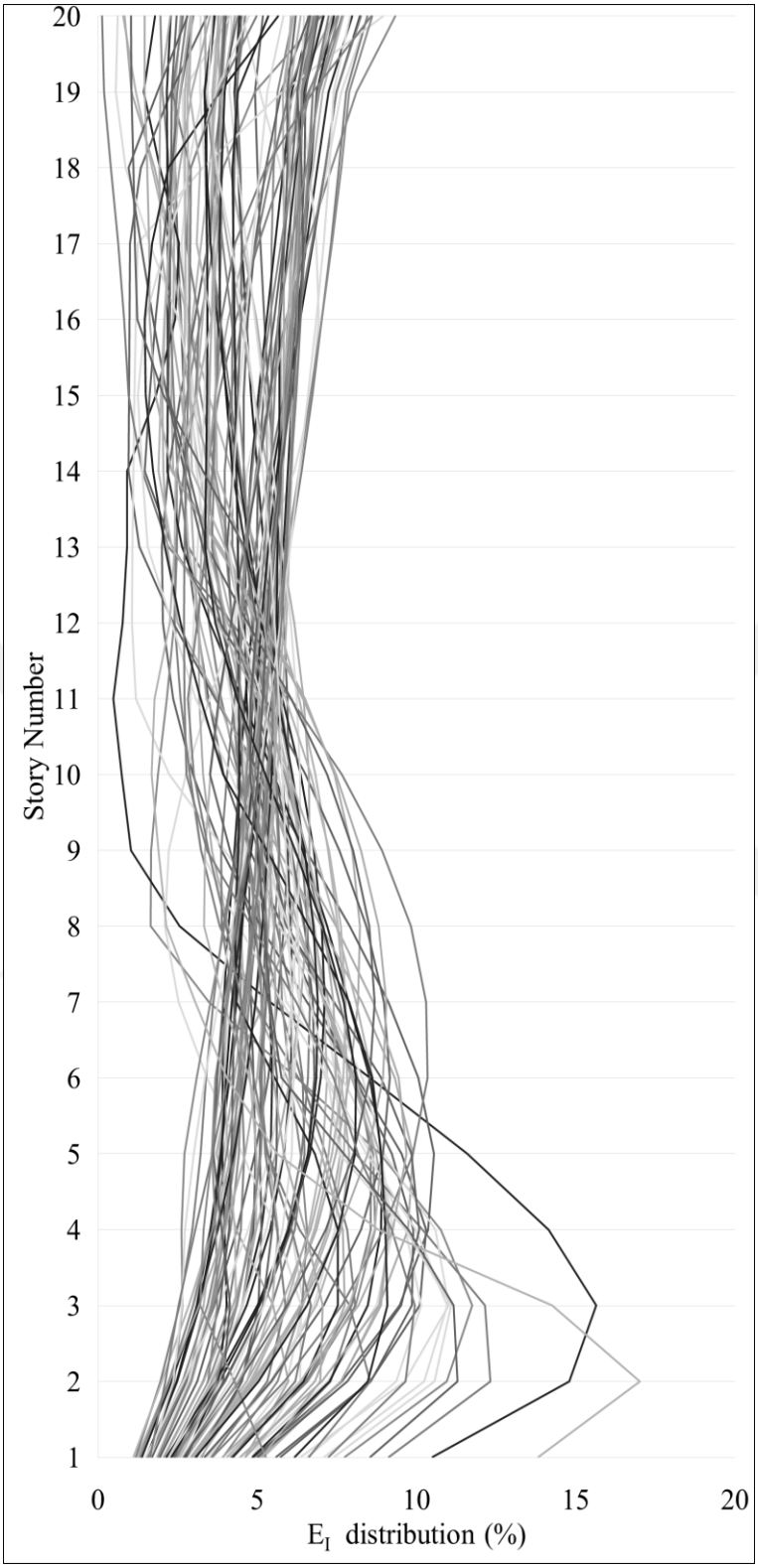

Figure 4.7 : E_I distribution of *SAC-LA* 20-St for 92 *EQ* records.

4.3 Discussion on the Results

Arithmetic means of ε for E_I predictions on story levels using 92 *EQ* records were calculated as 37.04%, 15.4%, 16.9%, 16.5%, and 29.4% for *Manoukas* 3-St, *Akbas* 3-St, *Akbas* 6-St, *SAC-LA* 9-St, and *SAC-LA* 20-St frames, respectively, Table 4.1.

Table 4.1 : Arithmetic means of relative percentage differences for input energy predictions on story levels using 92 *EQ* records.

Story #	*Manoukas* 3-St	*Akbas* 3-St	*Akbas* 6-St	*SAC-LA* 9-St	*SAC-LA* 20-St
1	33.4	11.7	12.9	13.7	15.1
2	36.3	11.2	11.1	9.8	11.1
3	41.3	23.3	12.6	17.4	13.6
4			14.8	19.7	20.5
5			16.9	18.1	25.0
6			33.2	15.7	24.4
7				15.1	22.1
8				18.0	19.3
9				21.2	20.0
10					21.8
11					25.3
12					28.9
13					32.1
14					31.2
15					35.4
16					45.5
17					51.2
18					46.1
19					49.3
20					49.4
Mean	37.0	15.4	16.9	16.5	29.4

Arithmetic means of ε for E_I predictions on story levels using the *EQ* records with a $PGV \leq 50$ cm/s were calculated as 18.7%, 13.1%, 12.3%, 10.1%, and 19.3% for *Manoukas* 3-St, *Akbas* 3-St, *Akbas* 6-St, *SAC-LA* 9-St, and *SAC-LA* 20-St frames, respectively, Table 4.2.

Table 4.2 : Arithmetic means of relative percentage differences for input energy predictions on story levels using the *EQ* records with a $PGV \leq 50$ cm/s.

Story #	*Manoukas* 3-St	*Akbas* 3-St	*Akbas* 6-St	*SAC-LA* 9-St	*SAC-LA* 20-St
1	16.2	10.1	11.2	11.7	18.1
2	16.8	7.9	5.7	5.7	8.2
3	23.2	21.1	5.8	13.6	5.9
4			7.8	14.4	12.2
5			12.7	12.4	16.4
6			30.4	5.5	16.2
7				9.9	12.9
8				7.5	9.1
9				10.7	11.4
10					12.8
11					15.0
12					15.6
13					20.1
14					17.8
15					23.4
16					30.4
17					39.9
18					35.0
19					31.7
20					34.8
Mean	18.7	13.1	12.3	10.1	19.3

It can be observed from the result that the relative percentage differences between the numerical and estimated story input energies are higher for the *RC* frame (*Manoukas* 3-St) and twenty-story steel frame (*SAC-LA* 20-St). Yet, it can be said that the methodology results in story input energies with an acceptable level of accuracy for the case of far-fault motion ($PGV \leq 50$ cm/s).

5. INELASTIC TOP DISPLACEMENT DEMAND PREDICTION

For some general nonlinear static analysis procedures, it is vital to predict the inelastic top displacement demand of a *MDOF* system with an error as low as possible. With this thesis study, an alternative for the calculation of the maximum inelastic top displacement according to the *equal displacement rule* will be proposed.

Maximum inelastic top displacement of a *MDOF* system during an earthquake can be predicted using the estimated seismic input energy with an acceptable accuracy.

5.1 Suggested Method to Estimate the Inelastic Top Displacement Demand

In a *MDOF* system, the dynamic response can be represented with a reference period (T_{ref}) which is calculated by combining the effects of sufficient number of modes as suggested by Marasco and Cimellaro (2018), equation (5.1).

$$T_{ref} = \frac{\sum_{j=1}^{N} T_j \times \left|\Gamma_j\right|}{\sum_{j=1}^{N} \left|\Gamma_j\right|} \tag{5.1}$$

Relation between input energy and top displacement for a *MDOF* system, which was first introduced by Mollaioli et al. (2011), is modified in the suggested method for the prediction of the top displacement, equation (5.2). Here, E_I / m is the mass-normalized input energy estimated in Chapter 3 and ω_{ref} is the angular frequency corresponding to T_{ref}, equation (5.3). Instead of using the ω of the first vibrational mode, ω_{ref} is used in order to take other mode effects into account. A new parameter (β) is defined with the equation (5.3) and its change with respect to T_1 is shown in Figure 5.1. T_{ref} and ω_{ref} values calculated for the model frames are listed in Table 5.1.

$$\delta_{top} = \frac{\sqrt{E_I / m}}{\beta \times \omega_{ref}} \tag{5.2}$$

$$\beta = \begin{cases} 1.5 - T_1; & T_1 < 0.75s \\ 0.75; & T_1 \geq 0.75s \end{cases} \qquad (5.3)$$

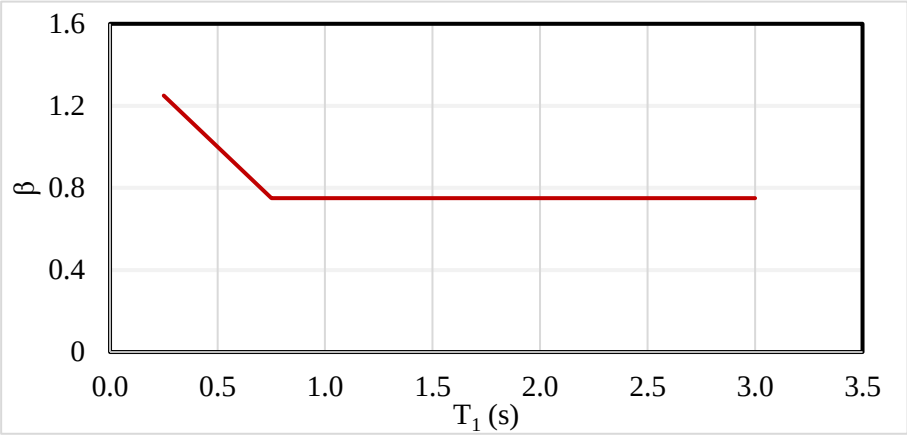

Figure 5.1 : Suggested bilinear β spectra.

Table 5.1 : Calculated reference periods and angular frequencies.

Frame	T_{ref} (s)	ω_{ref} (rad)
Manoukas 3-St	0.41	15.32
Akbas 3-St	0.67	9.38
Akbas 6-St	1.15	5.46
SAC-LA 9-St	1.70	3.70
SAC-LA 20-St	2.82	2.23

Second degree parabolic relation is obtained between input energy and top displacement for the set of five model frames used in this study, Figure 5.2.

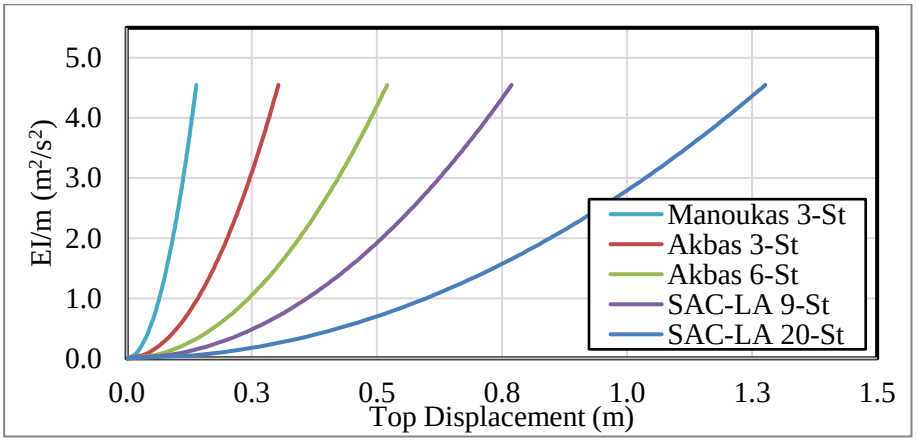

Figure 5.2 : Input energy – top displacement relationship.

Inelastic top displacement demand predictions ($(\delta_{top})_{pre}$) were made using the suggested method in this study, equation (5.2). After that, they were compared with

the numerical results obtained after running nonlinear time history analysis in Perform 3D software ($(\delta_{top})_{num}$). The relative percentage differences between the predictions and numerical results (ε_{EI}) were calculated using equation (5.4).

$$\varepsilon_{\delta} = \frac{\left|(\delta_{top})_{pre} - (\delta_{top})_{num}\right|}{\left[(\delta_{top})_{pre} + (\delta_{top})_{num}\right]/2} \tag{5.4}$$

With the proposed method, an accurate relation between mass-normalized input energy and inelastic top displacement demand of a MDOF system is obtained. The comparison of the relation obtained by the suggested method and Perform 3D results of 92 earthquake records are shown in Figure 5.3.

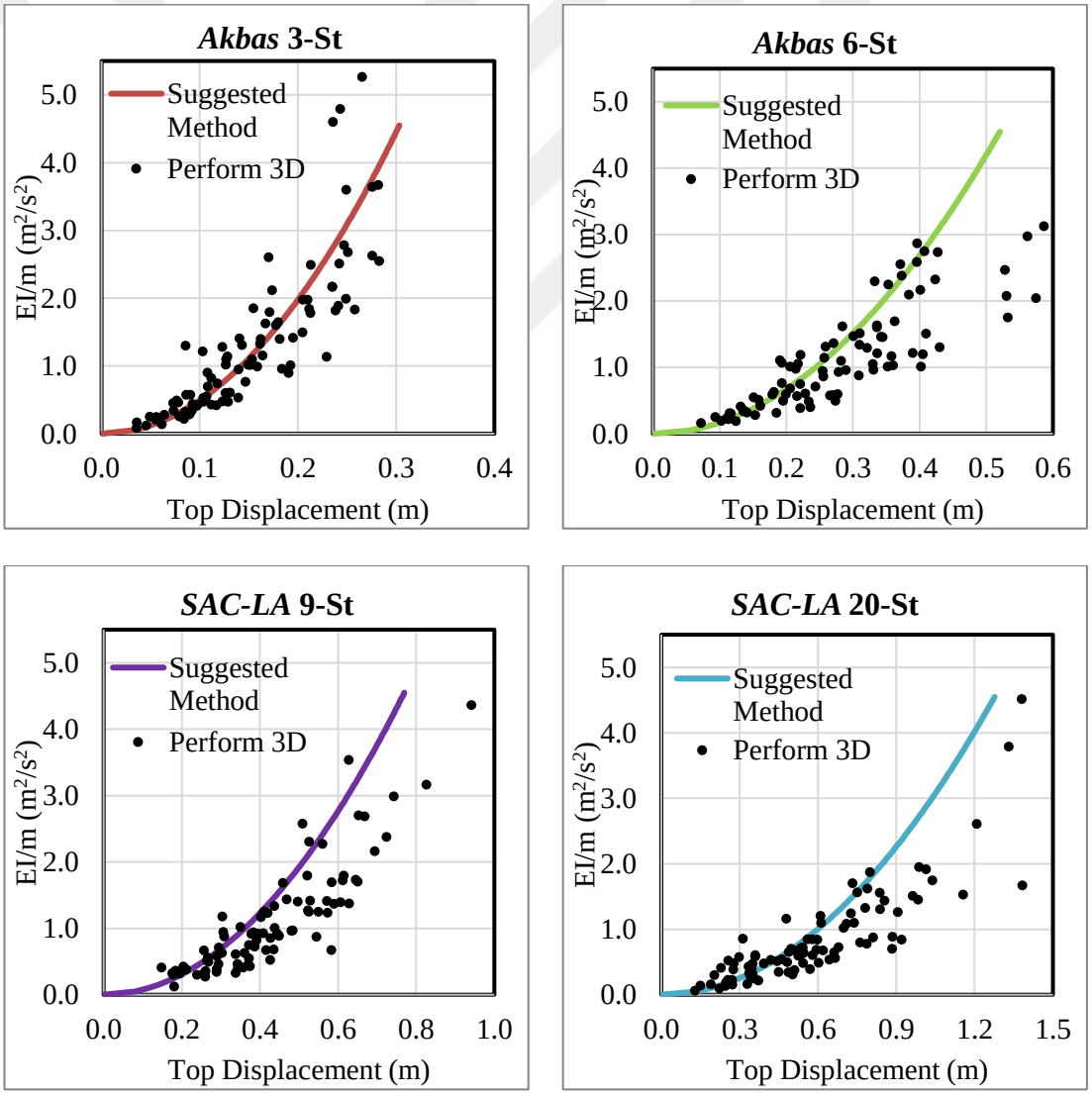

Figure 5.3 : Comparison for input energy – top displacement relation for the set of 92 *EQ* records on steel frames.

The comparison of the relation obtained by the suggested method and Perform 3D results for the *EQ* records with a $PGV \leq 50$ cm/s are shown in Figure 5.4.

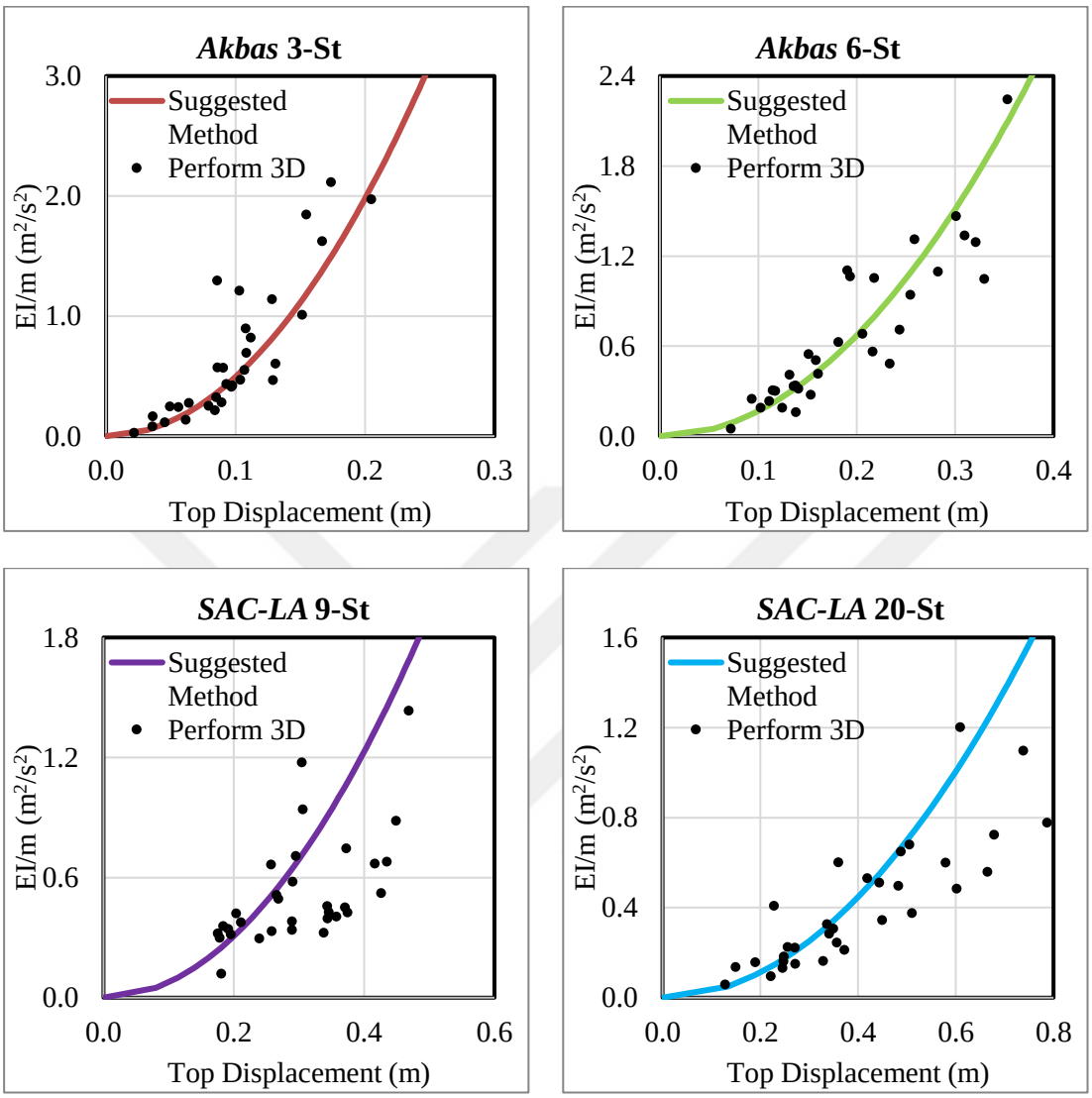

Figure 5.4 : Comparison for input energy – top displacement relation for the *EQ* records with a $PGV \leq 50$ cm/s on steel frames.

5.2 Discussion on the Results

Numerical and predicted inelastic top displacement demands and the relative percentage differences between them are listed in Tables C.1 and C.2 and also visualized in Figures C.1, C.2, C.3, C.4 and C.5 for the set of five model frames. Like E_I/m estimations in the previous chapter, it can be observed that the methodology proposed in this study gives better results for ordinary type (far fault characteristics and lower *PGV*) earthquake records in terms of predicting the displacement demand of *MDOF* systems.

Using the suggested method in this study, for the set of 92 earthquake records on *Manoukas* 3-St *RC* frame, arithmetic mean of ε_{EI} was calculated as 53.1%. The correlation coefficient was calculated as 0.546 indicating a moderate correlation, Figure 5.5.

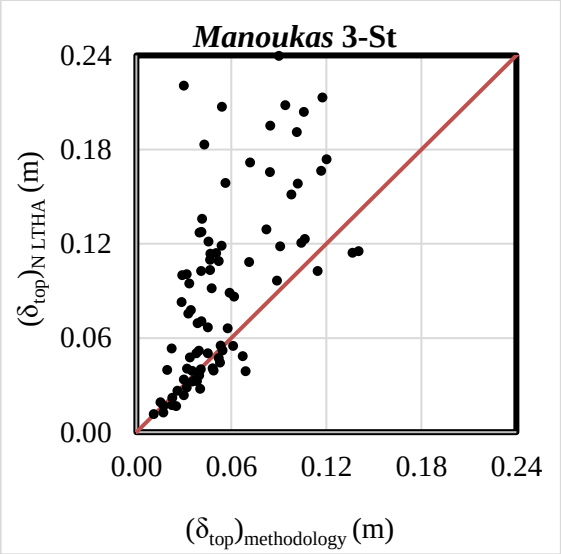

Figure 5.5 : Correlation between the estimated and numerical δ_{top} for the set of 92 *EQ* records on *RC* frame.

For 35 *EQ* records with a $PGV \leq 50$ cm/s on *Manoukas* 3-St, arithmetic mean of ε_{EI} was calculated as 20.9%. The correlation coefficient was calculated as 0.866 indicating a very strong correlation, Figure 5.6.

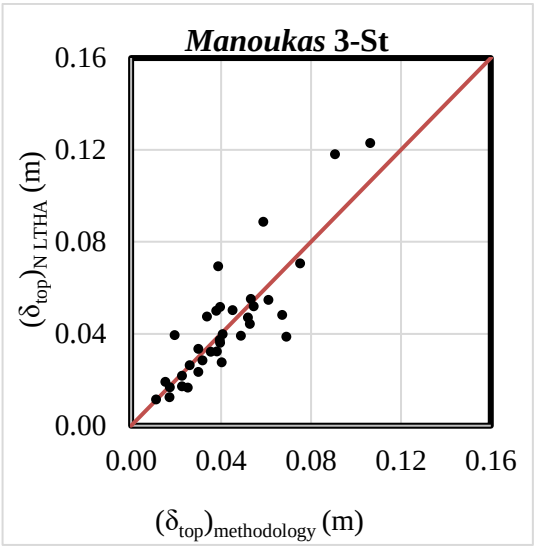

Figure 5.6 : Correlation between the estimated and numerical δ_{top} for the *EQ* records with a $PGV \leq 50$ cm/s on *RC* frame.

Using the suggested method in this study, for the set of 92 earthquake records on *Akbas* 3-St, *Akbas* 6-St, *SAC-LA* 9-St, and *SAC-LA* 20-St steel frames, arithmetic means of ε_δ were calculated as 18.3%, 20.6%, 18.8%, and 20.9%, respectively.

The correlation coefficients for the steel frames examined in this study were calculated as 0.857, 0.849, 0.878, and 0.883, respectively. These results represent that there is a very strong correlation between the estimated and numerical inelastic top displacement demands of the selected *MDOF* systems, Figure 5.7.

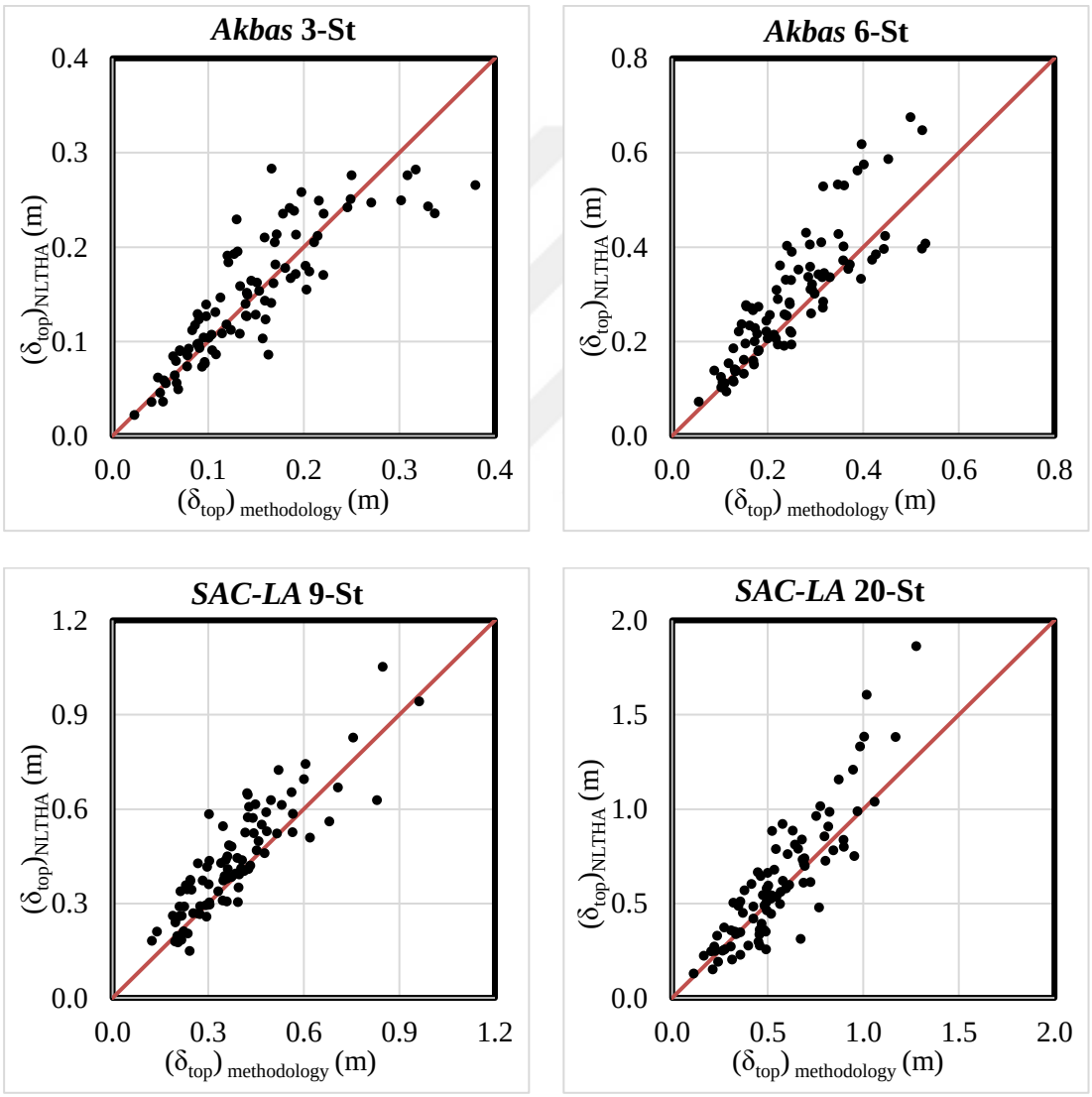

Figure 5.7 : Correlation between the estimated and numerical δ_{top} for the set of 92 *EQ* records on steel frames.

Using the suggested method in this study, for 35 *EQ* records with a $PGV \leq 50$ cm/s on *Akbas* 3-St, *Akbas* 6-St, *SAC-LA* 9-St, and *SAC-LA* 20-St steel frames, arithmetic means of ε_δ were calculated as 17.7%, 13.4%, 18.9%, and 16.4%, respectively.

The correlation coefficients for the steel frames examined in this study were calculated as 0.882, 0.917, 0.841, and 0.866, respectively. These results represent that there is a very strong correlation between the estimated and numerical inelastic top displacement demands of the selected *MDOF* systems, Figure 5.8.

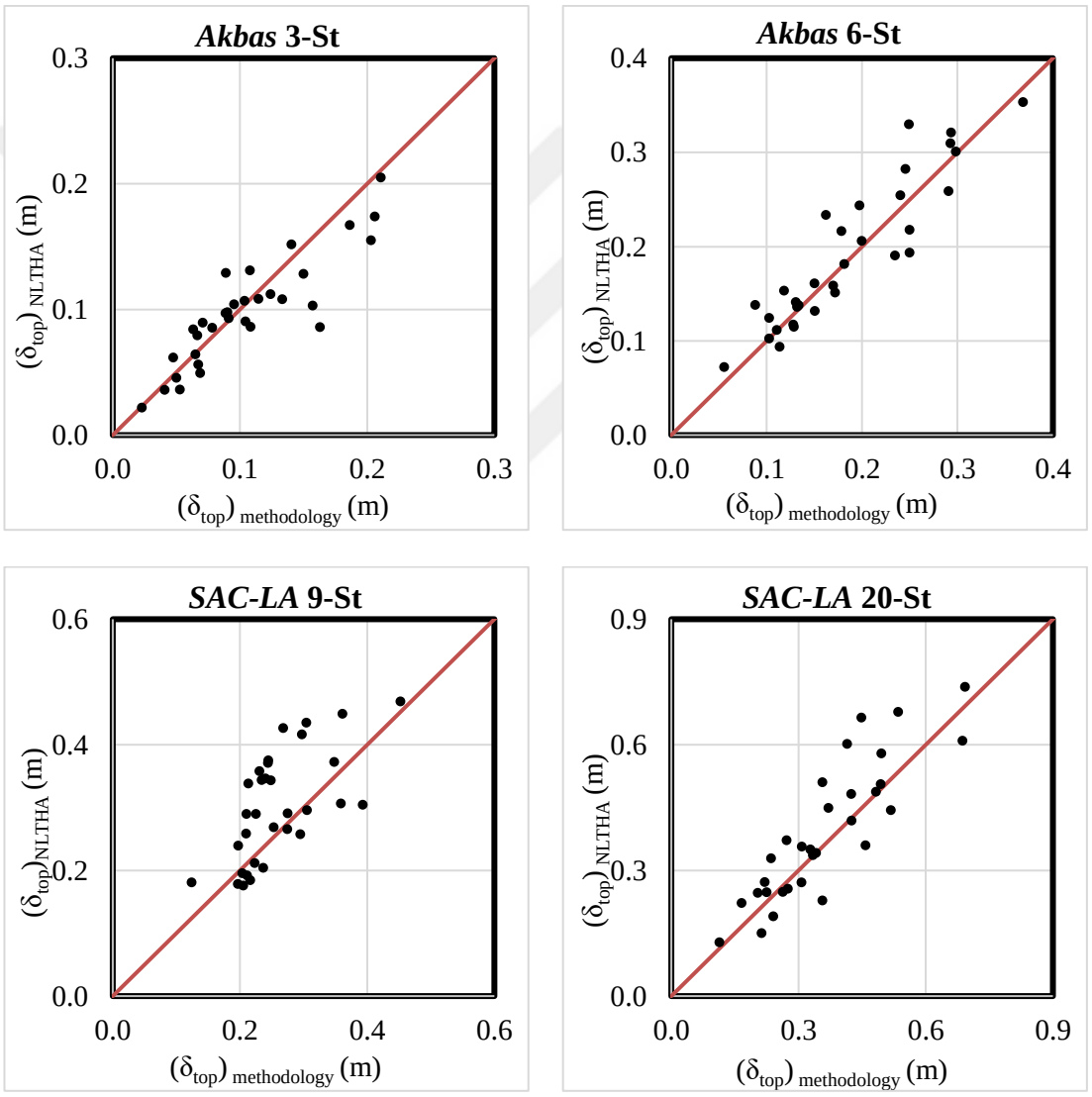

Figure 5.8 : Correlation between the estimated and numerical δ_{top} for the *EQ* records with a $PGV \leq 50$ cm/s on steel frames.

Distribution of the relative percentage differences between top displacements calculated with the suggested method and "true" top displacements obtained using Perform 3D software with respect to 35 *EQ* records with a $PGV \leq 50$ cm/s are shown in Figure 5.9.

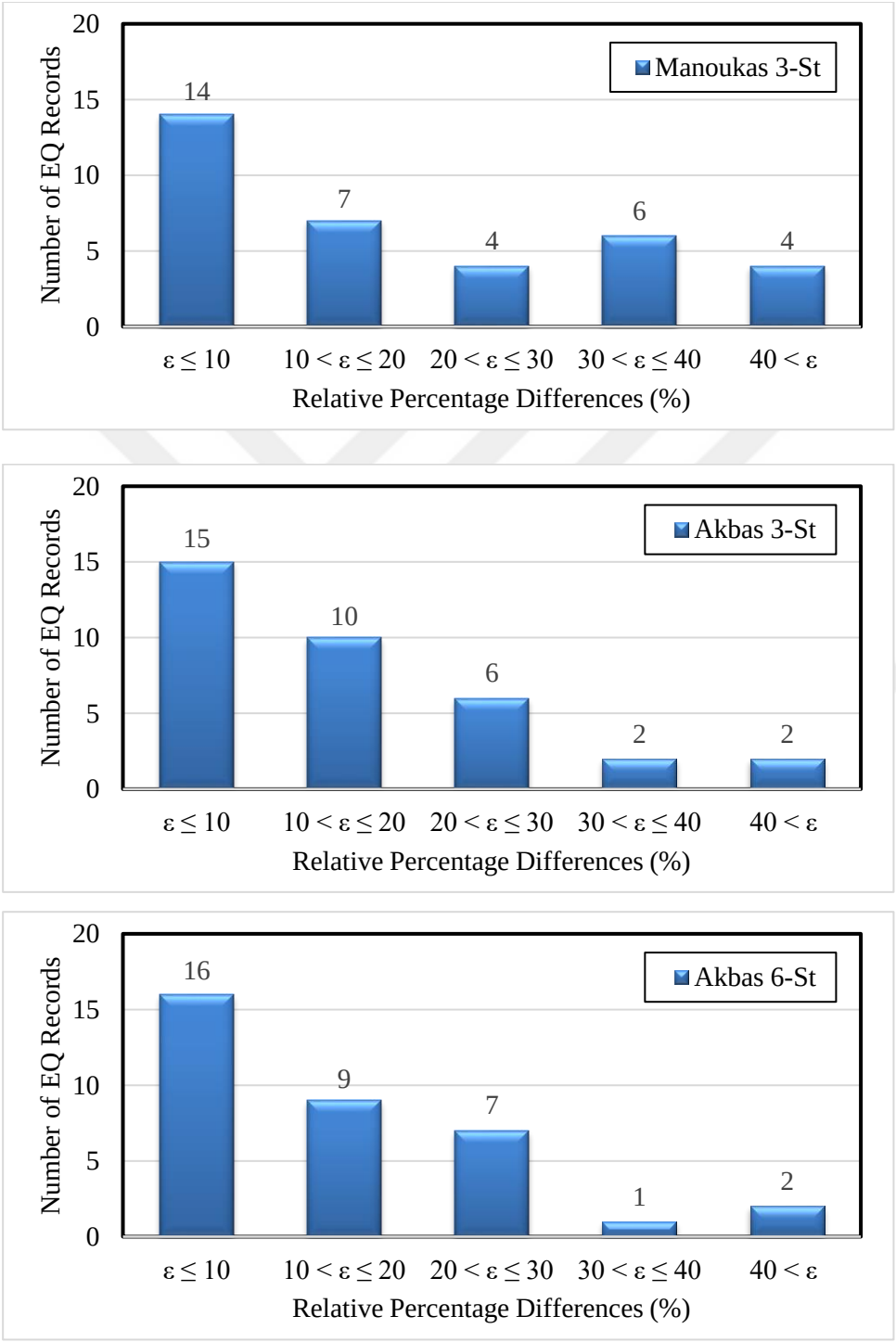

Figure 5.9 : Relative percentage difference distribution for δ_{top} estimation.

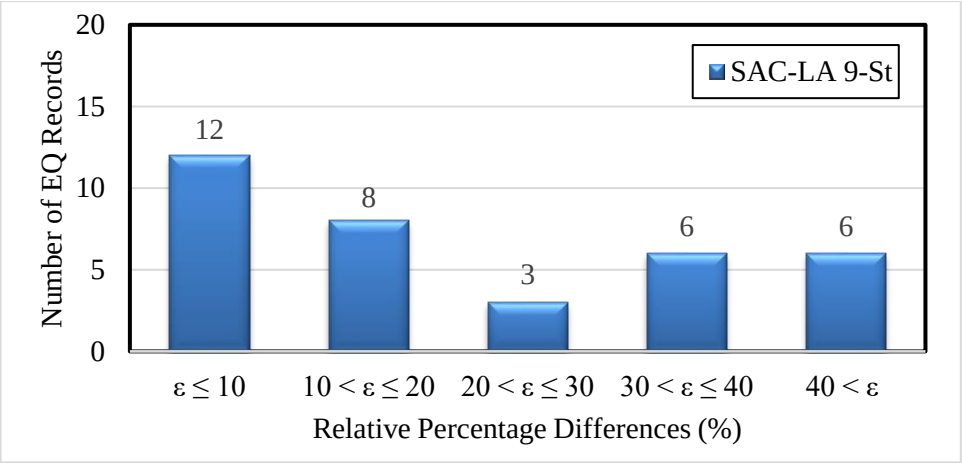

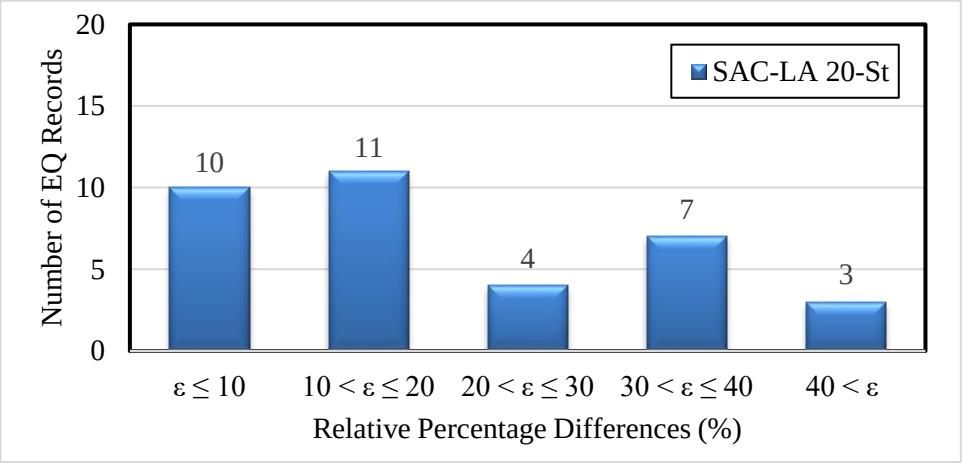

Figure 5.9 (continued) : Relative percentage difference distribution for δ_{top} estimation.

5.3 Comparison with Other Methods in the Literature

5.3.1 Method proposed by Manoukas et al. (2011)

An energy-based pushover procedure is suggested by Manoukas et al. (2011) in order to estimate the story displacements under an *EQ* record.

According to the suggested methodology, lateral incremental forces with a distribution pattern proportional to $M \cdot \Phi_1$ vector are applied to the created structural model as the first step. The strain energy-displacement curve (E_1-u_{N1}) is obtained where E_1 is the work of external forces and u_{N1} stands for top displacement of the *MDOF* system. Then, the strain energy-displacement curve for the *E-SDOF* system (E_1-D_1) is calculated dividing u_{N1} value by the quantity $\Gamma_1 \cdot \Phi_{N1}$. Using E_1-D_1 curve, the force-displacement curve for the *E-SDOF* system (V_1-D_1) is obtained. Story displacements are then calculated using displacement modification procedures.

In this study, story displacement predictions were made for 0.5 × El Centro, 1.0 × El Centro, and 1.5 × El Centro and they were compared with the *NLTHA* results for the reinforced concrete *Manoukas* 3-St frame.

In order to make a comparison between the method proposed by Manoukas et al. (2011) and the methodology suggested in this study, seismic demands of Manoukas 3-St frame were estimated for El Centro record (Figure 5.10) with scales of 0.5, 1.0, 1.5 as well. First, mass-normalized input energy spectrum was constructed for *SDOF* systems, Figure 5.11.

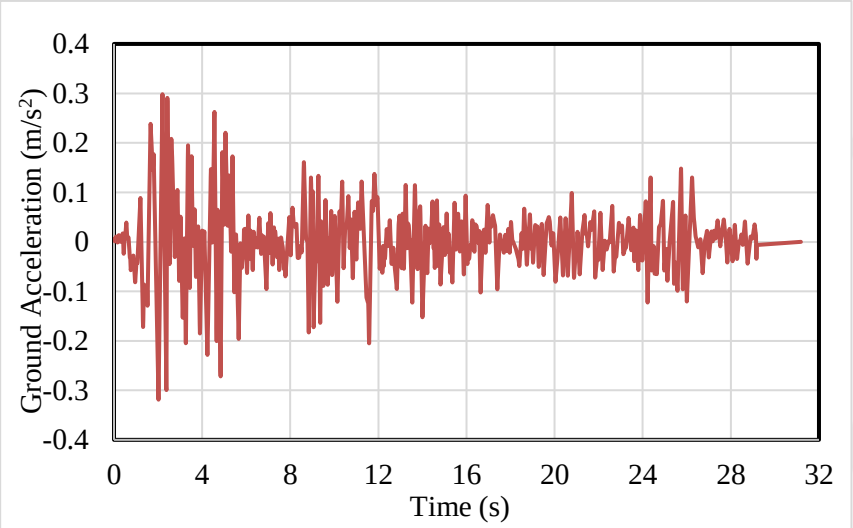

Figure 5.10 : Ground acceleration for 1.0 × El Centro.

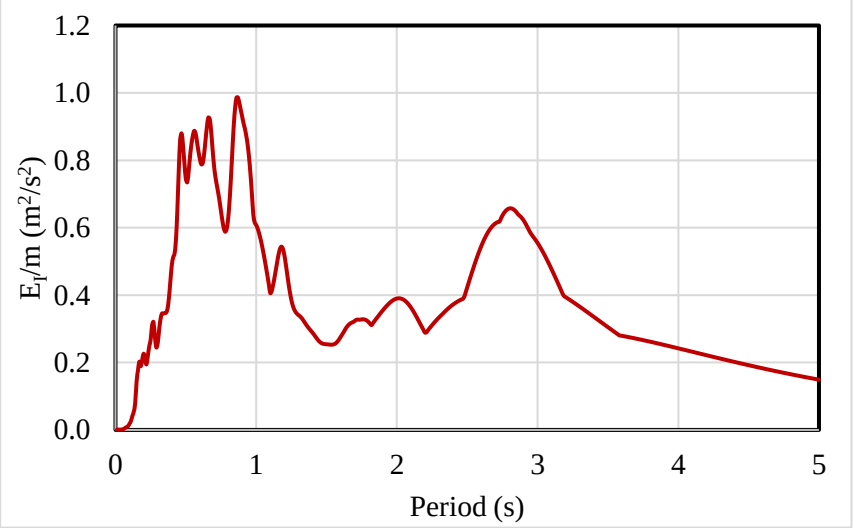

Figure 5.11 : Mass-normalized input energy spectrum for 1.0 × El Centro.

Using the suggested method, E_I/m values were calculated for *MDOF* system. Then, by using the suggested relationship between input energy and top displacement, inelastic

top displacement demands were predicted and a comparison was made between *NLTHA* results and the top displacement predictions, Table 5.2.

As it can be seen from the table, the methodology yields better top displacement prediction results than the method proposed by Manukas et al. (2011) for 0.5 × El Centro, 1.0 × El Centro, and 1.5 × El Centro records.

Table 5.2 : Comparison with Manoukas et al. (2011) for δ_{top} predictions.

EQ	$(\delta_{top})_{NLTHA}$ (cm)	Manoukas et al. (2011)		This study	
		$(\delta_{top})_{pre.}$ (cm)	ε_{δ} (%)	$(\delta_{top})_{pre.}$ (cm)	ε_{δ} (%)
0.5 × El Centro	2.988	3.656	**20.1**	3.944	27.6
1.0 × El Centro	5.627	5.697	1.2	5.577	**0.9**
1.5 × El Centro	7.803	11.076	34.7	6.831	**13.3**

5.3.2 Method proposed by Güllü (2018)

Güllü (2018) used the velocity spectra and displacement spectra to predict the relationship between seismic input energy and the top displacement demand of a *MDOF* moment resisting steel frame system.

A hybrid spectrum is constructed by an inclined line with a slope of "α" which is calculated using spectral velocity ($SV(T_1,\zeta)$) and displacement ($SD(T_1,\zeta)$) corresponding to the first mode and a variable "n" defining the relation between SV and (E_I / m), equation (5.5). The value of the variable "n" is obtained from the equation of trendline of the graph and it varies between 0.5 and 2.0, Figure 5.12.

$$\alpha = \frac{SV(T_1,\xi)^2}{n \times SD(T_1,\xi)} \tag{5.5}$$

Spectral displacement (SD) is obtained from the hybrid spectrum (Figure 5.13) by drawing a vertical line from the point where horizontal line from estimated mass-normalized input energy value intersects with the inclined line with slope of "α". After that, the physical top displacement of the *MDOF* system is calculated using equation (5.6).

$$u_{jn} = \sum_{j=1}^{N} \Gamma_j \cdot \phi_{jn} \cdot SD \tag{5.6}$$

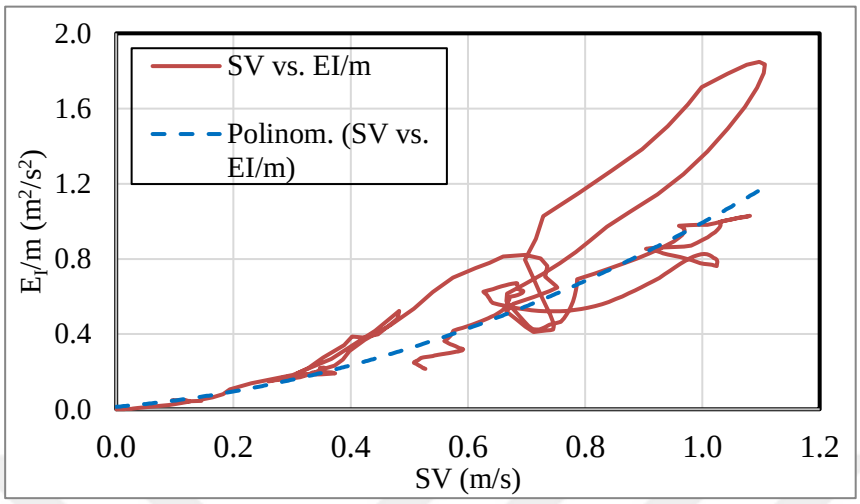

Figure 5.12 : Relation between *SV* and (E_I / *m*).

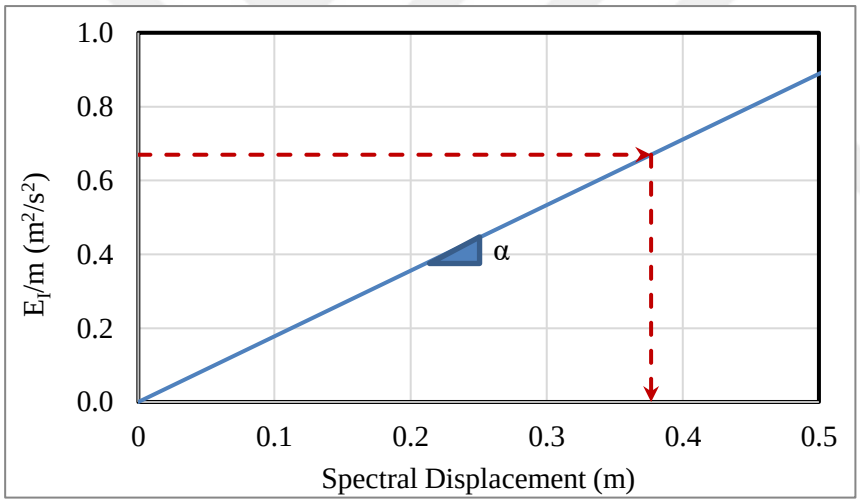

Figure 5.13 : Hybrid spectrum suggested by Güllü (2018).

After $(\delta_{top})_{pre}$ values were also calculated with the method proposed by Güllü (2018), they were compared with the "true" inelastic top displacement demands.

Using the method proposed by Güllü (2018), for the set of 92 earthquake records on *Akbas* 3-St, *Akbas* 6-St, *SAC-LA* 9-St, and *SAC-LA* 20-St frames, arithmetic means of ε_δ were calculated as 41.3%, 37.8%, 41.7%, and 40.7%, respectively.

It shows that the proposed method in this study gives better results than the one Güllü (2018) suggested in terms of making a prediction about the top displacement demand in *MDOF* systems.

6. CONCLUSIONS AND RECOMMENDATIONS

In the content of this M.Sc. thesis study, a methodology to estimate the input energy distribution and inelastic top displacement demand of steel moment resisting frame type structures was suggested. Its verification was made by applying the methodology on four steel model frames with different story numbers and performing nonlinear time history analyses using 92 earthquake records.

In order to check the applicability of the methodology on reinforced concrete frames, the methodology developed for the steel frames was tested on an *RC* frame as well. Thus, the number of model frames used in the verification of the methodology was increased to five.

For the implementation of the proposed methodology, these steps are followed:

Step 1. Create the structural model and run the modal analysis.

Step 2. Decide how many vibrational modes to use.

Step 3. Calculate the mass-normalized input energy spectra using the relative input energy approach.

Step 4. Calculate the input energy on each story level using mode shape, modal participation factor, and E_I/m values corresponding to each mode on the input energy spectra, equation (4.1). By summing them up and dividing by the total mass of the structure, obtain the mass-normalized seismic input energy for the whole structure.

Step 5. Calculate the inelastic top displacement demand of the structure using the mass-normalized input energy of the whole structure, reference angular frequency, and a period-dependent coefficient, equation (5.2).

6.1 Conclusions

- Maximum mass-normalized input energies imparted into the *MDOF* systems were shown to be estimated fast and accurately by only using their modal properties and

seismic input energy spectrum created for *SDOF* systems. The suggested methodology produced a mean relative percentage difference of around 12% with the results of the *NLTHA* for the steel frames of three-, six-, nine- and twenty-stories.

- Input energy distribution among the stories of three-, six-, and nine-story steel frames were estimated with a mean relative percentage difference of around 15%. Yet, the methodology yielded less accurate results for input energy distribution on twenty-story frame even though total input energy estimation was precise enough. The reason of this might be that the input energy distribution is sensitive to higher mode effects. Thus, less accurate results were obtained as the number of stories increased.
- Maximum top displacements experienced by the *MDOF* systems during an earthquake excitation -which can be used as an input values in some general nonlinear static analysis procedures- were shown to be estimated accurately by using mass-normalized input energy, angular frequency corresponding to their reference period, and a suggested parameter called "β". The suggested methodology produced a mean relative percentage difference of around 18% with the results of the *NLTHA* for the selected steel frames.
- For the set of all 92 *EQ* records applied on *Manoukas* 3-St *RC* frame, seismic demands were calculated with higher relative percentage differences, meaning less accuracy compared to the steel frames, Table 6.1. The reason of this might be that the suggested methodology loses its validity for the low-period structures: *Manoukas* 3-St *RC* frame has the lowest period (T_1 = 0.51 s) out of the selected model frames.

Table 6.1 : Arithmetic means of relative percentage differences for seismic demand predictions (using the set of all 92 records).

Frame	$(E_I/m)_{total}$	$(E_I/m)_{story}$	δ_{top}
Manoukas 3-St	38.6	37.0	53.1
Akbas 3-St	11.3	15.4	18.3
Akbas 6-St	13.6	16.9	20.6
SAC-LA 9-St	11.7	16.5	18.8
SAC-LA 20-St	13.9	29.4	20.9

- The methodology resulted in more accurate seismic input energy and nonlinear displacement demand values for earthquake records with a *PGV* value less than 50 m/s (ordinary non-pulse-like ground motions with the characteristics of far-fault earthquake excitation) used in the analyses, especially for *Manoukas* 3-St reinforced concrete frame.
- Using the *EQ* records with a $PGV \leq 50$ cm/s, it was observed that the methodology yields seismic demand components with acceptable approximation levels even though the relative percentage differences for *EI/m* estimation were computed slightly larger for the *RC* frame (*Manoukas* 3-St) in comparison with the steel frames (*Akbas* 3-St, *Akbas* 6-St, *SAC-LA* 9-St, and *SAC-LA* 20-St), Table 6.2.

Table 6.2 : Arithmetic means of relative percentage differences for seismic demand predictions (using the records with a $PGV \leq 50$ cm/s).

Frame	$(E_I/m)_{total}$	$(E_I/m)_{story}$	δ_{top}
Manoukas 3-St	17.1	18.7	20.9
Akbas 3-St	5.8	13.1	15.8
Akbas 6-St	7.7	12.3	14.8
SAC-LA 9-St	6.0	10.1	19.8
SAC-LA 20-St	9.3	19.3	18.8

- Effects of the number of modes used in the methodology was also investigated. It was observed that the methodology yields better results for the mass-normalized input energy predictions as the number of modes increases, Table 6.3.

  However, no direct correlation between the number of modes and the inelastic top displacement demand predictions was observed, Table 6.4.
- The results obtained using the suggested methodology were compared with some other procedures existing in the literature. After E_I/m imparted into the selected model frames in this study were predicted using the methods proposed by Kalkan and Kunnath (2007) and Güllü (2018) as well, a comparison between them and the methodology was made. In order to make a comparison for δ_{top} prediction, the method proposed by Güllü (2018) was applied to the model frames. Additionally, inelastic top displacements were predicted for the *RC* frame (*Manoukas* 3-St) using

the suggested methodology and compared with the predictions given in the study of Manoukas et al. (2011). It was observed that the methodology suggested in this study yields better results compared to the ones in the literature.

Table 6.3 : Effects of the number of modes used in the methodology for the seismic input energy predictions.

Frame	Arithmetic Means of Relative Percentage Differences (%)				
	First Mode	First 2 Modes	First 3 Modes	First 4 Modes	First 5 Modes
Manoukas 3-St	39.6	**38.6**	37.9	-	-
Akbas 3-St	16.4	**11.3**	11.2	-	-
Akbas 6-St	21.0	15.8	**13.6**	13.2	12.9
*SAC-LA*9-St	22.1	12.9	**11.7**	11.1	11.0
SAC-LA20-St	33.5	16.8	**13.9**	12.8	12.3

Table 6.4 : Effects of the number of modes used in the methodology for the inelastic top displacement demand predictions.

Frame	Arithmetic Means of Relative Percentage Differences (%)				
	First Mode	First 2 Modes	First 3 Modes	First 4 Modes	First 5 Modes
Manoukas 3-St	53.6	**53.1**	51.1	-	-
Akbas 3-St	18.6	**18.3**	18.4	-	-
Akbas 6-St	20.2	20.1	**20.6**	20.7	20.9
*SAC-LA*9-St	20.1	18.4	**18.8**	19.0	19.1
SAC-LA20-St	20.4	20.5	**20.9**	20.4	21.6

6.2 Recommendations

- The applicability of the methodology should be studied on different frame types (such as braced frames).
- The proposed methodology in this study should be extended for mid-rise and high-rise reinforced concrete frames as well.
- The methodology should be taken a step further by eliminating the negative effects of pulse-like seismic excitations on the methodology.

REFERENCES

Akbas, B. (1997). *Energy-based earthquake resistant design of steel moment resisting frames.* (Doctoral thesis). Illinois Institute of Technology, Graduate College, CHICAGO.

Akbas, B., Shen, J., & Hao, H. (2001). Energy approach in performance-based seismic design of steel moment resisting frames for basic safety objective. *Structural Design of Special and Tall Frames*, *10*, 193-217.

Akiyama, H. (1985). *Earthquake-Resistant Limit-State Design for Frames*. Tokyo: University of Tokyo Press.

BS EN 1998 (2005). *Eurocode 8: Design of Structures for Earthquake Resistance. General Rules, Seismic Actions and Rules for Frames.* Retrieved from https://bsol.bsigroup.com/PdfViewer/Viewer?pid=000000000030256900

Chopra, A.K. (2012), *Dynamics of Structures, Theory and Applications to Earthquake Engineering*. San Francisco, CA.: Prentice Hall.

Chou, C.C., Uang, C.M. (2003). A procedure for evaluating seismic energy demand of framed structures. *Earthquake Engineering and Structural Dynamics*, *32*, 229–244. doi: 10.1002/eqe.221

Chou, C.C., Uang, C.M. (2004). Evaluating distribution of seismic energy in multistory frames, *13th World Conference on Earthquake Engineering,* Vancouver, B.C., Canada, August 1-6.

D'Ambrissi, A., Mezzi, M. (2015). An energy-based approach for nonlinear static analysis of structures. *Bull Earthquake Eng*, *13*, 1513–1530. doi: 10.1007/s10518-014-9673-2

Decanini, L., Mollaioli, F. (2001). An energy based methodology for the assessment of seismic demand. *Soil Dynamics and Earthquake Engineering*, *21*, 113-137.

Decanini, L., Mollaioli, F., & Mura, A. (2001). Equivalent *SDOF* systems for the estimation of seismic response of multistory frame structures. *WIT Transactions on The Built Environment, 57*, 101-110.

Decanini, L., Mollaioli, F., & Saragoni, R. (2000). Energy and displacement demands imposed by near-source ground motions, *12th World Conference on Earthquake Engineering,* Auckland, New Zealand, January 30-February 4.

Deger, Z.T., Sutcu, F. (2017). Evaluation of earthquake input energy distribution in an *RC* frame for an energy-based seismic design approach, *16th World Conference on Earthquake Engineering,* Santiago, Chile, January 9-13.

Donaire-Ávila, J., Benavent-Climent, A., Lucchini, A., & Mollaioli, F. (2017). Energy-based seismic design methodology: a preliminary approach, *16th World Conference on Earthquake Engineering,* Santiago, Chile, January 9-13.

Fajfar P. (1992). Equivalent ductility factors taking into account low-cycle fatigue. *Earthquake Engineering and Structural Dynamics, 21*, 837–848.

Fajfar P., Vidic T. (1994). Consistent inelastic design spectra: hysteretic and input energy, *Earthquake Engineering and Structural Dynamics, 23*, 523-537.

FEMA 356 (2000). *Prestandard and Commentary for the Seismic Rehabilitation of Frames.* Retrieved from https://www.fema.gov/media-library-data/20130726-1444-20490-5925/fema_356.pdf

Ganjavi, B., Rezagholilou, A.R. (2018). An intensity measure for seismic input energy demand of multi-degree-of-freedom systems. *Civil Engineering Infrastructures Journal, 51(2),* 373-388.

Gupta, A., Krawinkler, H. (1999). Seismic demands for performance evaluation of steel moment resisting frame structures (SAC Task 5.4.3) (Report No: 132). Stanford, CA: The John A. Blume Earthquake Engineering Center.

Güllü, A. (2018). *Determination of the inelastıc displacement demand and response control of steel frame type structures by seismic energy equations.* (Doctoral thesis). Istanbul Technical University, Institute of Science and Technology, ISTANBUL.

Housner, G.W. (1956). Limit design of the structures to resist earthquakes, Proceedings of the *1st World Conference on Earthquake Engineering*, Berkeley, California.

Kalkan, E., Kunnath, S.K. (2007). Effective cyclic energy as a measure of seismic demand. *Journal of Earthquake Engineering, 11(5),* 725-751. doi: 10.1080/13632460601033827

Khashaee, P., Mohraz, B., Sadek, F., Lew, H.S., & Gross, J.L. (2003), Distribution of earthquake input energy in structures (Report No: NISTIR 6903). Gaithersburg: National Institute of Standards and Technology.

Kuwamura, H., Galambos, T.V. (1989). Earthquake load for structural reliability. *ASCE Journal of Structural Engineering 115(6).*

Leelatavivat, S., Saewon, W., & Subhash, C.G. (2009). Application of energy balance concept in seismic evaluation of structures. *ASCE J. Struct. Eng*., *135*, 113-121.

Manoukas, G., Athanatopoulou, A., & Avramidis, I. (2011). Static pushover analysis based on an energy-equivalent SDOF system. *Earthquake Spectra, 27(1),* 89-105.

Marasco, S., Cimellaro, G. P. (2018). A new energy-based ground motion selection and modification method limiting the dynamic response dispersion and preserving the median demand. *Bull Earthquake Eng, 16*, 561–581. doi: 10.1007/s10518-017-0232-5

MATLAB (version 2019) [Computer Software]. Natick, MA : The MathWorks, Inc.

Mezgebo, M.G. (2015). *Estimation of earthquake input energy, hysteretic energy and its distribution in MDOF structures.* (Doctoral dissertation). Syracuse University, NEW YORK.

Mezgebo, M.G., Lui, E.M. (2017). A new methodology for energy-based seismic design of steel moment frames. *Earthquake Engineering and*

Engineering Vibration, 16(1), 131-162. doi: 10.1007/s11803-017-0373-1.

Mollaioli, F., Bruno, S., Decanini, L., & Saragoni, R. (2004). On the correlation between energy and displacement, *13th World Conference on Earthquake Engineering*, Vancouver, B.C., Canada, August 1-6.

Mollaioli, F., Bruno, S., Decanini, L., & Saragoni, R. (2011). Correlations between energy and displacement demands for performance-based seismic engineering. *Pure and Applied Geophysics, 168*, 237-259.

PEER Ground Motion Database, NGA-West2. http://ngawest2.berkeley.edu/

Perform 3D (Version 7) [Computer Software]. Walnut Creek, CA : Computers and Structures, Inc.

Rajasekaran, S. (2009). *Structural Dynamics of Earthquake Engineering: Theory and Application Using Mathematica and MATLAB.* Cambridge: Woodhead Publishing Limited.

SAP2000 (Version 20) [Computer Software]. Walnut Creek, CA : Computers and Structures, Inc.

SeismoSoft, SeismoSignal 2016.

Shiwua, A.J., Rutman, Y. (2016). Assessment of seismic input energy by means of new definition and the application to earthquake resistant design. *Architecture and Engineering, 1(4),* 26-35.

Surmeli, M., Yuksel, E. (2015). A variant of modal pushover analyses (VMPA) based a non-incremental procedure. *Bull Earthquake Eng*, *13*, 3353-3379.

TBEC (2018). *Turkish Building Earthquake Code-2018*. Retrieved from http://www.imo.org.tr/resimler/dosya_ekler/89227ad223d3b7a_ek.pdf

Teran-Gilmore A. (1998). A parametric approach to performance-based numerical seismic design, *Earthquake Spectra*, *14*, 3.

Uang, C.M., Bertero, V.V. (1990). Evaluation of seismic energy in structures. *Earthquake Engineering and Structural Dynamics*, *19*, 77-90.

Ucar, T. (2020). Computing input energy response of MDOF systems to actual ground motions based on modal contributions. *Earthquakes and Structures, 18:2*, 263-273. doi: 10.12989/eas.2020.18.2.263

Wang, F., Yi, T. (2012). A methodology for estimating seismic hysteretic energy of frames, *ASCE 2012 International Conference on Civil Engineering and Urban Planning*, Yantai, China.

XTRACT [Computer Software]. Rancho Cordova, CA : TRC.

APPENDICES

APPENDIX A: Earthquake Records
APPENDIX B: Input Energy Demand Predictions
APPENDIX C: Displacement Demand Predictions

APPENDIX A

Table A.1 : Selected earthquake records.

#	Earthquake Name	Year	Station Name	M_s	V_{s30} (m/sec)
1	Superstition Hills-02	1987	Imperial Valley Wildlife Liquefaction Array	6.54	179.00
2	Loma Prieta	1989	Foster City - APEEL 1	6.93	116.35
3	Superstition Hills-02	1987	Imperial Valley Wildlife Liquefaction Array	6.54	179.00
4	Kocaeli_ Turkey	1999	Ambarli	7.51	175.00
5	Chi-Chi_ Taiwan-06	1999	CHY047	6.30	169.52
6	Loma Prieta	1989	Treasure Island	6.93	155.11
7	Chuetsu-oki_ Japan	2007	NIG014	6.80	128.12
8	Loma Prieta	1989	Foster City - APEEL 1	6.93	116.35
9	Niigata_ Japan	2004	NIG013	6.63	174.55
10	Chi-Chi_ Taiwan	1999	TAP021	7.62	167.18
11	Kocaeli_ Turkey	1999	Ambarli	7.51	175.00
12	Chi-Chi_ Taiwan	1999	CHY054	7.62	172.10
13	Chi-Chi_ Taiwan	1999	CHY054	7.62	172.10
14	Christchurch_ New Zealand	2011	Christchurch Resthaven	6.20	141.00
15	Darfield_ New Zealand	2010	Christchurch Resthaven	7.00	141.00
16	Christchurch_ New Zealand	2011	Christchurch Resthaven	6.20	141.00
17	Parkfield-02_ CA	2004	Parkfield - Fault Zone 1	6.00	178.27
18	Imperial Valley-06	1979	El Centro Array #3	6.53	162.94
19	Parkfield-02_ CA	2004	Parkfield - Cholame 2WA	6.00	173.02
20	Tottori_ Japan	2000	TTR008	6.61	139.21
21	Parkfield-02_ CA	2004	Parkfield - Fault Zone 1	6.00	178.27
22	Darfield_ New Zealand	2010	Christchurch Resthaven	7.00	141.00
23	Imperial Valley-06	1979	Delta	6.53	242.05
24	Imperial Valley-06	1979	Bonds Corner	6.53	223.03
25	Imperial Valley-06	1979	Bonds Corner	6.53	223.03

Table A.1 (continued) : Selected earthquake records.

#	Earthquake Name	Year	Station Name	M_s	V_{s30} (m/sec)
26	Gazli_ USSR	1976	Karakyr	6.80	259.59
27	Imperial Valley-06	1979	Delta	6.53	242.05
28	Imperial Valley-02	1940	El Centro Array #9	6.95	213.44
29	Gazli_ USSR	1976	Karakyr	6.80	259.59
30	Imperial Valley-06	1979	El Centro Array #8	6.53	206.08
31	Imperial Valley-06	1979	Aeropuerto Mexicali	6.53	259.86
32	Northern Calif-03	1954	Ferndale City Hall	6.50	219.31
33	Imperial Valley-02	1940	El Centro Array #9	6.95	213.44
34	Imperial Valley-06	1979	El Centro Array #11	6.53	196.25
35	Managua_ Nicaragua-01	1972	Managua_ ESSO	6.24	288.77
36	Imperial Valley-06	1979	Chihuahua	6.53	242.05
37	Imperial Valley-06	1979	El Centro Array #8	6.53	206.08
38	Imperial Valley-06	1979	El Centro Array #7	6.53	210.51
39	Northridge-01	1994	Newhall - Fire Sta	6.69	269.14
40	Imperial Valley-06	1979	El Centro Array #6	6.53	203.22
41	Kobe_ Japan	1995	Takarazuka	6.90	312.00
42	Imperial Valley-06	1979	El Centro Array #5	6.53	205.63
43	Northridge-01	1994	Newhall - W Pico Canyon Rd.	6.69	285.93
44	Darfield_ New Zealand	2010	LINC	7.00	263.20
45	Chi-Chi_ Taiwan	1999	TCU051	7.62	350.06
46	Chi-Chi_ Taiwan	1999	CHY101	7.62	258.89
47	Kobe_ Japan	1995	KJMA	6.90	312.00
48	Kobe_ Japan	1995	Takarazuka	6.90	312.00
49	Imperial Valley-06	1979	El Centro - Meloland Geot. Array	6.53	264.57
50	Northridge-01	1994	Pardee - SCE	6.69	325.67

Table A.1 (continued) : Selected earthquake records.

#	Earthquake Name	Year	Station Name	M_s	V_{s30} (m/sec)
51	Darfield_ New Zealand	2010	HORC	7.00	326.01
52	Darfield_ New Zealand	2010	Riccarton High School	7.00	293.00
53	El Mayor-Cucapah_ Mexico	2010	Westside Elementary School	7.20	242.00
54	Northridge-01	1994	Newhall - Fire Sta	6.69	269.14
55	Christchurch_ New Zealand	2011	Pages Road Pumping Station	6.20	206.00
56	Northridge-01	1994	Pardee - SCE	6.69	325.67
57	Duzce_ Turkey	1999	Bolu	7.14	293.57
58	Chi-Chi_ Taiwan	1999	TCU052	7.62	579.10
59	Chi-Chi_ Taiwan	1999	TCU068	7.62	487.34
60	Chi-Chi_ Taiwan	1999	TCU102	7.62	714.27
61	Chi-Chi_ Taiwan	1999	TCU052	7.62	579.10
62	Northridge-01	1994	Jensen Filter Plant Administrative Frame	6.69	373.07
63	Northridge-01	1994	Sylmar - Olive View Med FF	6.69	440.54
64	Northridge-01	1994	Jensen Filter Plant Administrative Frame	6.69	373.07
65	Northridge-01	1994	Sylmar - Olive View Med FF	6.69	440.54
66	Northridge-01	1994	Jensen Filter Plant Generator Frame	6.69	525.79
67	Chi-Chi_ Taiwan	1999	TCU102	7.62	714.27
68	Northridge-01	1994	Jensen Filter Plant Generator Frame	6.69	525.79
69	Chi-Chi_ Taiwan	1999	TCU068	7.62	487.34
70	Northridge-01	1994	Sylmar - Converter Sta East	6.69	370.52
71	Northridge-01	1994	Sylmar - Converter Sta East	6.69	370.52
72	Northridge-01	1994	LA Dam	6.69	628.99
73	Chi-Chi_ Taiwan	1999	TCU063	7.62	476.14
74	Cape Mendocino	1992	Petrolia	7.01	422.17
75	Irpinia_ Italy-01	1980	Sturno (STN)	6.90	382.00

Table A.1 (continued) : Selected earthquake records.

#	Earthquake Name	Year	Station Name	M_s	V_{s30} (m/sec)
76	Chuetsu-oki_ Japan	2007	Joetsu Kakizakiku Kakizaki	6.80	383.43
77	Northridge-01	1994	LA - Sepulveda VA Hospital	6.69	380.06
78	Kobe_ Japan	1995	Kobe University	6.90	1043.00
79	Kobe_ Japan	1995	Kobe University	6.90	1043.00
80	Tabas_ Iran	1978	Tabas	7.35	766.77
81	Tabas_ Iran	1978	Tabas	7.35	766.77
82	Loma Prieta	1989	Los Gatos - Lexington Dam	6.93	1070.34
83	Loma Prieta	1989	Los Gatos - Lexington Dam	6.93	1070.34
84	Landers	1992	Lucerne	7.28	1369.00
85	Kocaeli_ Turkey	1999	Izmit	7.51	811.00
86	Landers	1992	Lucerne	7.28	1369.00
87	Chi-Chi_ Taiwan	1999	HWA003	7.62	1525.85
88	Chi-Chi_ Taiwan	1999	HWA003	7.62	1525.85
89	San Fernando	1971	Pacoima Dam (upper left abut)	6.61	2016.13
90	Northridge-01	1994	Pacoima Dam (upper left)	6.69	2016.13
91	San Fernando	1971	Pacoima Dam (upper left abut)	6.61	2016.13
92	Northridge-01	1994	Pacoima Dam (upper left)	6.69	2016.13

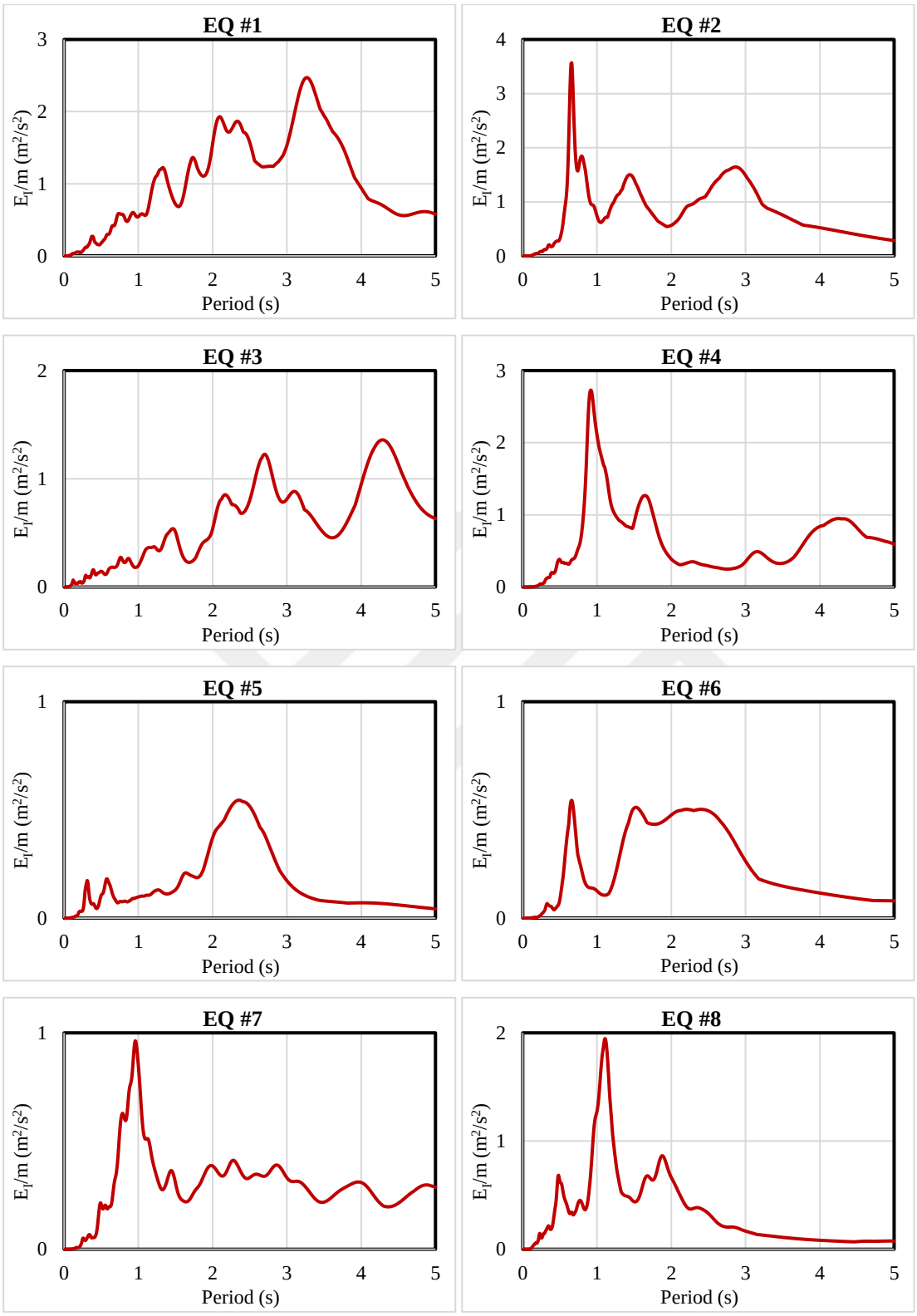

Figure A.1 : Mass-normalized input energy spectra for the *EQ* records.

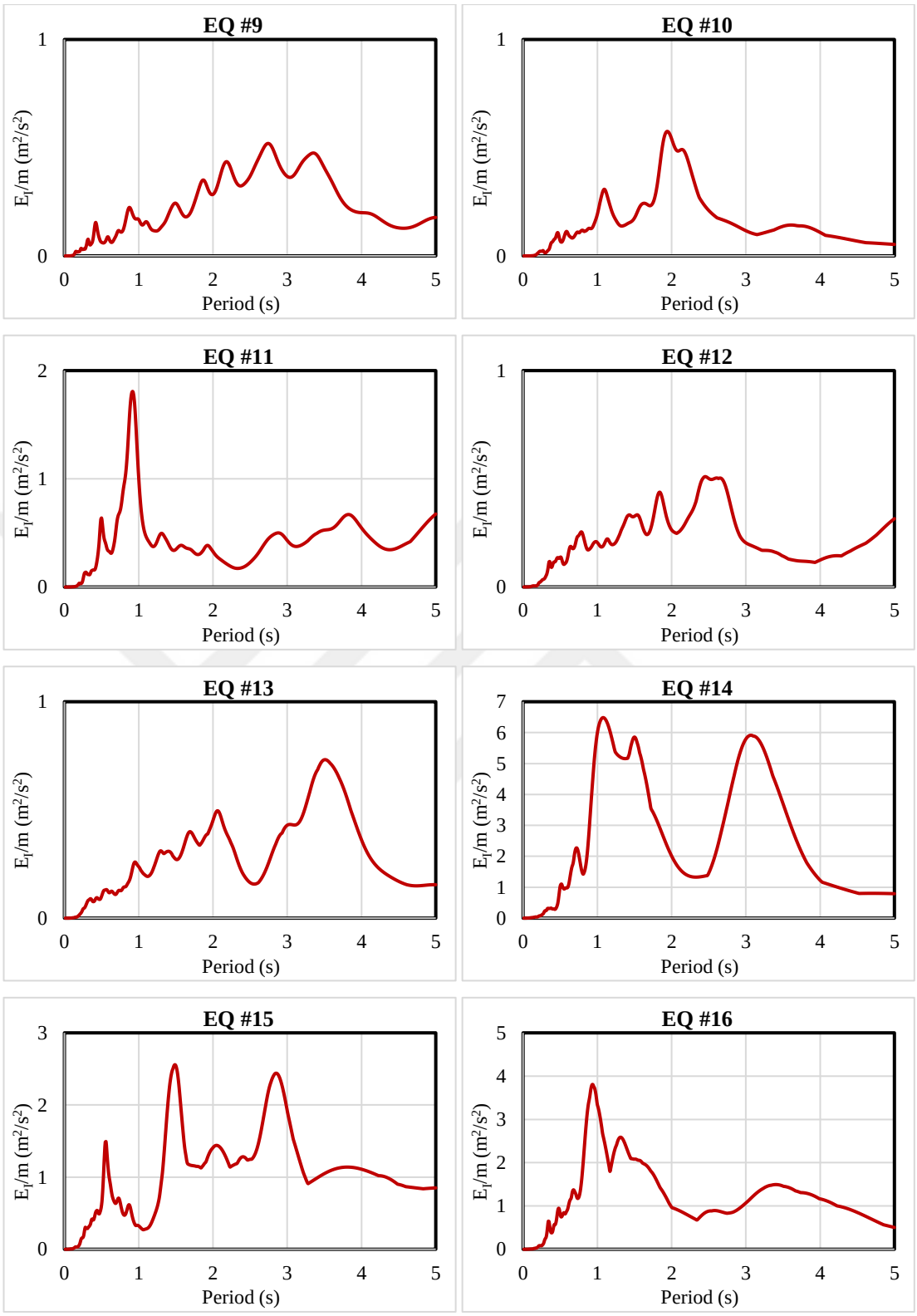

Figure A.1 (continued) : Mass-normalized input energy spectra for the *EQ* records.

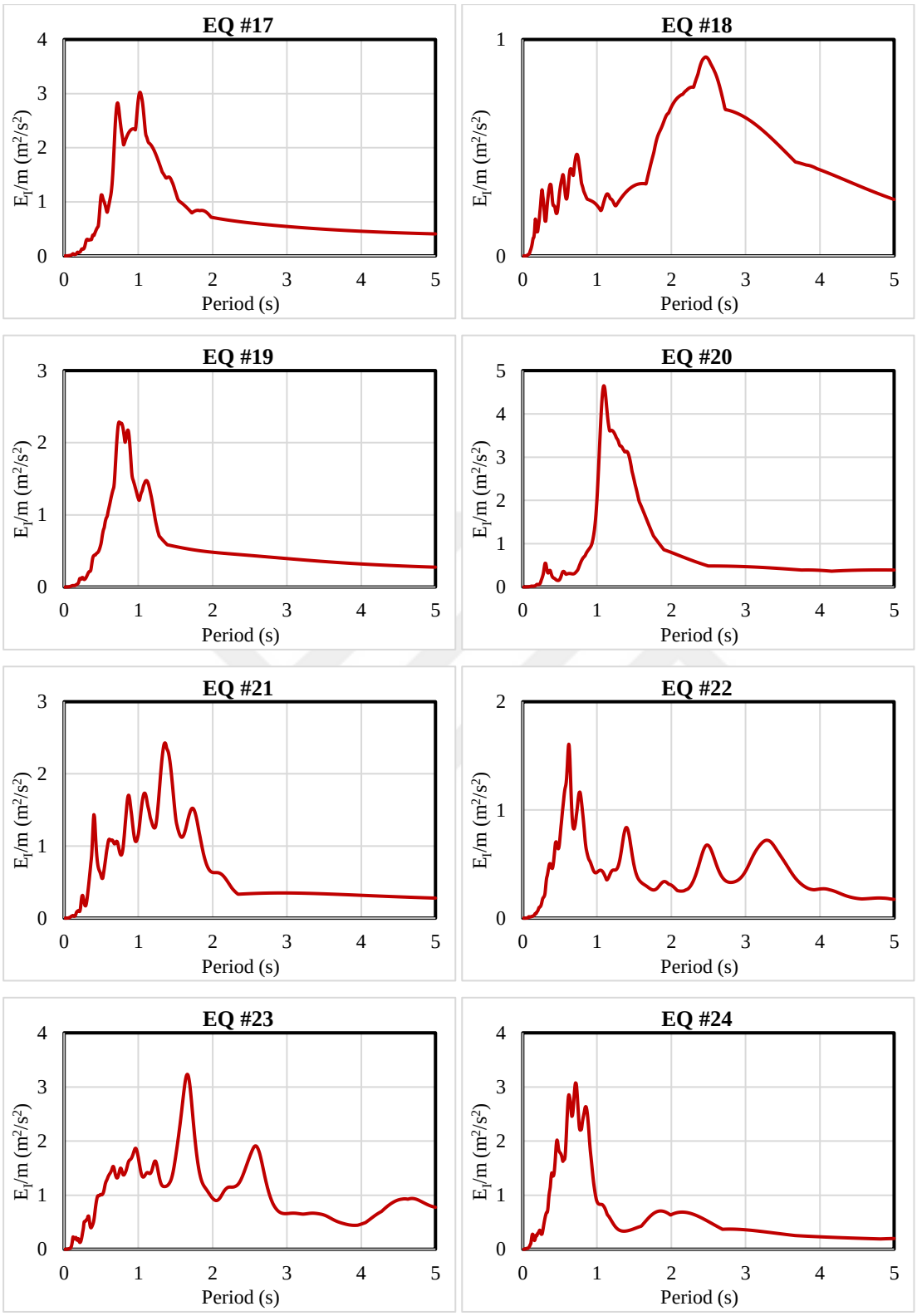

Figure A.1 (continued) : Mass-normalized input energy spectra for the *EQ* records.

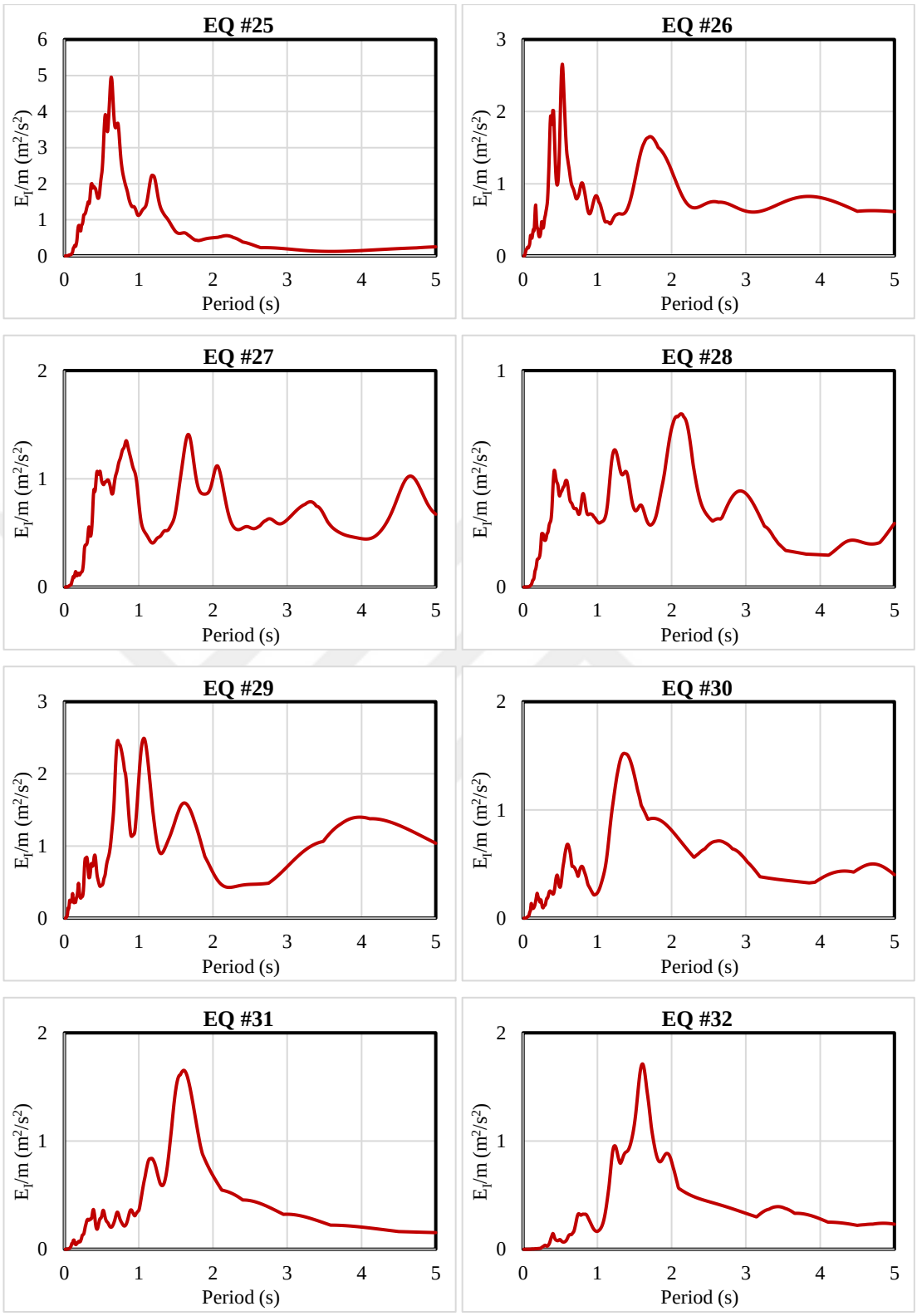

Figure A.1 (continued) : Mass-normalized input energy spectra for the *EQ* records.

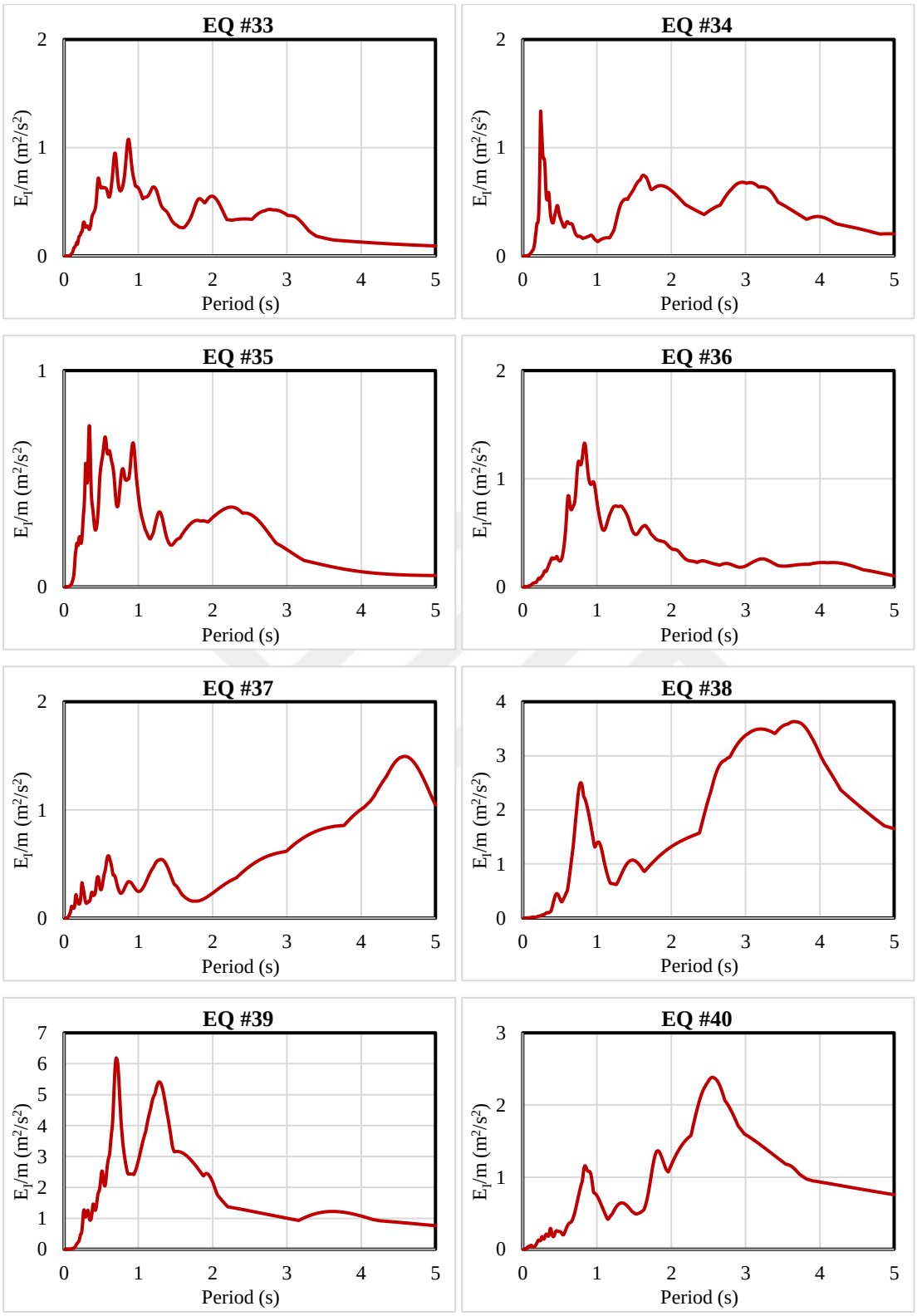

Figure A.1 (continued) : Mass-normalized input energy spectra for the *EQ* records.

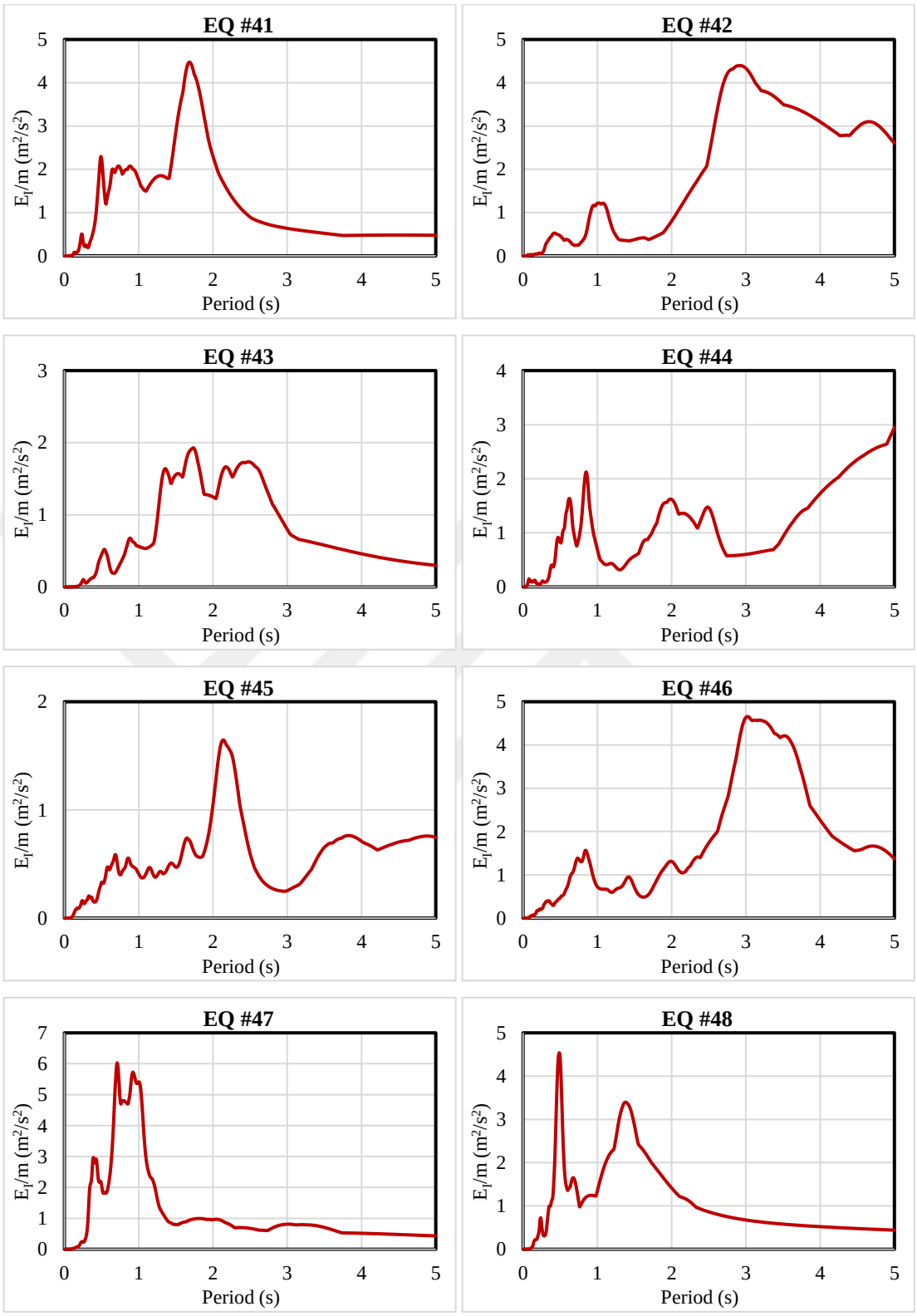

Figure A.1 (continued) : Mass-normalized input energy spectra for the *EQ* records.

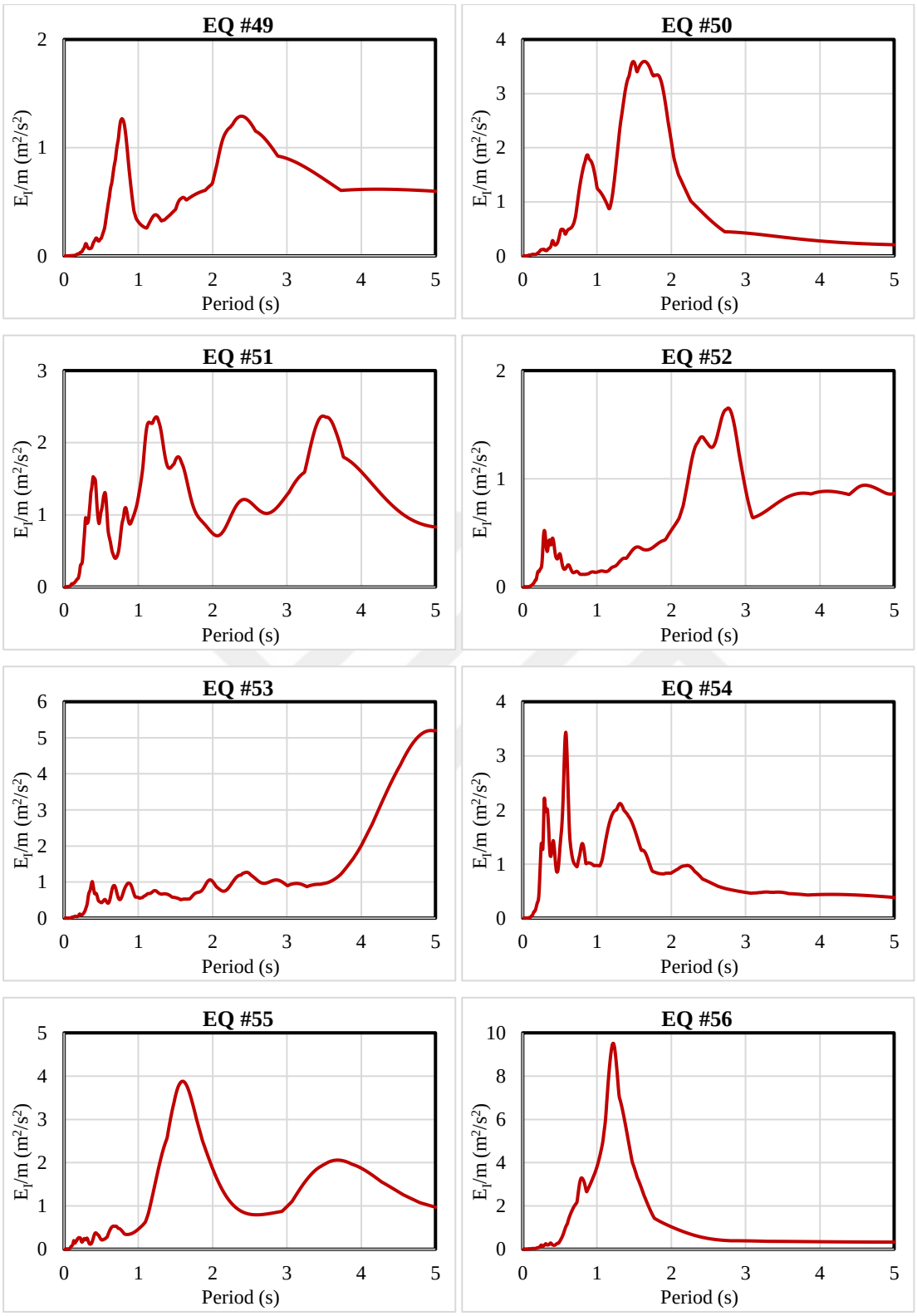

Figure A.1 (continued) : Mass-normalized input energy spectra for the *EQ* records.

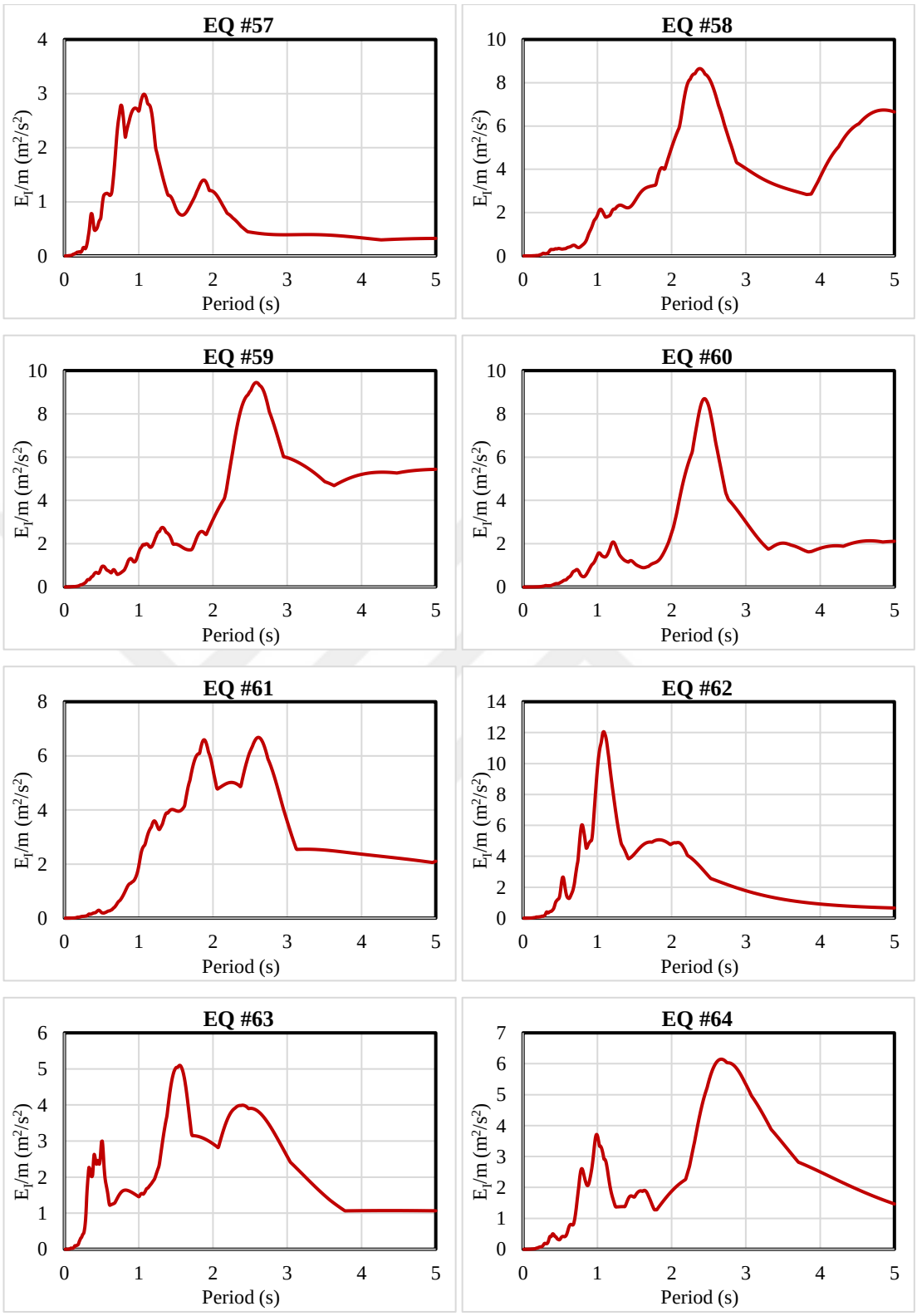

Figure A.1 (continued) : Mass-normalized input energy spectra for the *EQ* records.

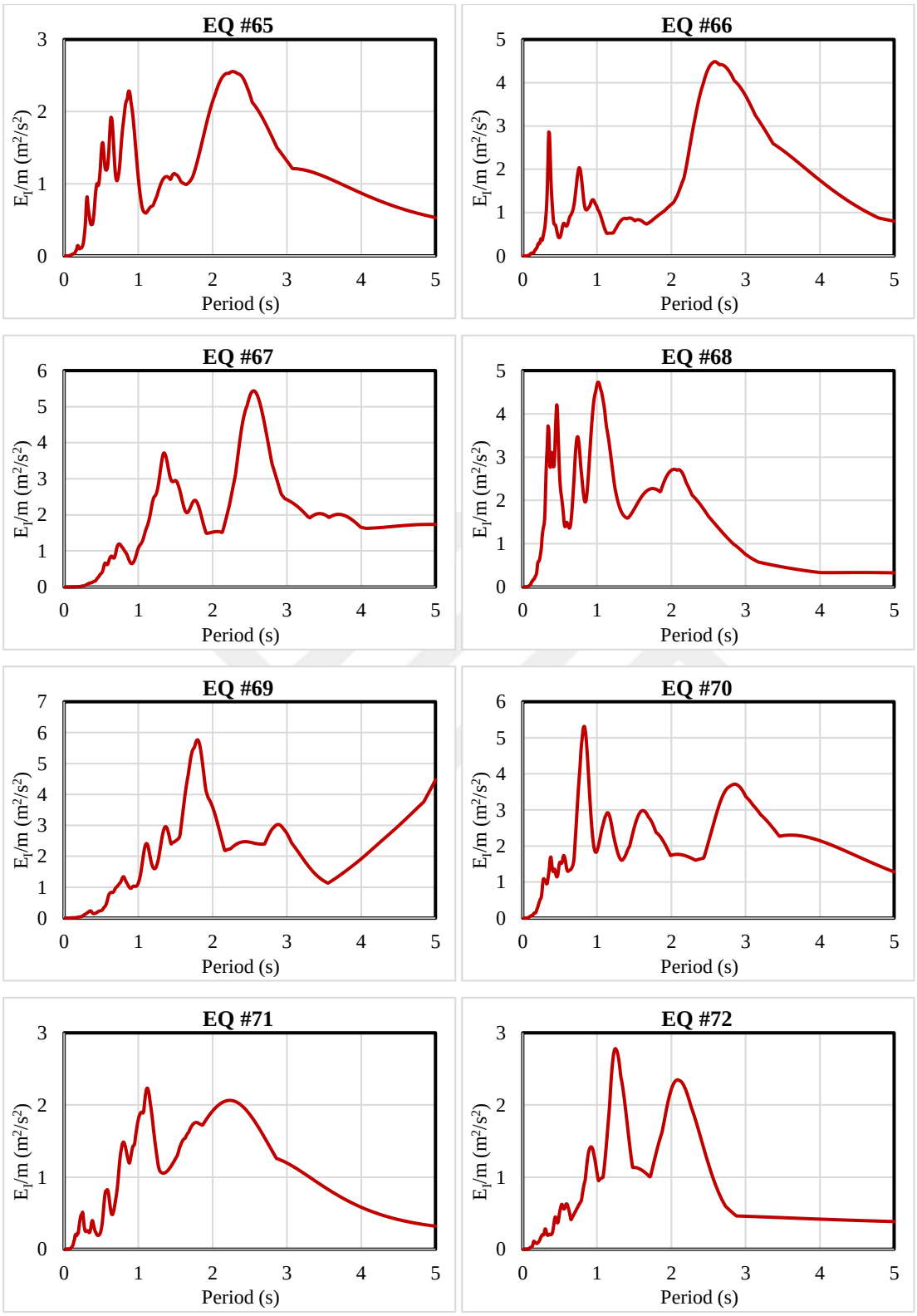

Figure A.1 (continued) : Mass-normalized input energy spectra for the *EQ* records.

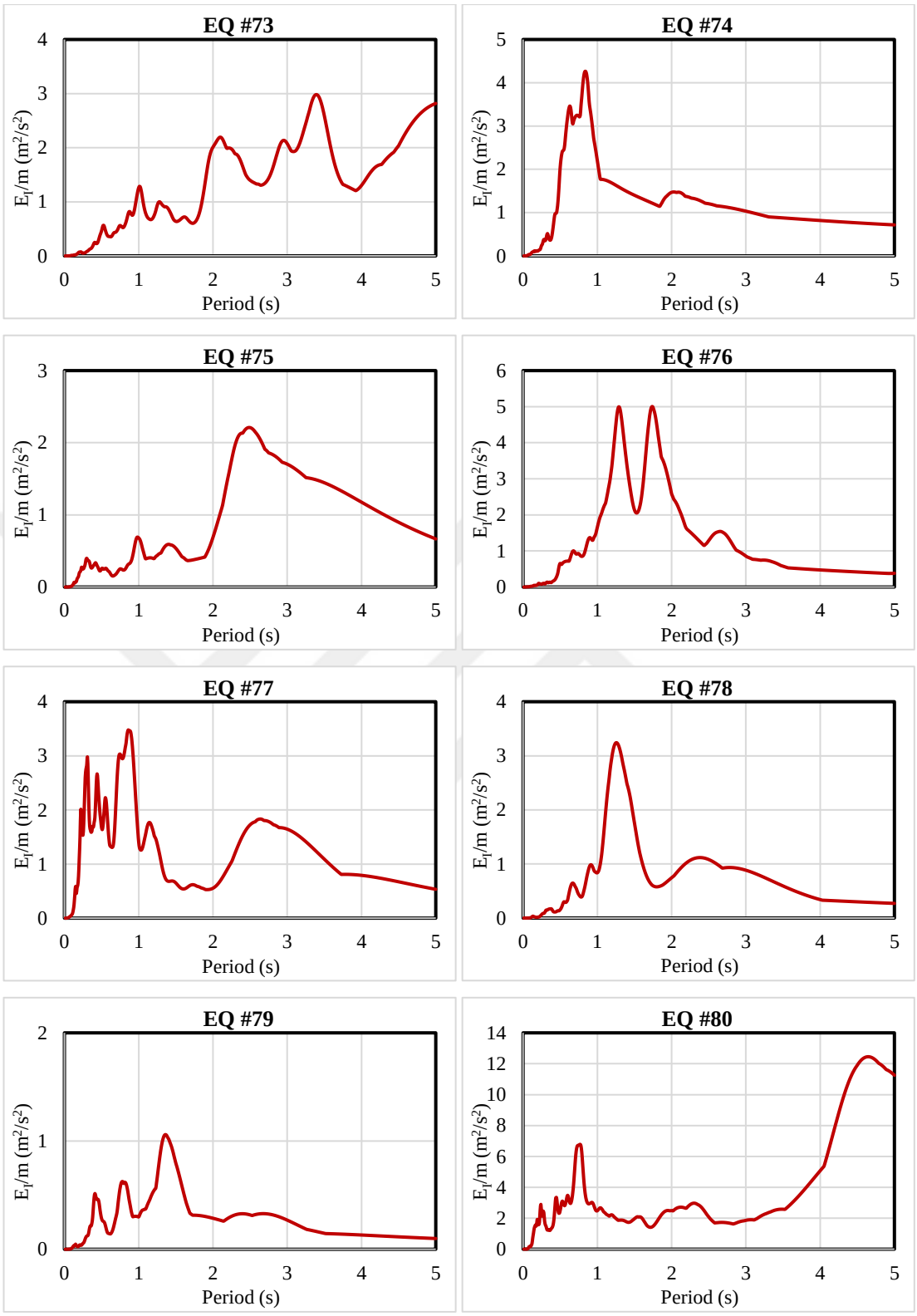

Figure A.1 (continued) : Mass-normalized input energy spectra for the *EQ* records.

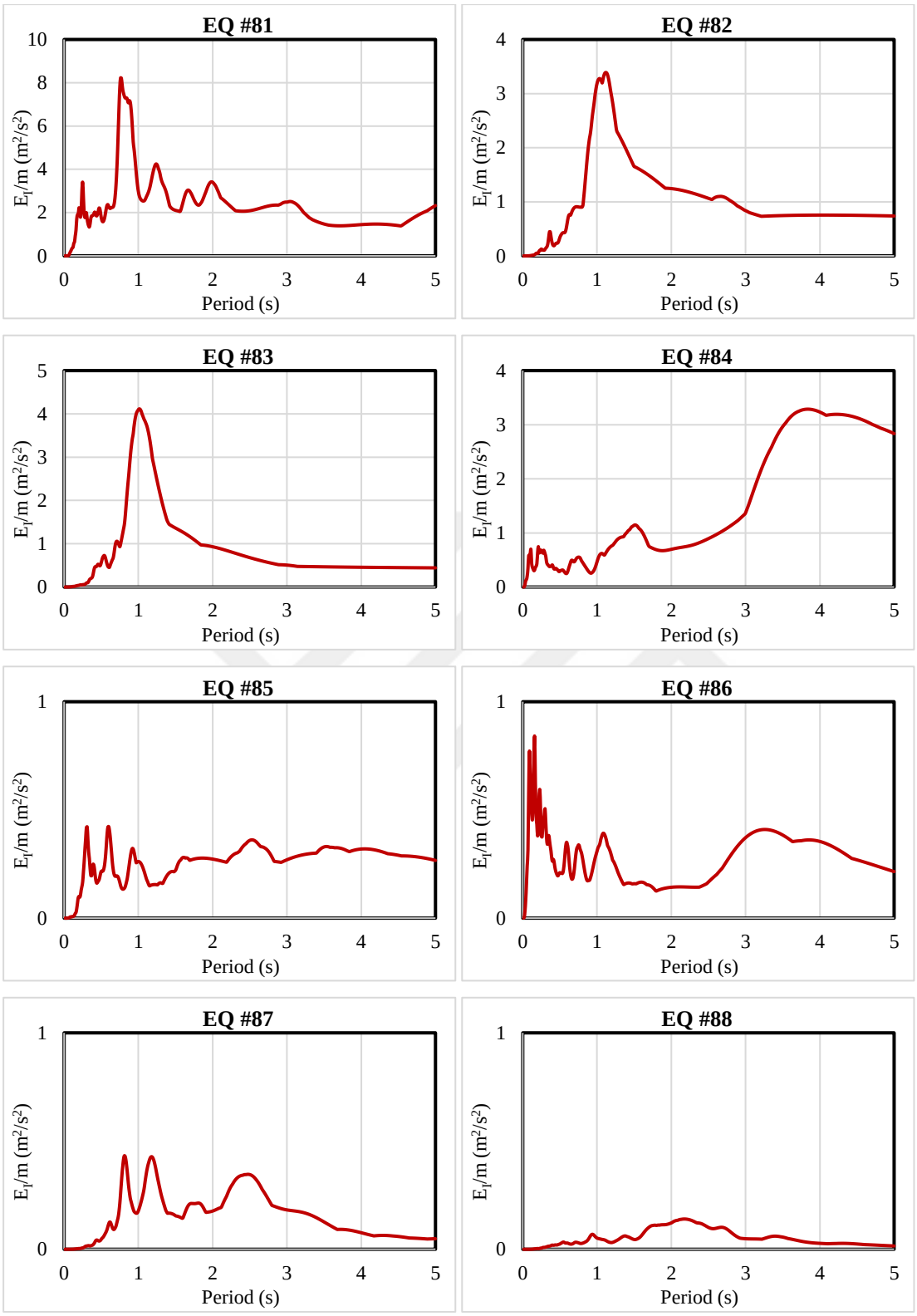

Figure A.1 (continued) : Mass-normalized input energy spectra for the *EQ* records.

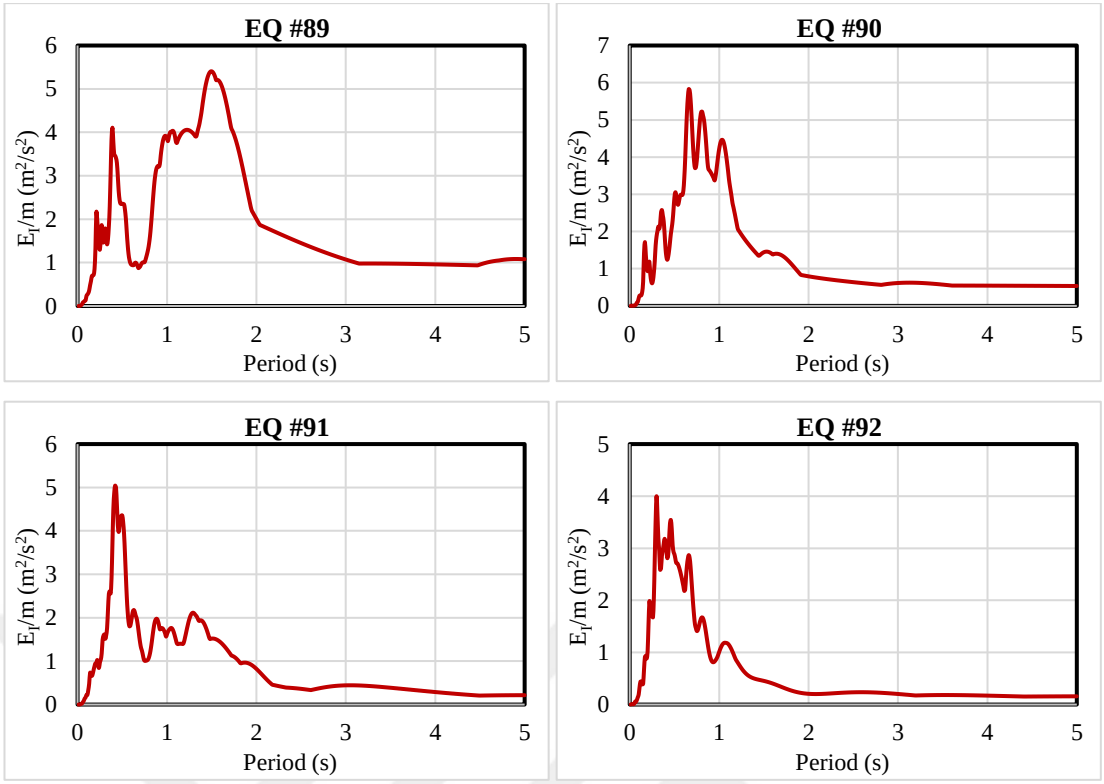

Figure A.1 (continued) : Mass-normalized input energy spectra for the *EQ* records.

APPENDIX B

Table B.1 : Input energy predictions for three- and six-story *Akbas* frames.

EQ #	*Akbas* 3-St			*Akbas* 6-St		
	$(E_I / m)_{pre}$ m^2/s^2	$(E_I / m)_{num}$ m^2/s^2	ε_{EI} %	$(E_I / m)_{pre}$ m^2/s^2	$(E_I / m)_{num}$ m^2/s^2	ε_{EI} %
1	0.516	0.491	4.8	0.653	0.631	3.3
2	1.663	1.442	14.3	1.042	0.894	15.3
3	0.217	0.210	3.3	0.286	0.278	2.9
4	0.738	0.760	2.9	1.046	0.955	9.1
5	0.080	0.085	5.8	0.176	0.169	4.1
6	0.192	0.180	6.8	0.440	0.397	10.4
7	0.562	0.533	5.3	0.216	0.211	2.4
8	0.390	0.373	4.2	0.494	0.497	0.5
9	0.120	0.122	1.7	0.177	0.171	3.7
10	0.108	0.103	4.7	0.205	0.195	4.6
11	0.850	0.840	1.2	0.379	0.371	2.3
12	0.226	0.214	5.4	0.277	0.267	3.6
13	0.134	0.132	1.6	0.274	0.263	4.0
14	1.329	2.354	55.7	4.598	2.649	53.8
15	0.449	0.443	1.3	1.678	1.462	13.8
16	1.647	1.692	2.7	1.830	1.432	24.4
17	1.872	1.603	15.4	0.950	0.900	5.5
18	0.307	0.296	3.7	0.327	0.344	5.1
19	1.955	1.445	30.0	0.548	0.573	4.5
20	0.610	0.674	9.9	1.698	1.288	27.5
21	0.948	0.923	2.6	1.026	1.056	2.9
22	0.930	0.841	10.0	0.395	0.487	20.9
23	1.278	1.251	2.1	2.283	2.090	8.9
24	2.137	1.790	17.7	0.551	0.617	11.2
25	2.040	1.922	6.0	0.923	1.102	17.7

Table B.1 (continued) : Input energy predictions for three- and six-story *Akbas* frames.

EQ #	*Akbas* 3-St			*Akbas* 6-St		
	$(E_I / m)_{pre}$ m^2/s^2	$(E_I / m)_{num}$ m^2/s^2	ε_{EI} %	$(E_I / m)_{pre}$ m^2/s^2	$(E_I / m)_{num}$ m^2/s^2	ε_{EI} %
26	0.957	0.893	6.9	1.493	1.282	15.2
27	1.188	1.161	2.3	1.046	1.004	4.2
28	0.400	0.394	1.4	0.377	0.372	1.4
29	1.981	1.676	16.7	1.437	1.170	20.5
30	0.439	0.416	5.4	0.967	0.803	18.6
31	0.214	0.228	6.3	1.442	1.135	23.9
32	0.294	0.284	3.4	1.418	1.184	18.0
33	0.632	0.640	1.2	0.299	0.322	7.6
34	0.205	0.287	33.6	0.669	0.586	13.3
35	0.524	0.513	2.1	0.291	0.297	1.9
36	1.078	1.060	1.7	0.484	0.462	4.7
37	0.244	0.245	0.7	0.234	0.242	3.2
38	2.204	1.627	30.1	0.858	0.856	0.2
39	3.000	2.412	21.7	2.943	2.363	21.8
40	0.857	0.845	1.4	0.462	0.487	5.2
41	1.770	1.573	11.8	3.297	2.400	31.5
42	0.333	0.359	7.6	0.403	0.498	21.2
43	0.392	0.398	1.5	1.363	1.042	26.7
44	1.324	1.299	1.9	0.703	0.738	4.8
45	0.422	0.415	1.5	0.544	0.535	1.7
46	1.228	1.211	1.4	0.500	0.526	5.0
47	4.367	3.363	26.0	0.930	1.106	17.2
48	1.015	0.998	1.7	2.321	1.539	40.5
49	1.129	0.986	13.5	0.480	0.473	1.4
50	1.389	1.233	11.9	3.055	1.918	45.7

Table B.1 (continued) : Input energy predictions for three- and six-story *Akbas* frames.

EQ #	*Akbas* 3-St			*Akbas* 6-St		
	$(E_I / m)_{pre}$ m^2/s^2	$(E_I / m)_{num}$ m^2/s^2	ε_{EI} %	$(E_I / m)_{pre}$ m^2/s^2	$(E_I / m)_{num}$ m^2/s^2	ε_{EI} %
51	0.934	0.977	4.5	1.639	1.345	19.7
52	0.140	0.197	34.2	0.356	0.339	5.0
53	0.683	0.688	0.7	0.504	0.518	2.7
54	1.384	1.342	3.1	1.406	1.340	4.8
55	0.363	0.346	4.9	3.332	2.144	43.4
56	2.973	2.470	18.5	2.619	2.107	21.7
57	2.233	1.762	23.6	0.761	0.839	9.7
58	0.459	0.519	12.2	2.522	2.778	9.6
59	0.706	0.837	16.9	1.681	2.277	30.1
60	0.444	0.422	4.9	0.821	0.840	2.4
61	0.809	0.984	19.5	3.438	2.931	15.9
62	5.441	4.343	22.4	4.173	2.879	36.7
63	1.570	1.593	1.5	4.587	2.683	52.4
64	2.339	1.987	16.3	1.658	1.457	12.9
65	1.732	1.673	3.5	1.053	1.055	0.1
66	1.525	1.445	5.4	0.801	0.749	6.7
67	0.953	0.930	2.4	2.176	1.914	12.8
68	2.335	2.463	5.3	2.015	1.828	9.7
69	1.218	1.189	2.4	2.637	3.147	17.6
70	4.560	3.400	29.1	2.700	1.865	36.6
71	1.361	1.172	14.9	1.320	1.122	16.3
72	0.695	0.753	8.1	1.020	0.796	24.7
73	0.487	0.480	1.5	0.651	0.677	3.8
74	3.515	2.566	31.2	1.393	1.341	3.8
75	0.240	0.254	5.7	0.405	0.415	2.6

Table B.1 (continued) : Input energy predictions for three- and six-story *Akbas* frames.

EQ #	*Akbas* 3-St			*Akbas* 6-St		
	$(E_I / m)_{pre}$ m^2/s^2	$(E_I / m)_{num}$ m^2/s^2	ε_{EI} %	$(E_I / m)_{pre}$ m^2/s^2	$(E_I / m)_{num}$ m^2/s^2	ε_{EI} %
76	0.777	0.872	11.5	2.033	2.554	22.7
77	2.909	2.329	22.1	0.793	0.943	17.3
78	0.381	0.401	5.3	1.012	0.945	6.8
79	0.557	0.532	4.6	0.533	0.492	8.1
80	5.257	4.571	14.0	2.160	2.008	7.3
81	6.926	5.046	31.4	2.149	2.392	10.7
82	0.823	1.260	42.0	1.404	1.019	31.8
83	1.215	1.775	37.5	1.170	0.897	26.3
84	0.473	0.512	7.9	0.969	0.865	11.4
85	0.149	0.198	28.1	0.277	0.282	2.0
86	0.310	0.331	6.5	0.187	0.198	5.6
87	0.376	0.366	2.6	0.130	0.124	4.6
88	0.025	0.026	2.3	0.051	0.049	4.4
89	1.427	2.279	46.0	4.722	2.723	53.7
90	4.834	3.439	33.7	1.573	1.529	2.9
91	1.119	1.271	12.7	1.669	1.559	6.8
92	1.772	1.736	2.1	0.822	0.912	10.4
Ar. Mean		11.3			13.6	
Geo. Mean		6.4			8.2	
Correlation		0.974			0.932	

Table B.2 : Input energy predictions for nine- and twenty-story *SAC-LA* frames.

EQ #	*SAC-LA* 9-St			*SAC-LA* 20-St		
	$(E_I / m)_{pre}$ m^2/s^2	$(E_I / m)_{num}$ m^2/s^2	ε_{EI} %	$(E_I / m)_{pre}$ m^2/s^2	$(E_I / m)_{num}$ m^2/s^2	ε_{EI} %
1	1.572	1.429	9.6	1.317	1.182	10.8
2	0.990	0.936	5.6	0.685	0.649	5.5
3	0.680	0.670	1.5	0.561	0.538	4.3
4	0.493	0.635	25.1	0.680	0.659	3.2
5	0.458	0.448	2.2	0.077	0.076	0.8
6	0.444	0.424	4.5	0.155	0.142	8.6
7	0.430	0.420	2.3	0.300	0.288	4.2
8	0.382	0.371	2.9	0.161	0.190	16.2
9	0.344	0.341	0.7	0.211	0.204	3.5
10	0.340	0.336	1.3	0.135	0.130	4.2
11	0.323	0.438	30.1	0.651	0.633	2.8
12	0.320	0.311	2.9	0.141	0.139	0.9
13	0.298	0.295	1.1	0.503	0.473	6.2
14	1.376	1.701	21.1	2.256	1.937	15.2
15	1.073	0.982	8.8	1.109	0.991	11.3
16	0.998	1.093	9.0	1.460	1.073	30.6
17	0.847	0.871	2.8	0.672	0.658	2.1
18	0.703	0.624	11.8	0.400	0.381	4.9
19	0.661	0.725	9.3	0.443	0.460	3.8
20	0.618	0.548	12.0	0.757	0.896	16.8
21	0.553	0.697	23.1	0.584	0.715	20.2
22	0.363	0.350	3.6	0.356	0.365	2.5
23	1.189	1.173	1.4	0.586	0.581	0.8
24	0.931	0.875	6.3	0.326	0.437	29.2
25	0.717	0.730	1.9	0.355	0.558	44.5

Table B.2 (continued) : Input energy predictions for nine- and twenty-story *SAC-LA* frames.

EQ #	*SAC-LA* 9-St			*SAC-LA* 20-St		
	$(E_I / m)_{pre}$ m^2/s^2	$(E_I / m)_{num}$ m^2/s^2	ε_{EI} %	$(E_I / m)_{pre}$ m^2/s^2	$(E_I / m)_{num}$ m^2/s^2	ε_{EI} %
26	0.713	0.676	5.3	0.798	0.738	7.9
27	0.668	0.664	0.6	0.504	0.519	2.9
28	0.581	0.576	1.0	0.206	0.242	16.0
29	0.579	0.639	9.9	1.338	1.084	21.0
30	0.551	0.528	4.4	0.479	0.565	16.5
31	0.475	0.452	5.0	0.265	0.258	2.6
32	0.460	0.429	7.1	0.383	0.367	4.2
33	0.422	0.468	10.2	0.193	0.216	11.2
34	0.410	0.409	0.1	0.354	0.368	3.9
35	0.390	0.379	3.0	0.126	0.155	20.5
36	0.360	0.483	29.2	0.310	0.315	1.4
37	0.350	0.338	3.3	0.821	0.755	8.3
38	1.547	1.786	14.4	3.134	1.722	58.2
39	1.512	1.587	4.8	1.793	1.452	21.0
40	1.496	1.404	6.3	0.932	0.841	10.3
41	1.437	1.228	15.7	0.698	0.693	0.7
42	1.386	1.725	21.8	2.818	1.672	51.1
43	1.385	1.228	12.0	0.628	0.628	0.0
44	1.337	1.262	5.8	1.288	1.295	0.5
45	1.319	1.187	10.5	0.706	0.659	6.9
46	1.270	1.331	4.7	2.624	1.926	30.6
47	1.251	1.789	35.4	0.760	0.935	20.7
48	1.207	1.085	10.7	0.892	0.901	1.0
49	1.151	0.917	22.7	0.597	0.559	6.5
50	1.074	0.946	12.7	0.612	0.747	19.9

Table B.2 (continued) : Input energy predictions for nine- and twenty-story *SAC-LA* frames.

EQ #	*SAC-LA* 9-St			*SAC-LA* 20-St		
	$(E_I / m)_{pre}$ m^2/s^2	$(E_I / m)_{num}$ m^2/s^2	ε_{EI} %	$(E_I / m)_{pre}$ m^2/s^2	$(E_I / m)_{num}$ m^2/s^2	ε_{EI} %
51	1.032	0.964	6.9	1.775	1.470	18.8
52	1.005	0.921	8.7	0.762	0.691	9.8
53	0.976	0.999	2.3	1.302	1.686	25.7
54	0.952	0.915	4.0	0.670	0.735	9.3
55	0.923	0.864	6.7	1.985	1.312	40.8
56	0.918	1.123	20.0	1.262	1.342	6.1
57	0.895	0.982	9.3	0.587	0.601	2.4
58	7.129	4.354	48.3	2.695	3.764	33.1
59	5.535	4.421	22.4	4.553	2.993	41.3
60	5.297	3.529	40.1	1.587	1.528	3.8
61	4.391	3.162	32.6	2.500	2.613	4.4
62	3.855	2.781	32.4	1.651	1.734	4.9
63	3.564	2.278	44.0	1.324	1.298	2.0
64	2.824	2.984	5.5	2.535	1.631	43.4
65	2.464	1.694	37.0	0.991	0.895	10.2
66	2.455	2.298	6.6	1.863	1.297	35.8
67	2.431	2.695	10.3	2.123	1.668	24.0
68	2.168	1.849	15.9	0.648	0.841	25.8
69	2.092	2.379	12.8	1.680	1.914	13.0
70	2.053	1.831	11.4	2.244	1.604	33.3
71	1.904	1.371	32.6	0.750	0.725	3.4
72	1.805	1.409	24.6	0.681	0.748	9.4
73	1.750	1.679	4.1	1.213	1.599	27.5
74	1.689	1.492	12.4	1.018	1.007	1.1
75	1.614	1.398	14.4	1.152	0.862	28.7

Table B.2 (continued) : Input energy predictions for nine- and twenty-story *SAC-LA* frames.

EQ #	*SAC-LA* 9-St			*SAC-LA* 20-St		
	$(E_I / m)_{pre}$ m^2/s^2	$(E_I / m)_{num}$ m^2/s^2	ε_{EI} %	$(E_I / m)_{pre}$ m^2/s^2	$(E_I / m)_{num}$ m^2/s^2	ε_{EI} %
76	1.412	1.390	1.5	1.048	1.211	14.4
77	1.403	1.286	8.7	0.900	0.918	2.0
78	1.004	0.878	13.3	0.749	0.829	10.2
79	0.339	0.328	3.3	0.264	0.330	22.2
80	2.951	2.577	13.5	3.818	4.519	16.8
81	2.782	2.627	5.7	1.897	1.735	8.9
82	1.178	1.051	11.4	0.936	0.882	5.9
83	0.954	0.966	1.3	0.669	0.674	0.7
84	0.705	0.674	4.4	2.889	1.997	36.5
85	0.275	0.276	0.4	0.286	0.285	0.5
86	0.151	0.158	4.2	0.337	0.339	0.7
87	0.299	0.292	2.4	0.116	0.118	2.1
88	0.118	0.116	2.2	0.036	0.035	2.1
89	1.793	1.668	7.2	1.343	1.393	3.7
90	1.215	1.306	7.2	0.832	0.964	14.7
91	0.714	0.955	28.9	0.568	0.765	29.6
92	0.453	0.667	38.1	0.274	0.449	48.6
Ar. Mean		11.7			13.9	
Geo. Mean		7.0			7.2	
Correlation		0.959			0.914	

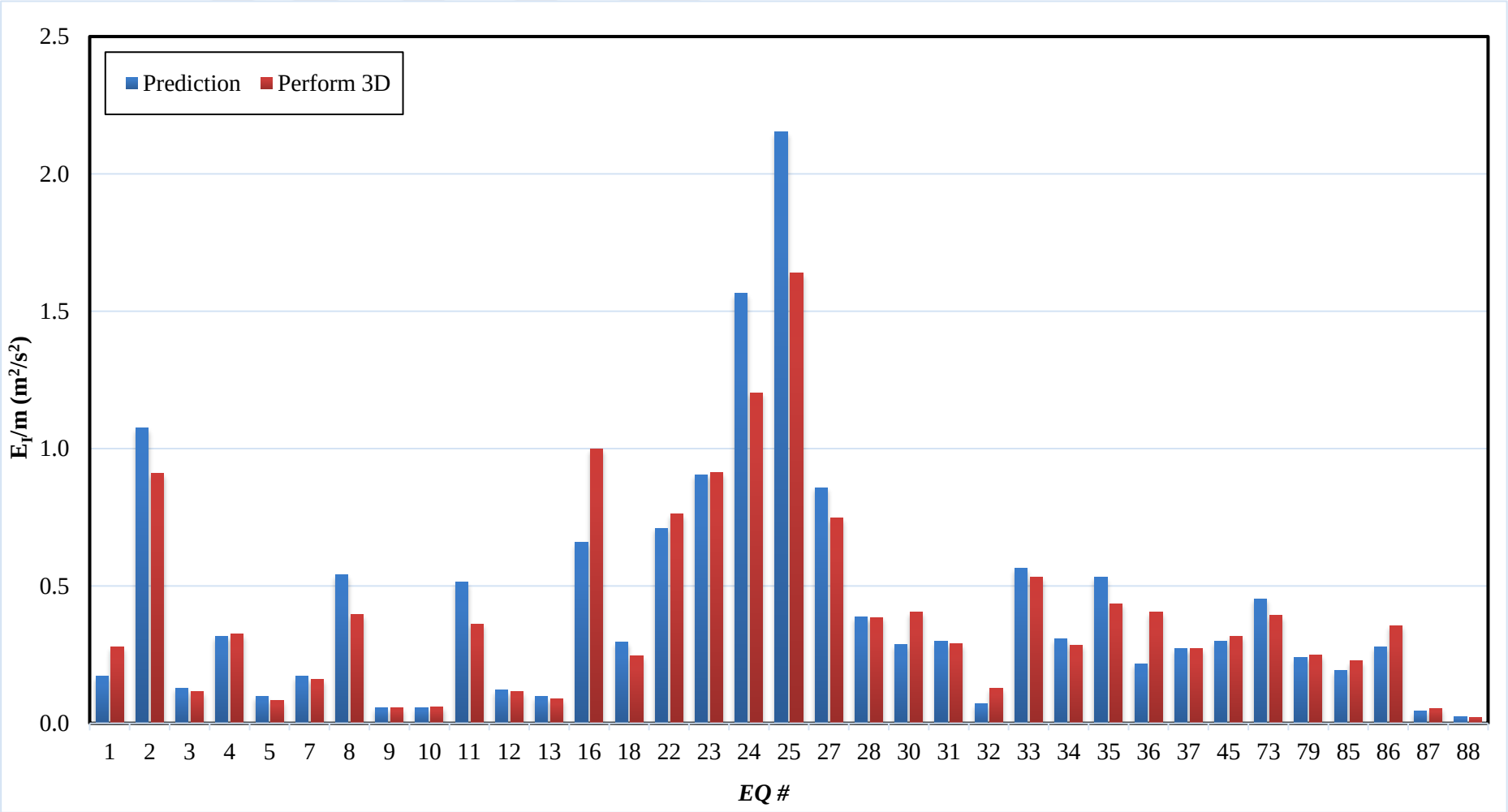

Figure B.1 : E_I/m comparison between methodology and *NLTHA* for *Manoukas* 3-St frame using the EQ records with a PGV ≤ 50 cm/s.

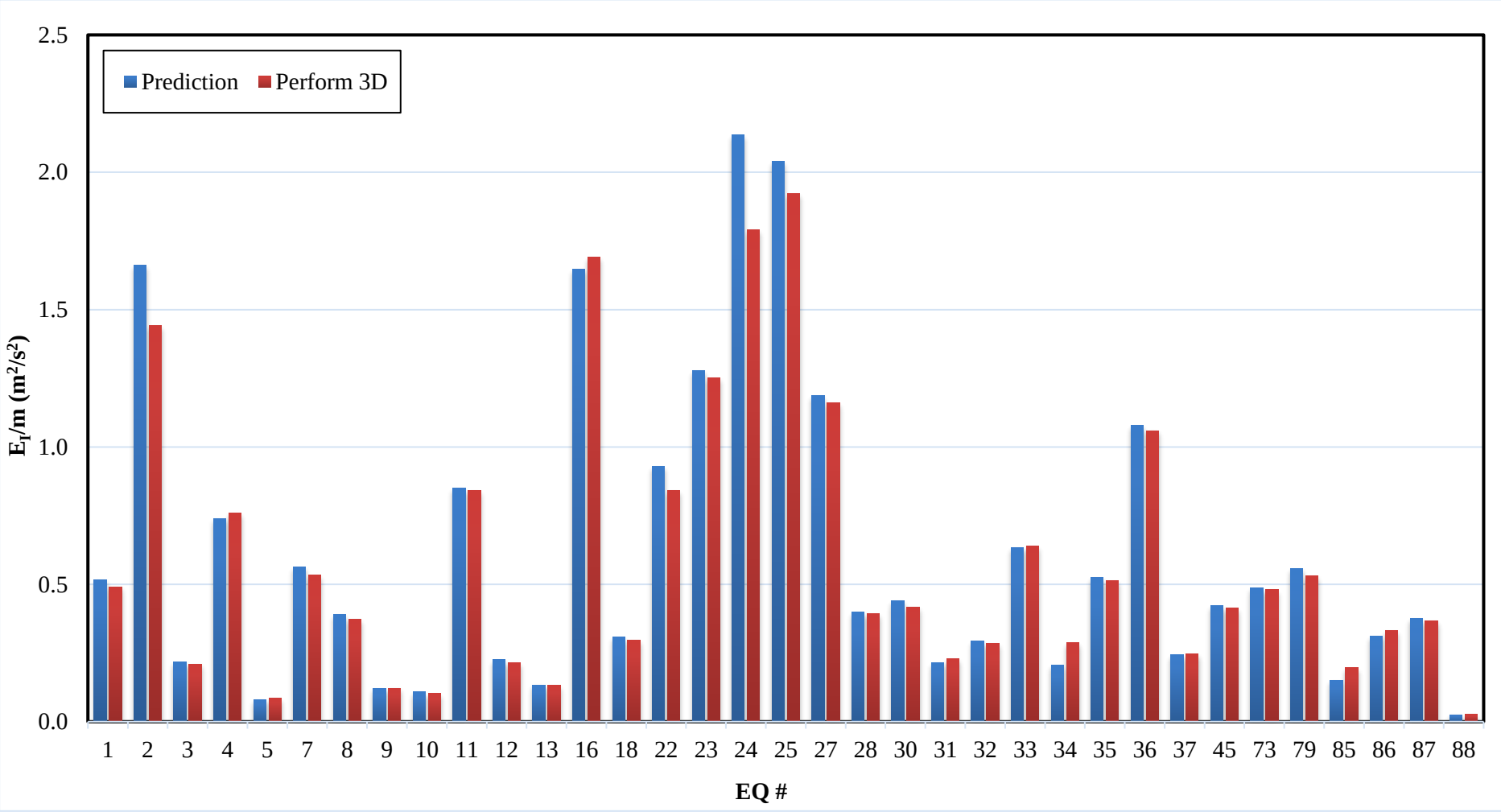

Figure B.2 : E_I/m comparison between methodology and *NLTHA* for *Akbas* 3-St frame using the EQ records with a PGV ≤ 50 cm/s.

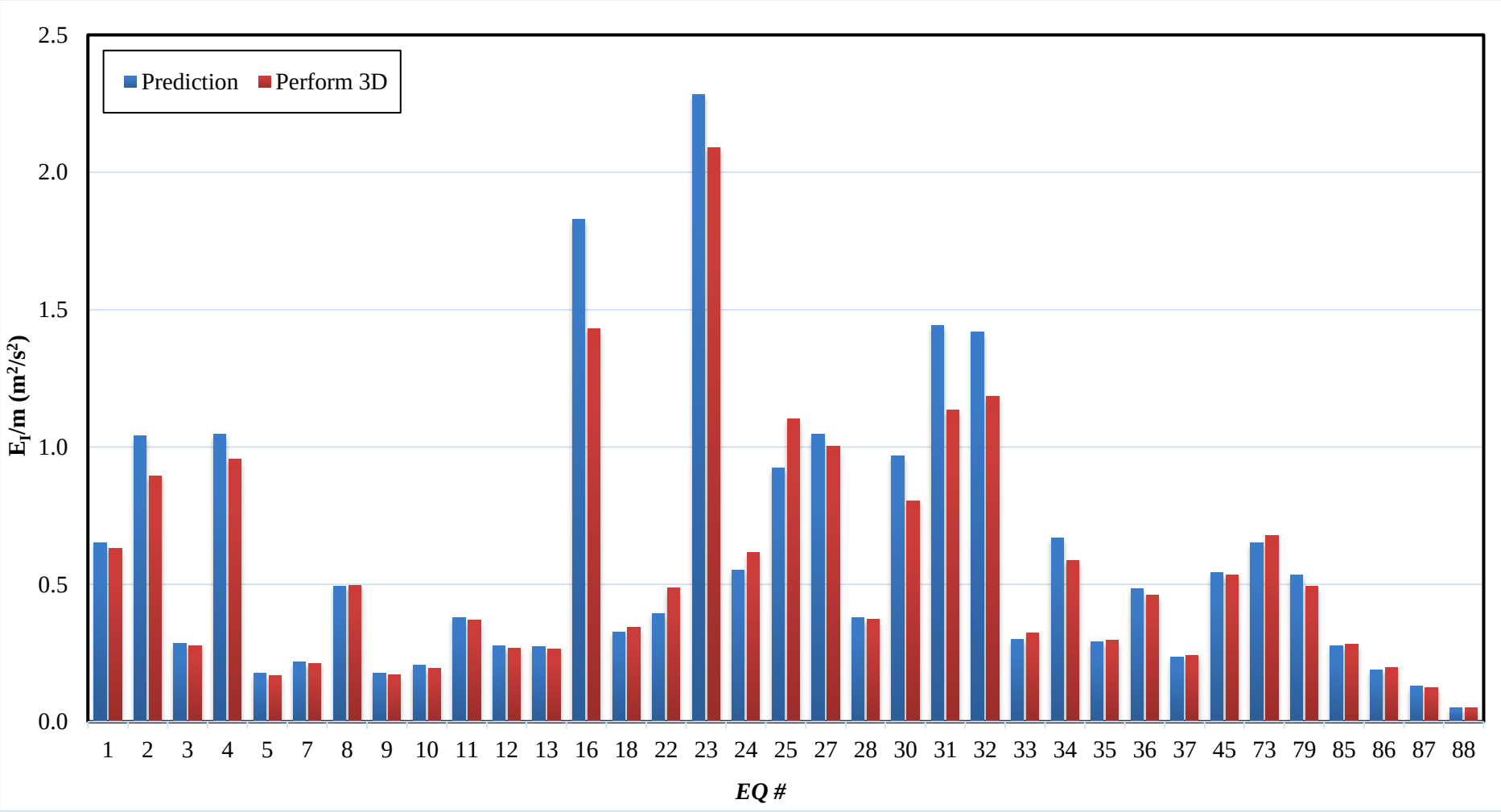

Figure B.3 : E_I/m comparison between methodology and *NLTHA* for *Akbas* 6-St frame using the EQ records with a PGV ≤ 50 cm/s.

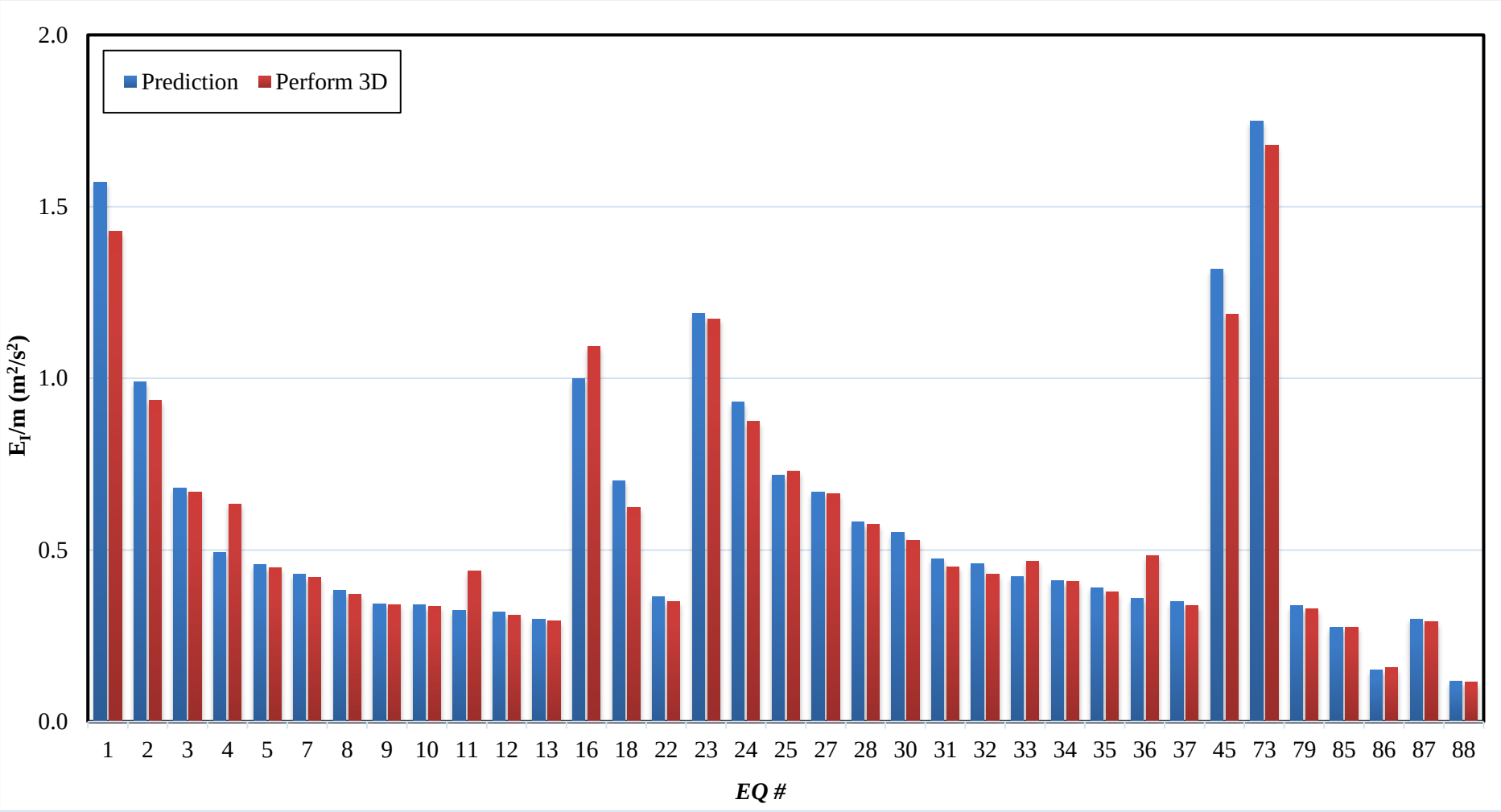

Figure B.4 : E_I/m comparison between methodology and *NLTHA* for *SAC-LA* 9-St frame using the EQ records with a PGV ≤ 50 cm/s.

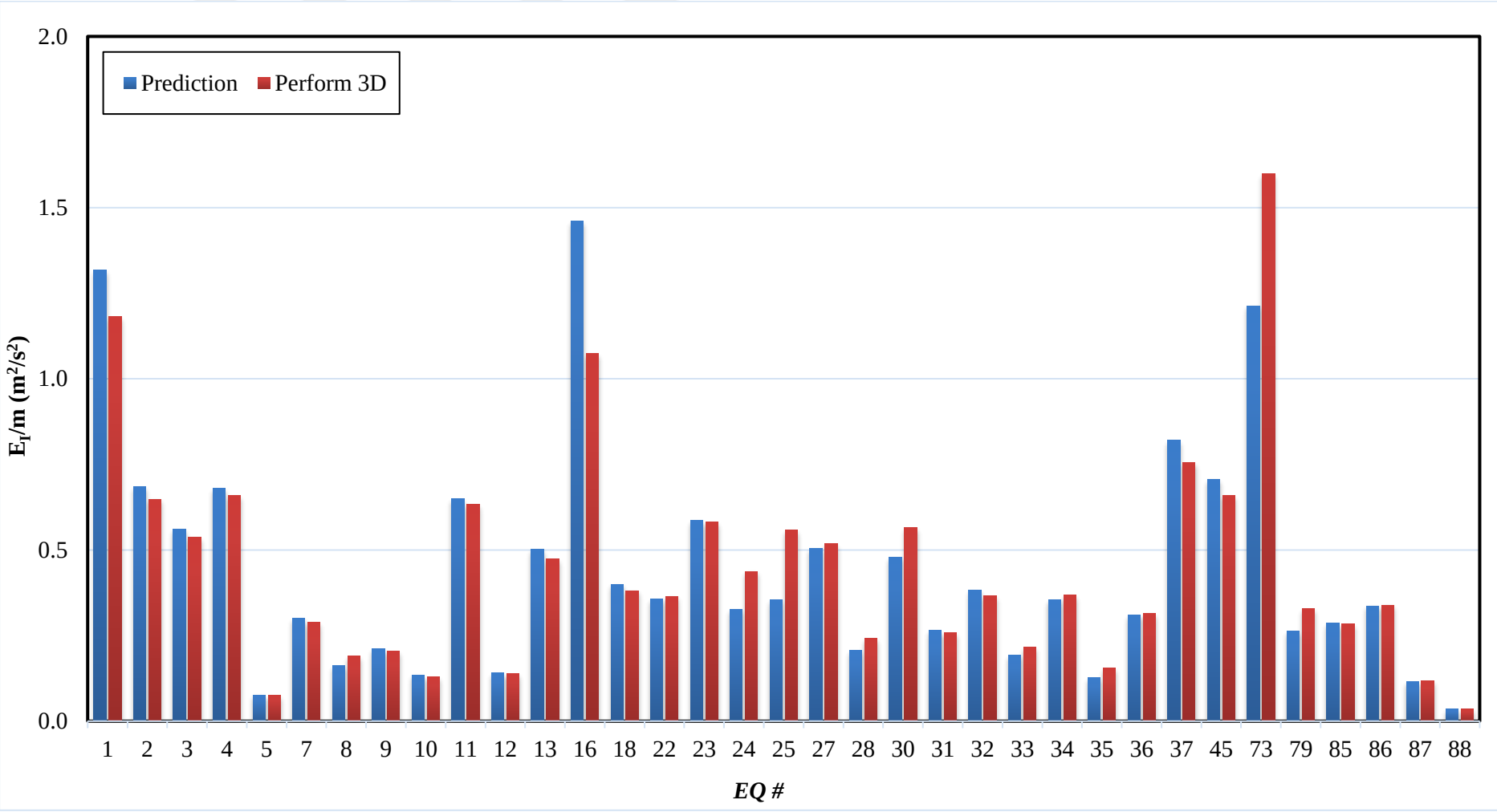

Figure B.5 : E_I/m comparison between methodology and *NLTHA* for *SAC-LA* 20-St frame using the EQ records with a PGV ≤ 50 cm/s.

APPENDIX C

Table C.1 : Top displacement predictions for three- and six-story *Akbas* frames.

EQ #	*Akbas* 3-St			*Akbas* 6-St		
	$(\delta_{top})_{pre}$ m	$(\delta_{top})_{num}$ m	ε_{δ} %	$(\delta_{top})_{pre}$ m	$(\delta_{top})_{num}$ m	ε_{δ} %
1	0.104	0.107	3.0	0.197	0.244	21.1
2	0.186	0.167	11.0	0.249	0.330	27.9
3	0.067	0.056	18.1	0.130	0.141	7.7
4	0.124	0.112	10.3	0.250	0.218	13.6
5	0.041	0.036	13.3	0.102	0.124	19.3
6	0.063	0.084	28.0	0.162	0.234	36.3
7	0.108	0.086	22.8	0.113	0.093	19.4
8	0.090	0.098	8.0	0.172	0.151	12.8
9	0.050	0.046	9.4	0.103	0.102	0.3
10	0.047	0.062	25.9	0.110	0.111	0.8
11	0.133	0.108	21.0	0.150	0.132	13.3
12	0.069	0.049	32.9	0.129	0.115	11.3
13	0.053	0.036	37.9	0.128	0.117	8.7
14	0.167	0.283	51.7	0.523	0.647	21.2
15	0.097	0.077	23.3	0.316	0.284	10.7
16	0.186	0.241	26.1	0.330	0.336	1.7
17	0.198	0.258	26.4	0.238	0.331	32.6
18	0.080	0.092	14.4	0.140	0.221	45.1
19	0.202	0.180	11.6	0.181	0.273	40.8
20	0.113	0.147	25.9	0.318	0.344	8.0
21	0.141	0.127	10.5	0.247	0.221	11.0
22	0.139	0.140	0.1	0.153	0.195	24.0
23	0.163	0.086	62.1	0.369	0.353	4.3
24	0.211	0.205	2.9	0.181	0.181	0.1
25	0.206	0.174	16.9	0.234	0.190	20.8

Table C.1 (continued) : Top displacement predictions for three- and six-story *Akbas* frames.

EQ #	*Akbas* 3-St			*Akbas* 6-St		
	$(\delta_{top})_{pre}$ m	$(\delta_{top})_{num}$ m	ε_{δ} %	$(\delta_{top})_{pre}$ m	$(\delta_{top})_{num}$ m	ε_{δ} %
26	0.141	0.152	7.5	0.298	0.301	0.9
27	0.157	0.103	41.7	0.250	0.193	25.4
28	0.091	0.093	1.8	0.150	0.161	7.1
29	0.203	0.155	27.0	0.293	0.310	5.7
30	0.095	0.104	8.4	0.240	0.254	5.9
31	0.067	0.079	17.3	0.293	0.321	9.1
32	0.078	0.085	8.4	0.291	0.259	11.6
33	0.115	0.108	5.7	0.133	0.138	3.3
34	0.065	0.064	1.6	0.200	0.206	3.1
35	0.104	0.090	14.3	0.132	0.136	3.2
36	0.150	0.128	15.7	0.170	0.159	6.8
37	0.071	0.089	23.1	0.118	0.153	25.8
38	0.215	0.212	1.4	0.226	0.360	45.8
39	0.250	0.276	9.7	0.419	0.373	11.5
40	0.134	0.158	16.9	0.166	0.270	47.9
41	0.192	0.213	10.2	0.443	0.396	11.3
42	0.083	0.112	29.2	0.155	0.277	56.6
43	0.090	0.123	30.6	0.285	0.337	16.6
44	0.166	0.141	16.7	0.205	0.256	22.1
45	0.094	0.073	24.7	0.180	0.179	0.6
46	0.160	0.123	26.0	0.173	0.200	14.6
47	0.302	0.249	19.2	0.235	0.257	8.9
48	0.145	0.164	12.2	0.372	0.363	2.5
49	0.154	0.153	0.1	0.169	0.266	44.4
50	0.170	0.181	6.3	0.427	0.384	10.5

Table C.1 (continued) : Top displacement predictions for three- and six-story *Akbas* frames.

EQ #	*Akbas* 3-St			*Akbas* 6-St		
	$(\delta_{top})_{pre}$ m	$(\delta_{top})_{num}$ m	ε_{δ} %	$(\delta_{top})_{pre}$ m	$(\delta_{top})_{num}$ m	ε_{δ} %
51	0.140	0.127	9.4	0.312	0.410	27.0
52	0.054	0.059	8.4	0.146	0.236	47.5
53	0.119	0.118	1.3	0.173	0.228	27.5
54	0.170	0.205	18.6	0.289	0.310	6.9
55	0.087	0.117	29.9	0.445	0.423	5.1
56	0.249	0.251	0.6	0.395	0.333	17.1
57	0.216	0.249	14.2	0.213	0.214	0.6
58	0.098	0.126	25.4	0.388	0.562	36.7
59	0.121	0.184	40.8	0.316	0.528	50.1
60	0.096	0.078	20.8	0.221	0.289	26.7
61	0.130	0.229	55.2	0.452	0.586	25.8
62	0.337	0.236	35.5	0.499	0.675	30.0
63	0.181	0.178	1.8	0.523	0.396	27.5
64	0.221	0.235	6.1	0.314	0.336	6.6
65	0.190	0.238	22.4	0.250	0.390	43.5
66	0.178	0.235	27.4	0.218	0.309	34.3
67	0.141	0.149	5.6	0.360	0.530	38.3
68	0.221	0.170	25.8	0.346	0.532	42.3
69	0.160	0.143	10.8	0.396	0.618	43.7
70	0.309	0.276	11.3	0.401	0.574	35.5
71	0.168	0.161	4.2	0.280	0.430	42.2
72	0.120	0.191	45.3	0.247	0.278	12.1
73	0.101	0.104	2.9	0.197	0.221	11.4
74	0.271	0.247	9.3	0.288	0.405	33.7
75	0.071	0.090	24.7	0.155	0.274	55.2

Table C.1 (continued) : Top displacement predictions for three- and six-story *Akbas* frames.

EQ #	*Akbas* 3-St			*Akbas* 6-St		
	$(\delta_{top})_{pre}$ m	$(\delta_{top})_{num}$ m	ε_{δ} %	$(\delta_{top})_{pre}$ m	$(\delta_{top})_{num}$ m	ε_{δ} %
76	0.127	0.193	40.8	0.348	0.427	20.4
77	0.246	0.242	1.6	0.217	0.206	5.5
78	0.089	0.129	36.7	0.245	0.282	14.0
79	0.108	0.131	19.3	0.178	0.216	19.3
80	0.330	0.243	30.5	0.359	0.401	11.2
81	0.380	0.266	35.4	0.358	0.371	3.7
82	0.131	0.195	39.3	0.289	0.358	21.2
83	0.159	0.210	27.4	0.264	0.352	28.6
84	0.098	0.139	34.4	0.240	0.402	50.4
85	0.056	0.055	0.5	0.128	0.185	36.2
86	0.078	0.073	6.1	0.106	0.113	6.7
87	0.089	0.097	8.9	0.088	0.138	44.3
88	0.023	0.022	5.7	0.055	0.072	26.2
89	0.172	0.213	21.6	0.530	0.407	26.3
90	0.317	0.282	11.9	0.306	0.342	11.1
91	0.151	0.162	7.0	0.315	0.271	15.1
92	0.192	0.171	11.4	0.221	0.193	13.5
Ar. Mean		18.3			20.6	
Geo. Mean		11.7			13.0	
Correlation		0.857			0.849	

Table C.2 : Top displacement predictions for nine- and twenty-story *SAC-LA* frames.

EQ #	*SAC-LA* 9-St			*SAC-LA* 20-St		
	$(\delta_{top})_{pre}$ m	$(\delta_{top})_{num}$ m	ε_{δ} %	$(\delta_{top})_{pre}$ m	$(\delta_{top})_{num}$ m	ε_{δ} %
1	0.452	0.469	3.6	0.687	0.609	12.0
2	0.359	0.306	15.9	0.495	0.579	15.6
3	0.297	0.416	33.3	0.448	0.665	38.9
4	0.253	0.269	5.9	0.494	0.505	2.3
5	0.244	0.371	41.2	0.166	0.222	29.0
6	0.240	0.346	36.1	0.235	0.329	33.2
7	0.237	0.204	14.8	0.328	0.350	6.4
8	0.223	0.211	5.4	0.240	0.190	23.6
9	0.212	0.192	9.8	0.275	0.256	7.2
10	0.210	0.290	31.7	0.220	0.272	21.0
11	0.205	0.176	15.5	0.483	0.488	1.0
12	0.204	0.196	4.2	0.225	0.247	9.6
13	0.197	0.178	9.9	0.424	0.482	12.8
14	0.423	0.650	42.3	0.899	0.799	11.7
15	0.374	0.481	25.1	0.630	0.886	33.7
16	0.360	0.379	4.9	0.723	0.612	16.7
17	0.332	0.338	1.8	0.490	0.256	62.7
18	0.302	0.361	17.6	0.379	0.569	40.3
19	0.293	0.294	0.3	0.398	0.276	36.2
20	0.284	0.372	27.0	0.521	0.532	2.2
21	0.268	0.267	0.4	0.457	0.334	31.1
22	0.217	0.261	18.2	0.357	0.347	2.9
23	0.393	0.304	25.5	0.458	0.359	24.1
24	0.348	0.373	6.8	0.342	0.341	0.1
25	0.305	0.296	3.3	0.356	0.228	44.0

Table C.2 (continued) : Top displacement predictions for nine- and twenty-story *SAC-LA* frames.

EQ #	*SAC-LA* 9-St			*SAC-LA* 20-St		
	$(\delta_{top})_{pre}$ m	$(\delta_{top})_{num}$ m	ε_{δ} %	$(\delta_{top})_{pre}$ m	$(\delta_{top})_{num}$ m	ε_{δ} %
26	0.305	0.435	35.3	0.535	0.678	23.7
27	0.295	0.257	13.6	0.425	0.419	1.4
28	0.275	0.291	5.5	0.272	0.372	31.1
29	0.274	0.265	3.3	0.692	0.738	6.4
30	0.268	0.427	45.7	0.414	0.602	37.0
31	0.249	0.343	32.0	0.308	0.357	14.7
32	0.245	0.375	42.0	0.370	0.449	19.3
33	0.234	0.344	37.8	0.263	0.248	5.8
34	0.231	0.358	43.1	0.356	0.510	35.6
35	0.225	0.290	25.0	0.212	0.150	34.6
36	0.216	0.184	16.1	0.333	0.336	0.8
37	0.213	0.338	45.3	0.542	0.787	36.9
38	0.449	0.614	31.2	1.059	1.038	2.1
39	0.444	0.523	16.5	0.801	0.726	9.9
40	0.441	0.571	25.7	0.578	0.920	45.7
41	0.433	0.420	2.9	0.500	0.662	27.8
42	0.425	0.645	41.2	1.005	1.382	31.6
43	0.425	0.573	29.8	0.474	0.543	13.5
44	0.417	0.525	22.9	0.679	0.838	20.9
45	0.414	0.403	2.8	0.503	0.594	16.6
46	0.407	0.437	7.2	0.969	0.987	1.8
47	0.403	0.411	1.8	0.522	0.542	3.8
48	0.396	0.350	12.4	0.565	0.496	13.0
49	0.387	0.395	2.0	0.462	0.644	32.8
50	0.374	0.384	2.6	0.468	0.393	17.6

Table C.2 (continued) : Top displacement predictions for nine- and twenty-story *SAC-LA* frames.

EQ #	*SAC-LA* 9-St			*SAC-LA* 20-St		
	$(\delta_{top})_{pre}$ m	$(\delta_{top})_{num}$ m	ε_{δ} %	$(\delta_{top})_{pre}$ m	$(\delta_{top})_{num}$ m	ε_{δ} %
51	0.366	0.484	27.7	0.797	0.854	6.9
52	0.362	0.409	12.3	0.522	0.883	51.4
53	0.356	0.438	20.6	0.683	0.732	7.0
54	0.352	0.379	7.4	0.490	0.545	10.7
55	0.347	0.545	44.5	0.843	0.780	7.7
56	0.346	0.309	11.3	0.672	0.312	73.3
57	0.341	0.428	22.5	0.458	0.277	49.5
58	0.963	0.942	2.3	0.982	1.331	30.1
59	0.849	1.052	21.4	1.277	1.861	37.2
60	0.830	0.628	27.7	0.754	0.963	24.3
61	0.756	0.827	8.9	0.946	1.208	24.3
62	0.708	0.668	5.8	0.769	0.478	46.6
63	0.681	0.560	19.5	0.689	0.710	3.0
64	0.606	0.743	20.3	0.953	0.750	23.8
65	0.566	0.584	3.1	0.596	0.578	3.0
66	0.565	0.526	7.1	0.817	0.906	10.4
67	0.562	0.653	14.9	0.872	1.156	28.0
68	0.531	0.613	14.2	0.482	0.359	29.2
69	0.522	0.724	32.5	0.776	1.014	26.7
70	0.517	0.522	0.9	0.897	0.837	6.9
71	0.498	0.628	23.2	0.518	0.524	1.2
72	0.485	0.529	8.8	0.494	0.462	6.7
73	0.477	0.459	3.9	0.659	0.789	17.9
74	0.469	0.550	15.9	0.604	0.761	23.1
75	0.458	0.497	8.2	0.642	0.811	23.2

Table C.2 (continued) : Top displacement predictions for nine- and twenty-story *SAC-LA* frames.

EQ #	*SAC-LA* 9-St			*SAC-LA* 20-St		
	$(\delta_{top})_{pre}$ m	$(\delta_{top})_{num}$ m	ε_{δ} %	$(\delta_{top})_{pre}$ m	$(\delta_{top})_{num}$ m	ε_{δ} %
76	0.429	0.607	34.4	0.612	0.598	2.5
77	0.427	0.408	4.5	0.568	0.560	1.3
78	0.361	0.449	21.7	0.518	0.444	15.4
79	0.210	0.258	20.7	0.307	0.271	12.6
80	0.620	0.509	19.6	1.169	1.380	16.6
81	0.602	0.694	14.3	0.824	0.984	17.6
82	0.392	0.445	12.7	0.579	0.619	6.7
83	0.352	0.387	9.4	0.490	0.350	33.2
84	0.303	0.583	63.3	1.017	1.605	44.8
85	0.189	0.260	31.6	0.320	0.503	44.4
86	0.140	0.210	40.1	0.347	0.487	33.5
87	0.197	0.239	19.2	0.204	0.246	18.7
88	0.124	0.181	37.3	0.113	0.128	12.6
89	0.483	0.590	19.9	0.693	0.698	0.7
90	0.398	0.392	1.4	0.546	0.536	1.9
91	0.305	0.303	0.6	0.451	0.297	41.2
92	0.243	0.148	48.4	0.313	0.202	42.9
Ar. Mean		18.8			20.9	
Geo. Mean		12.0			12.9	
Correlation		0.878			0.883	

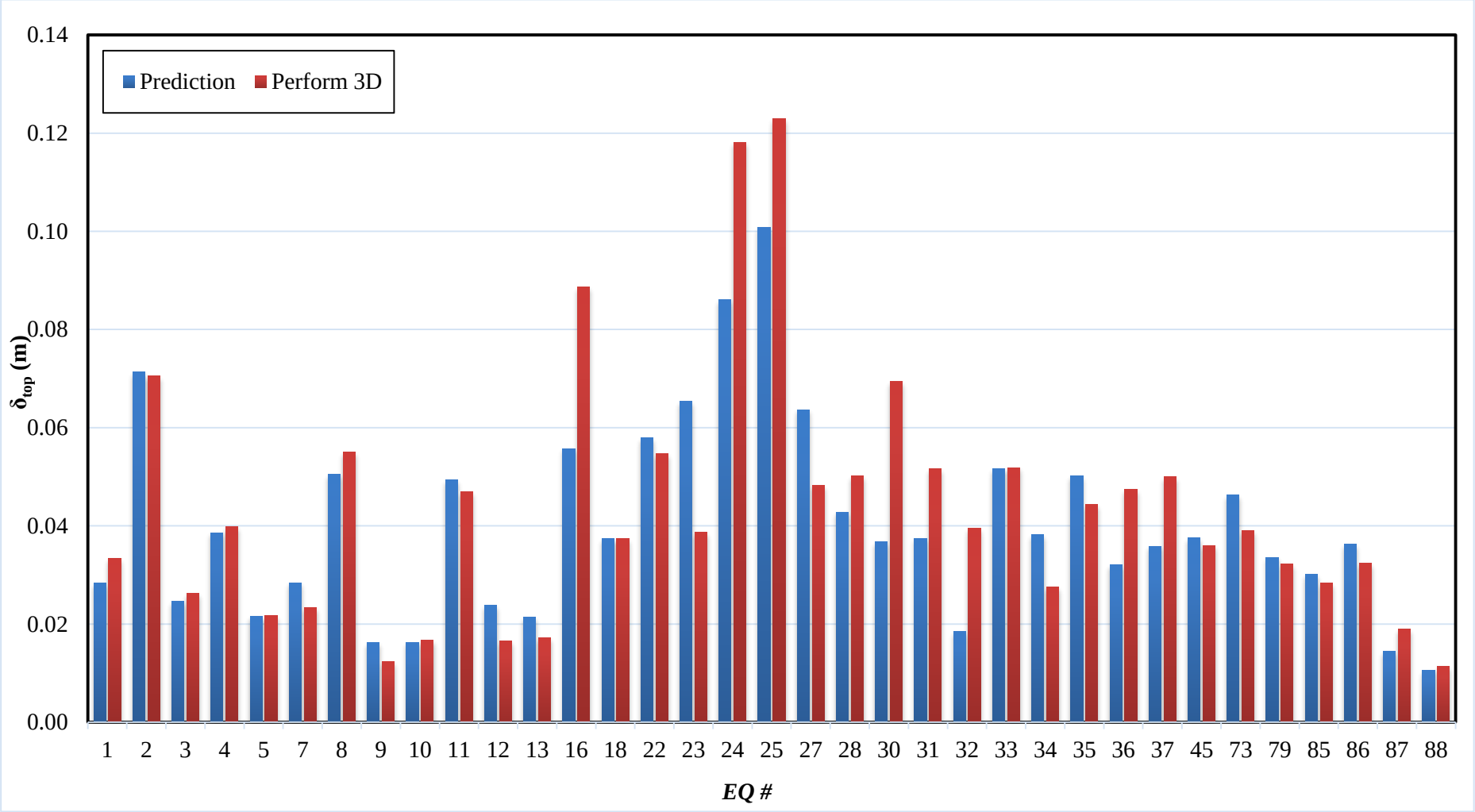

Figure C.1 : δ_{top} comparison between methodology and *NLTHA* for *Manoukas* 3-St frame using the EQ records with a PGV ≤ 50 cm/s.

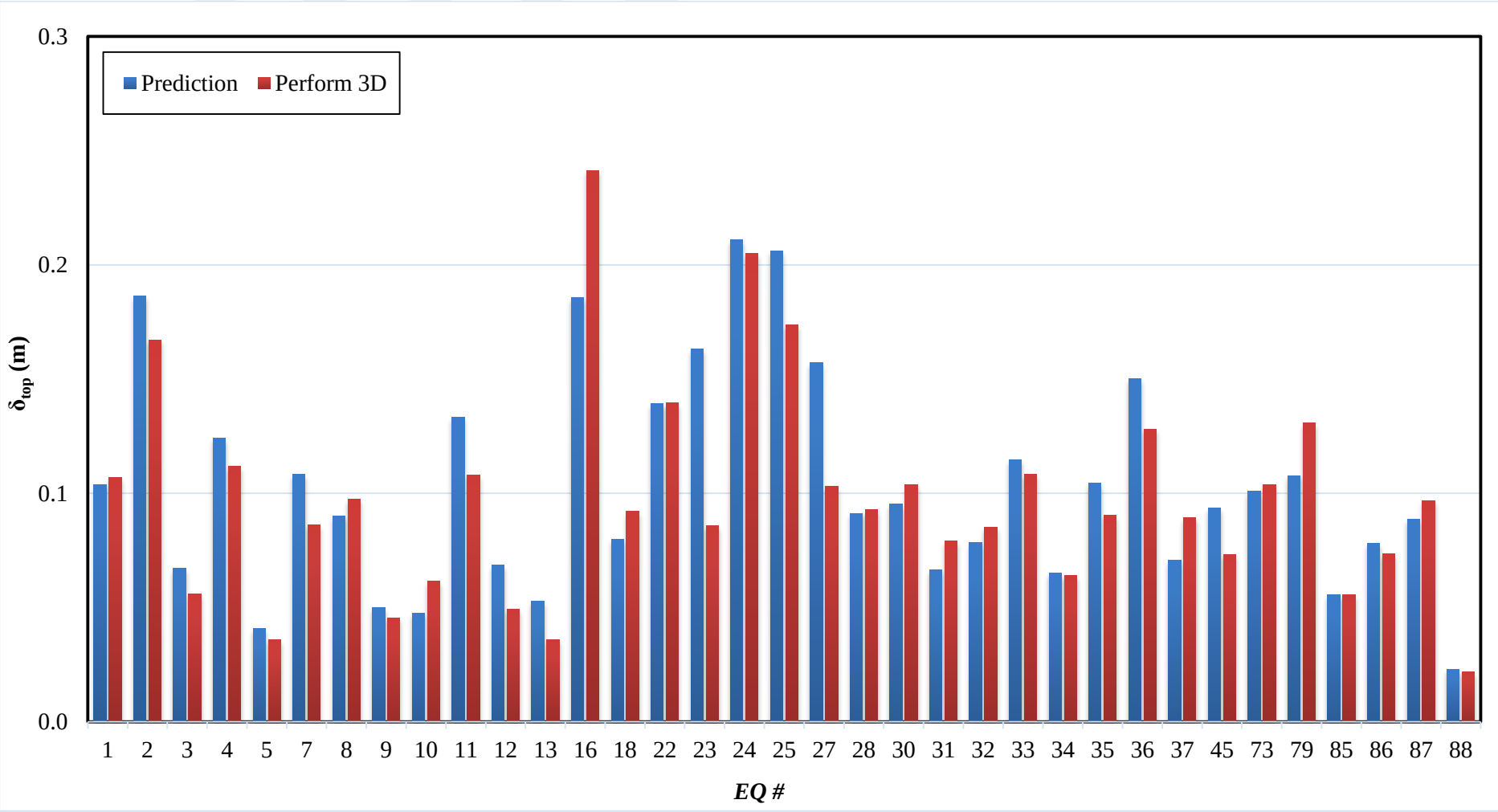

Figure C.2 : δ_{top} comparison between methodology and *NLTHA* for *Akbas* 3-St frame using the EQ records with a PGV ≤ 50 cm/s.

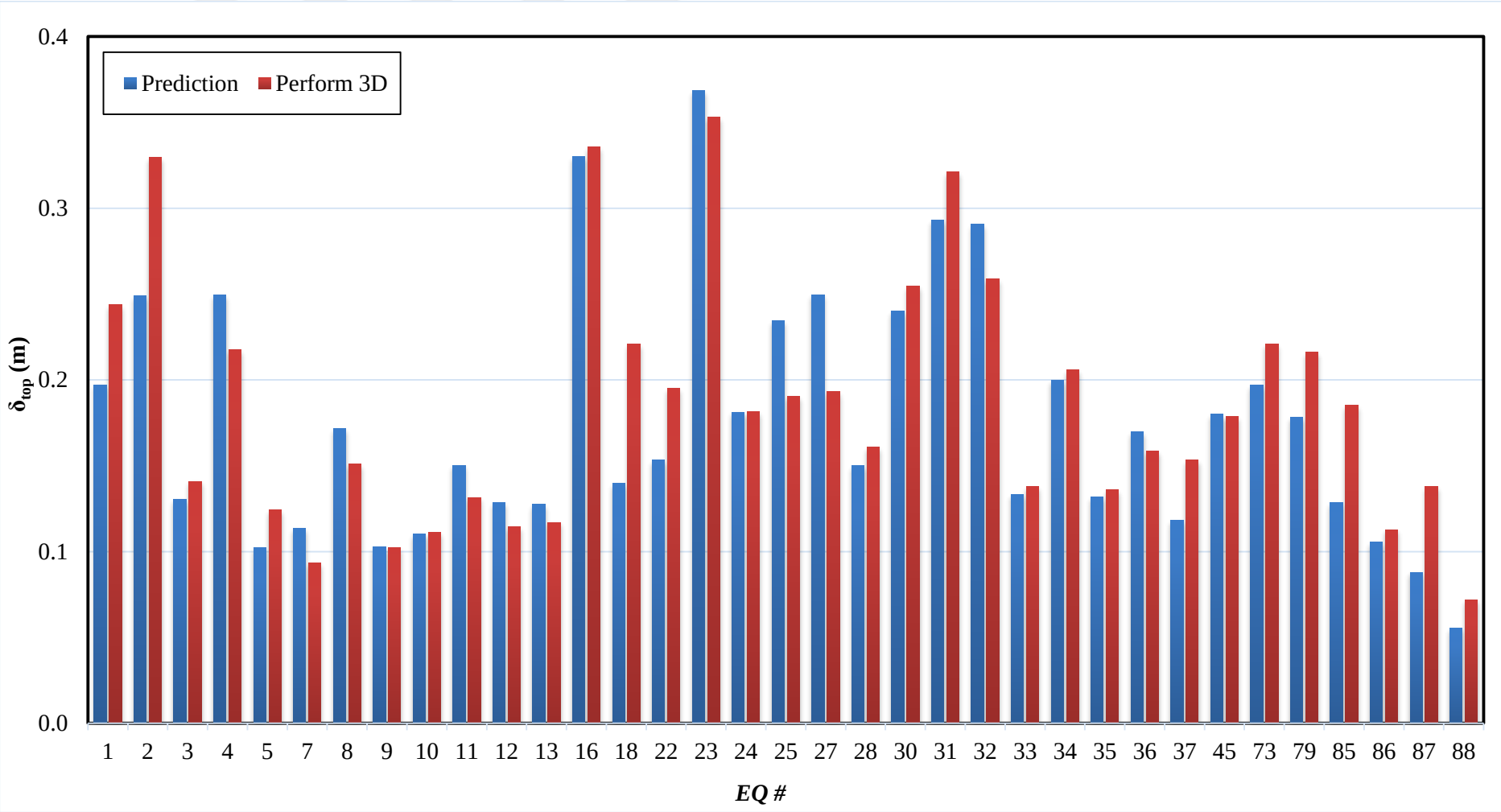

Figure C.3 : δ_{top} comparison between methodology and *NLTHA* for *Akbas* 6-St frame using the EQ records with a PGV ≤ 50 cm/s.

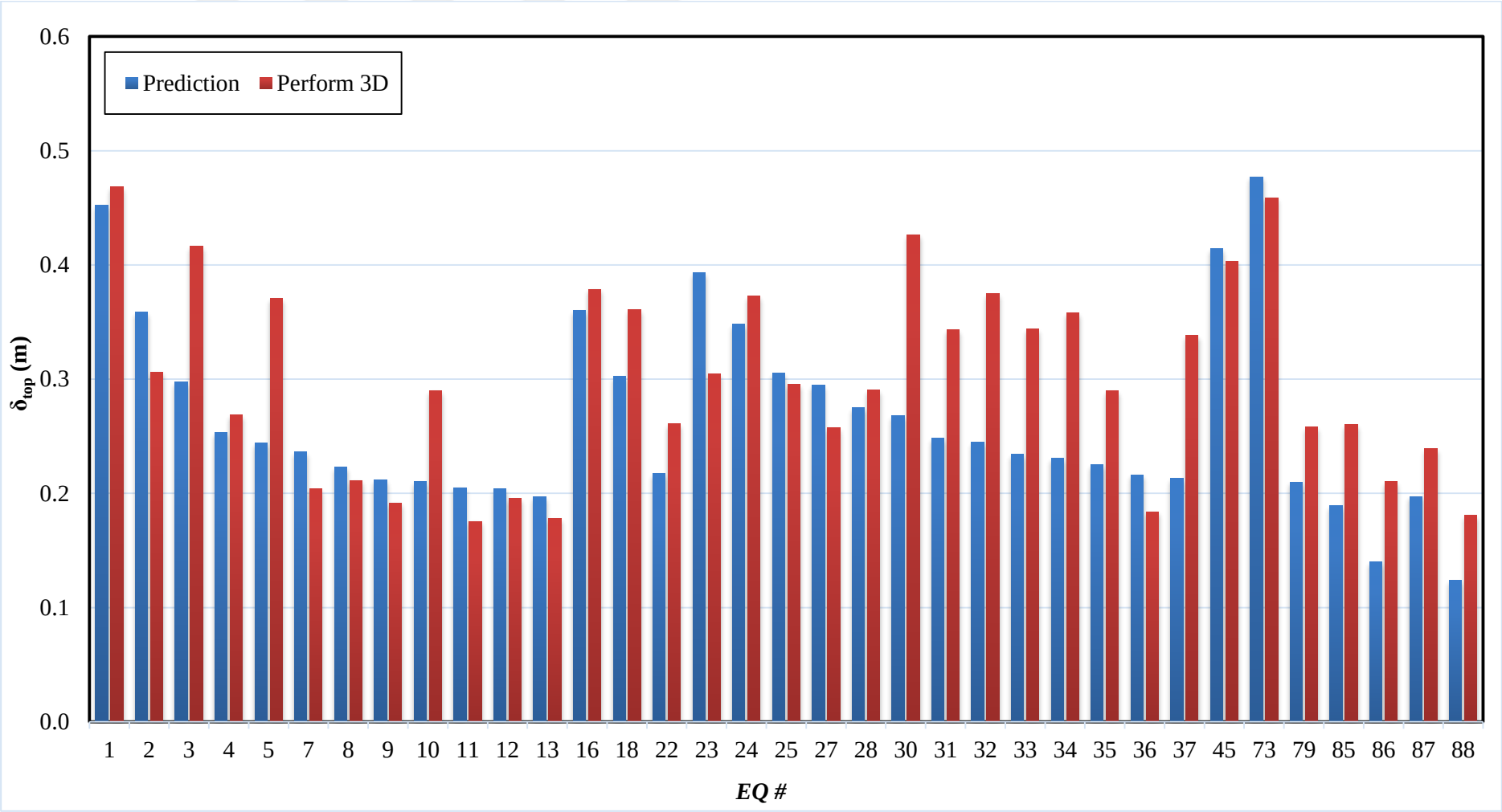

Figure C.4 : δ_{top} comparison between methodology and *NLTHA* for *SAC-LA* 9-St frame using the EQ records with a PGV ≤ 50 cm/s.

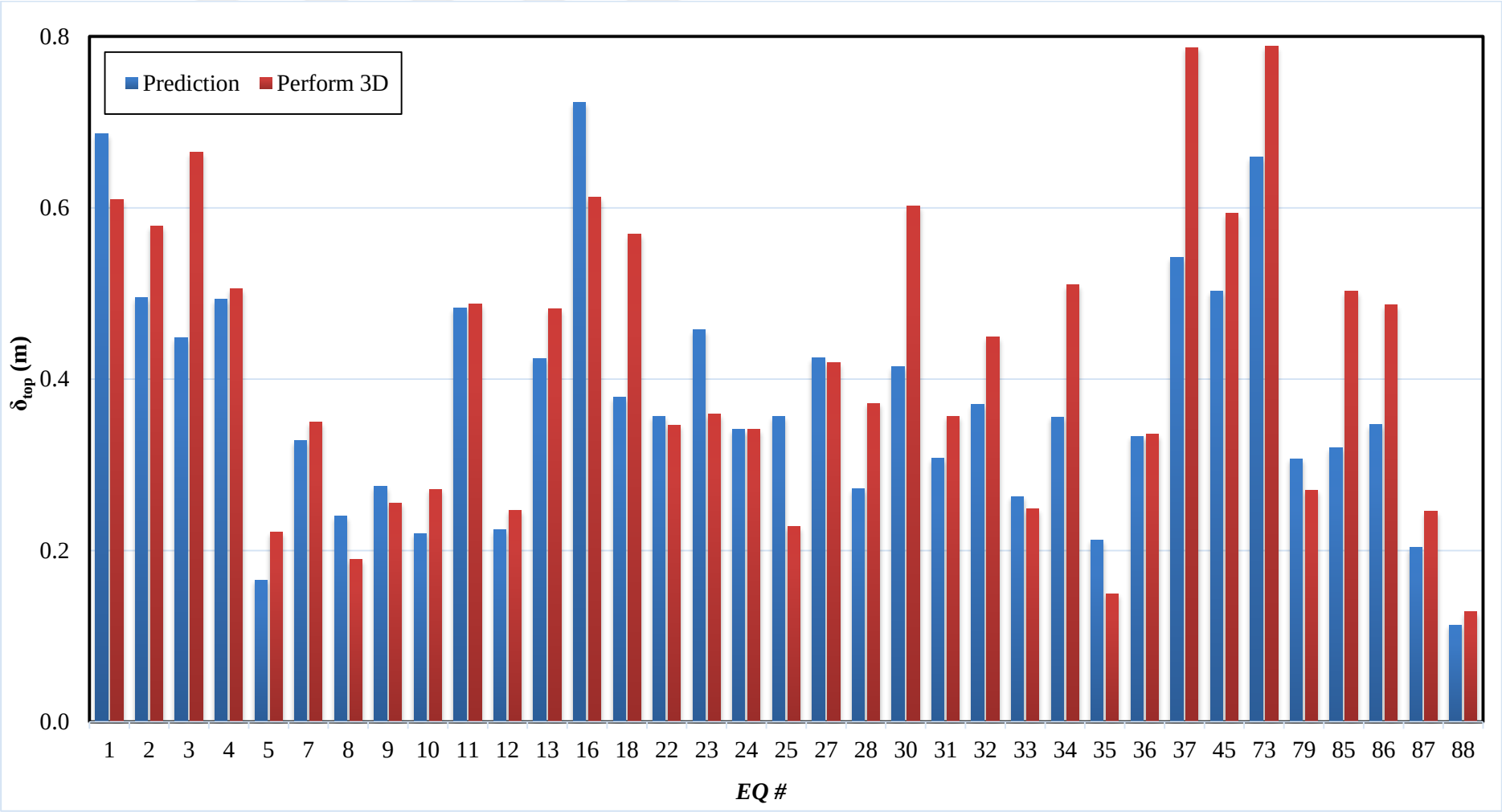

Figure C.5 : δ_{top} comparison between methodology and *NLTHA* for *SAC-LA* 20-St frame using the EQ records with a PGV ≤ 50 cm/s.

CURRICULUM VITAE

Name Surname **:** Furkan ÇALIM

Place and Date of Birth **:** Istanbul / 07.11.1995

E-Mail **:** furkancalim05@gmail.com

EDUCATION **:**

- **B.Sc.** **:** 2018, Istanbul Technical University, Faculty of Civil Engineering, Civil Engineering Department

PROFESSIONAL EXPERIENCE AND REWARDS:

- 2019- Research Assistant at Civil Engineering Department of ITU.

- 19.09.2019 Structural Dynamics Workshop Hackathon (Izmir Institute of Technology) – 1st Place Reward
- 01.07.2020 Graduate Research Poster Day (Istanbul Technical University) – 2nd Place Reward